University of Alberta

Semiclassical dynamics of constrained molecular systems in Cartesian coordinates

by

Ben Harland

©

A thesis submitted to the Faculty of Graduate Studies and Research in partial fulfillment of the requirements for the degree of **Master of Science**.

Department of Chemistry

Edmonton, Alberta
Fall 2002

National Library of Canada
Acquisitions and Bibliographic Services
395 Wellington Street
Ottawa ON K1A 0N4
Canada

Bibliothèque nationale du Canada
Acquisitions et services bibliographiques
395, rue Wellington
Ottawa ON K1A 0N4
Canada

Your file Votre référence

Our file Notre référence

The author has granted a non-exclusive licence allowing the National Library of Canada to reproduce, loan, distribute or sell copies of this thesis in microform, paper or electronic formats.

L'auteur a accordé une licence non exclusive permettant à la Bibliothèque nationale du Canada de reproduire, prêter, distribuer ou vendre des copies de cette thèse sous la forme de microfiche/film, de reproduction sur papier ou sur format électronique.

The author retains ownership of the copyright in this thesis. Neither the thesis nor substantial extracts from it may be printed or otherwise reproduced without the author's permission.

L'auteur conserve la propriété du droit d'auteur qui protège cette thèse. Ni la thèse ni des extraits substantiels de celle-ci ne doivent être imprimés ou autrement reproduits sans son autorisation.

0-612-81406-8

Canada

University of Alberta

Library Release Form

Name of Author: Ben Harland

Title of Thesis: Semiclassical dynamics of constrained molecular systems in Cartesian coordinates

Degree: Master of Science

Year this Degree Granted: 2002

Permission is hereby granted to the University of Alberta Library to reproduce single copies of this thesis and to lend or sell such copies for private, scholarly or scientific research purposes only.

The author reserves all other publication and other rights in association with the copyright in the thesis, and except as hereinbefore provided, neither the thesis nor any substantial portion thereof may be printed or otherwise reproduced in any material form whatever without the author's prior written permission.

Ben Harland
221 7th St. S.
Kenora, ON
CANADA, P9N 1P9

Date: 11 June 2002

University of Alberta

Faculty of Graduate Studies and Research

The undersigned certify that they have read, and recommend to the Faculty of Graduate Studies and Research for acceptance, a thesis entitled **Semiclassical dynamics of constrained molecular systems in Cartesian coordinates** submitted by Ben Harland in partial fulfillment of the requirements for the degree of **Master of Science**.

Pierre-Nicholas Roy

Wolfgang Jäger

Frank Marsiglio

Date: 11 June 2002

Abstract

Our present work endeavours to develop practical methods for implementing the Semiclassical Initial Value Representation (SC-IVR) based on the propagator of Herman and Kluk in cases where a reduction in the total number of degrees of freedom has been accomplished by applying holonomic constraints. By freezing out selected high frequency motions, the semiclassical propagator becomes less oscillatory, facilitating its evaluation, and integration of the classical equations of motion becomes less computationally expensive. Although the idea of eliminating undesirable molecular motions is certainly not new, it is usual to carry this out by going to some new coordinate of lower dimension which naturally describes the motions of interest. It is our view that a simpler and more general approach would be to remain in Cartesian coordinates throughout.

First, we show that our approach is theoretically justified for a simple model system consisting of two particles in a one dimensional harmonic potential, connected by a rigid "bond". Then, we turn our attention to a simple molecular problem: a constrained "water-bender" with one effective degree of freedom, namely, the bend mode. This problem was assessed using the standard methods of quantum molecular dynamics, and the existing prescription for the application of SC-IVR to constrained systems. It is shown that our new approach is quantitatively accurate *vis-a-vis* these methods.

Acknowledgements

I would like to express my gratitude for having had the opportunity to share a workspace with Dr. Nick Blinov. Not only did he provide clear and articulate answers to all my many questions on the spot (despite his constant insistence, "my English is not too good"), but I don't know if he even once didn't politely stand out of his chair at the sound of (chair swiveling) "uhh, Nick?"

Of course, I would also like to sincerely acknowledge my supervisor, Pierre-Nicholas Roy, for inviting me into his group as a Biochem. drop-out, for providing me with truly exceptional guidance and for tolerating my idiosyncrasies with kind patience. Inevitably, my future will include some heartfelt campaigning for the virtues of one or more of: C++, Linux, LaTeX, Maple, and AMD processors, and I would like to believe that this may be some small part of his legacy.

Contents

1 Introduction 1
- 1.1 The Theoretical Study of Molecules . . . 1
- 1.2 The Born-Oppenheimer Approximation . . . 2
- 1.3 Classical MD . . . 3
- 1.4 Quantum MD . . . 4
- 1.5 Semiclassical Methods . . . 5
- 1.6 Reduced Dimensionality Techniques . . . 6

2 Theory and Methods 8
- 2.1 The Importance of the Propagator in Quantum MD . . . 8
- 2.2 The Classical Limit of Quantum Mechanics . . . 10
- 2.3 Dirac's "Crude" Semiclassical Approximation . . . 11
- 2.4 The WKB Semiclassical Approximation . . . 14
- 2.5 The Van Vleck Propagator . . . 17
  - 2.5.1 Quasi-derivation of the Van Vleck propagator . . . 17
- 2.6 Heller's Gaussian Wavepackets . . . 20
  - 2.6.1 Dynamics with "thawed" Gaussians . . . 21
  - 2.6.2 The frozen Gaussian approximation . . . 22
- 2.7 The Herman-Kluk Initial Value Representation . . . 24
  - 2.7.1 The coherent state approximation: Arriving at the HK-IVR propagator . . . 24
  - 2.7.2 Application of the HK-IVR . . . 28

3 Results and Discussion 32
- 3.1 Proof of Principle: A Harmonic Oscillator Model . . . 33
  - 3.1.1 The quantum energy levels . . . 33
  - 3.1.2 The semiclassical energy levels . . . 34
- 3.2 A Physical Example: A Water Bender . . . 37
  - 3.2.1 Exact quantum results . . . 39
  - 3.2.2 HK-IVR in curvilinear coordinates . . . 43
  - 3.2.3 HK-IVR in Cartesian coordinates . . . 56

4 Conclusions 88

A Multidimensional Gaussian Integrals 94

B The Stationary-Phase Approximation 96

C The Power Spectrum from the Autocorrelation Function 98

D The Gaussian Window Function Applied to the Autocorrelation Function 101

E Selection of the Coherent State Width Parameters 104

F Miller's Log-Derivative Formulation for the Herman-Kluk Prefactor 105

G Schematic for Computer Code Used in this Thesis 109

List of Figures

3.1 The quantum autocorrelation function for two particles in a harmonic well. 37
3.2 The quantum power spectrum for two particles in a harmonic well taken as the Fourier transform of the windowed autocorrelation function. 38
3.3 The HK-IVR autocorrelation function for two particles in a harmonic well. 39
3.4 The HK-IVR power spectrum for two particles in a harmonic well. 40
3.5 The curvilinear coordinate for water. The O-H bonds will be frozen by setting $r_1 = r_2 = r_0$. 40
3.6 The 1D potential for the water-bender. O-H bonds are fixed at the equilibrium value, $r_0 = 0.958$ Å. 41
3.7 The 1D potential with first 5 energy levels. $|\Psi_0(\theta)|$ is shown as the bold curve, superimposed at a height $\langle\Psi_0|\hat{H}|\Psi_0\rangle = 5295.8\text{cm}^{-1}$. 42
3.8 The quantum autocorrelation function for the 1D water-bender. 43
3.9 The quantum power spectrum for the 1D water-bender. 44
3.10 A sample trajectory of the water-bender with initial conditions, $(p_{\theta 0} = 0, \theta_0 = 80°)$. . 46
3.11 Determining a suitable timestep: looking at conservation of energy for a sample trajectory of the water-bender in 1D. In all figures, the dotted line is potential energy, the dashed line, kinetic energy, and the solid line is total energy. Top figure, dt = 100.0 au. Centre figure, dt = 10.0 au. Bottom figure, dt = 1.0 au. The timestep of the bottom figure was used for all trajectories computed subsequently. 47
3.12 Phase-space plot for the water-bender in 1D. 48
3.13 The distributions of θ sampled from $\theta_0 = 80°$ in angular coordinates using a wavepacket width, $\gamma = 10.0$. The solid line indicates the distribution when an energy cutoff was used ($E_{max} = 10000\text{cm}^{-1}$), while for the dashed line, there was no such cutoff. This figure was generated from 80000 sets of initial conditions. 50
3.14 The distributions of p_θ sampled from $p_{\theta 0} = 0$ in angular coordinates using a wavepacket width, $\gamma = 10.0$. The solid line indicates the distribution when an energy cutoff was used ($E_{max} = 10000\text{cm}^{-1}$), while for the dashed line, there was no such cutoff. This figure was generated from 80000 sets of initial conditions. 51
3.15 The primitive Heller autocorrelation function for the water-bender, calculated in 1D. This function was obtained from 4402 bound trajectories. 52
3.16 The primitive Heller power spectrum for the water-bender, calculated in 1D. 53
3.17 The square frequencies obtained by diagonalising **GF**. The dashed line corresponds to the bend mode in 1D, calculated as $G_{33}F_{33}$. 55
3.18 The convergence of the HK-IVR autocorrelation function for the water-bender in 1D. The origin of the vertical axis corresponds to exact agreement with the corresponding quantum results. The dashed line corresponds to the ACF with the exact expression for the HK-prefactor, while the solid line was produced by the ACF with the approximate prefactor. 57

3.19 The HK-IVR autocorrelation function for the water-bender calculated in 1D using the exact expression for the prefactor. This function was obtained from 4402 bound trajectories. 58
3.20 The HK-IVR power spectrum for the water-bender calculated in 1D using the exact expression for the prefactor. 59
3.21 The HK-IVR autocorrelation function for the water-bender calculated in 1D using the "multichannel-WKB" approximation to the prefactor. This function was obtained from 4402 bound trajectories. 60
3.22 The HK-IVR power spectrum for the water-bender calculated in 1D using the "multichannel-WKB" approximation to the prefactor. 61
3.23 The effect of the value of the tolerance on Rattle's ability to hold the O-H bond length to the constrained value ($r_0 = 0.957927$ Å) over a sample trajectory. In the upper figure, the dotted line corresponds to a tolerance of 1.0, the dashed line, 0.1, and the solid line, 0.01. In the lower figure, the dotted line corresponds to a tolerance of 1×10^{-3}, the dashed line, 1×10^{-4}, and the solid line, 1×10^{-5}. A tolerance value of 1×10^{-6} was used in subsequent calculations. 63
3.24 The number of iterations used by Rattle to apply the contraints to the molecular configuration as a function of time, over a short sample trajectory. This figure shows the relationship between the number of these iterations and the value of the tolerance. In the upper figure, the circles correspond to a tolerance of 1.0, the squares, 0.1, and the triangles, 0.01. In the lower figure, the circles correspond to a tolerance of 1×10^{-3}, the squares, 1×10^{-4}, and the triangles, 1×10^{-5}. Notice that as the tolerance is decreased, more iterations (on average) are required. 64
3.25 The number of iterations used by Rattle to apply the contraints to the velocities as a function of time, over a short sample trajectory. This figure shows the relationship between the number of these iterations and the value of the tolerance. The tolerance values and associated symbols match with the preceeding figure. Notice that as the tolerance is decreased, more iterations (on average) are required. 65
3.26 A comparison of a trajectory obtained by integrating the angular equations of motion (the solid line) with the corresponding trajectory calculated in Cartesian coordinates by Rattle (the circles). The initial conditions are ($p_{\theta 0} = 0, \theta_0 = 80°$) and a tolerance of 1×10^{-6} was used. 66
3.27 A plot of the action calculated along a trajectory with initial conditions ($\theta_0 = 80.0°, p_{\theta 0} = 0.0$). For the solid line, the dynamics were performed in angular coordinates, and the circles, in Cartesian coordinates. 67
3.28 A "top view" of the distribution of configurations initially sampled (*ie.* they don't obey the constraints). The hydrogens are depicted by crosses and the oxygens, by circles. Configurations were sampled about $\theta_0 = 80°$ with wavepacket widths, ($\gamma_H = 2.868, \gamma_O = 9.807$). 1000 sets of initial conditions are represented. 68
3.29 A "top view" of the distribution of momenta initially sampled (*i.e.* they do not obey the constraints). The momenta associated with the hydrogens are depicted by crosses and those of the oxygens, by circles. Momenta were sampled about $p_{\theta 0} = 0$ with wavepacket widths, ($\gamma_H = 2.868, \gamma_O = 9.807$). 1000 sets of initial conditions are represented. 69
3.30 The distribution of initial configurations, after the application of Rattle and removal of centre-of-mass motions. 71
3.31 The distribution of initial momenta, after the application of Rattle and removal of centre-of-mass motions. 72

3.32 The distributions of kinetic energy of the initial conditions (sampled in Cartesian coordinates) at the different stages of preparation. The distribution directly sampled is shown with circles, after the application of Rattle in crosses, after removing translations in squares, and the distribution (not completely shown) after removing rigid-body rotations is shown as the bold solid line. These plots were obtained from 80000 sets of initial conditions. 73
3.33 The distributions of θ sampled from Ψ_0 in Cartesian coordinates. The dashed line is the distribution obtained from coordinates sampled directly (subject to an energy cutoff, $E_{max} = 10000\text{cm}^{-1}$), while the solid line shows this distribution after Rattle is applied. This plot was obtained from 80000 sets of initial conditions. 74
3.34 The distributions of p_θ sampled from Ψ_0 in Cartesian coordinates. The dashed line is the distribution obtained from momenta sampled directly (subjected to an energy cutoff, $E_{max} = 10000\text{cm}^{-1}$), while the solid line shows the distribution after Rattle is applied and centre-of-mass motion is subtracted. This plot was obtained from 80000 sets of initial conditions. 75
3.35 A comparison of the values of θ used in the initial conditions, obtained in both angular (solid line) and Cartesian (dashed line) coordinates. 76
3.36 A comparison of the values of p_θ used in the initial conditions, obtained in both angular (solid line) and Cartesian (dashed line) coordinates. 77
3.37 The HK-IVR autocorrelation function calculated for the water-bender in Cartesian coordinates, except for the prefactor, which is calculated from the 1D Hessian. . . . 78
3.38 The HK-IVR power spectrum calculated for the water-bender in Cartesian coordinates, except for the prefactor, which is calculated from the 1D Hessian. 79
3.39 The eigenvalues of the unprojected, mass-weighted Hessian matrix in Cartesian coordinates ($\mu^{-1} \cdot \mathbf{F} \cdot \mu^{-1}$). The three modes corresponding to translations are zero. Those corresponding to the three rigid-body rotations are negative (*i.e.* give imaginary frequencies) for most non-equilibrium conformations. The remaining three solid lines correspond to the internal modes. The dashed line indicates the bend mode, calculated in 1D as $G_{33}F_{33}$. 81
3.40 Square frequencies obtained by diagonalising $\Delta \cdot \mu^{-1} \cdot \Delta \cdot \mathbf{F} \cdot \Delta \cdot \mu^{-1} \cdot \Delta$. The dashed line corresponds to the bend mode calculated in 1D by $G_{33}F_{33}$. Notice that in two places, our bend mode is imaginary (*i.e.* the curve goes below zero), and this can lead to problems in the evaluation of the HK-prefactor. The region around 160° indicates a transition state (we are approaching the inversion barrier of the potential), while the "dip" near 40° is a feature of the curvature of the potential (perhaps not physically relevant). Either way, these regions correspond to high energies and are not visited frequently in our trajectories. 84
3.41 The HK-IVR autocorrelation function calculated for the water-bender in Cartesian coordinates, using the "multichannel-WKB" approximation to the prefactor. 85
3.42 The HK-IVR power spectrum calculated for the water-bender in Cartesian coordinates, using the "multichannel-WKB" approximation to the prefactor. 86

C.1 The quantum autocorrelation function for two particles in a harmonic well. 99
C.2 The quantum power spectrum for two particles in a harmonic well, taken as the Fourier transform of the autocorrelation function. 100

D.1 The windowed quantum autocorrelation function for two particles in a harmonic well. 102
D.2 The quantum power spectrum for two particles in a harmonic well taken as the Fourier transform of the windowed autocorrelation function. 103

List of Tables

3.1 The calculated energy levels for the two particles in a harmonic trap. Values are given in E_h. The numbers in brackets indicate the uncertainty on the last digit. 37

3.2 Accuracy in capturing zero point energy. This accuracy is due entirely to the HK-prefactor. By introducing the approximate form, we gain an additional 0.6% error; by going to the projected 9D Hessian, our error roughly doubles. The latter result can be explained by noticing that the frequency of our bend mode spends more time in the imaginary region than does the frequency computed in 1D. 85

3.3 Final table of calculated energy levels (raw data) in cm^{-1}. The numbers in brackets are uncertainties. 86

3.4 The percent errors on the peak positions, compared to the corresponding quantum results. This error reflects peak spacings only; peaks values were shifted so that the error associated with zero point energy is 0. 87

List of Abbreviations

ACF	*autocorrelation function*
BO	*Born-Oppenheimer*
CPU	*computer processing unit*
EJH	*Eric J. Heller*
FG	*frozen Gaussian*
FGA	*frozen Gaussian approximation*
FP	*free particle*
GWP	*Gaussian wavepacket*
HJ	*Hamilton-Jacobi*
HK	*Herman-Kluk*
IVR	*initial value representation*
MD	*molecular dynamics*
MM	*molecular mechanics*
mw	*mass-weighted*
PB	*Poisson bracket*
PES	*potential energy surface*
QCMD	*quantum chemistry - molecular dynamics*
QM	*quantum mechanics*
QMD	*quantum molecular dynamics*
SC	*semiclassical*
SP	*stationary-phase*
st.pts	*stationary points*
TDSE	*time-dependent Schrödinger equation*
TISE	*time-independent Schrödinger equation*
traj.	*classical trajectory*
VV	*Van Vleck*
WKB	*Wigner, Kramers, and Brillouin*

Chapter 1

Introduction

1.1 The Theoretical Study of Molecules

Our understanding of a large class of natural phenomena lies in a molecular picture of some sort. This picture, along with its associated terminology, usually derives directly from the theoretical model used to rationalise experimental observations. Theoretical chemistry as a discipline has enjoyed tremendous advances in the past decades in the details with which we can predict and explain the properties of matter at the atomic and molecular level.

At this level, the description of matter leads to the many-body problem, a problem we can not hope to solve analytically. Because efforts are therefore restricted to numerical methods, the development of methodologies for the study of molecules has been linked to the development of the digital computer. The recent advent of affordable large scale parallel computing from commodity hardware (*e.g.* Beowulf clusters) has allowed theoretical chemists to tackle the simulation of systems of much greater complexity than ever before possible.

This chapter begins with a molecular picture consisting of a set of charged point particles (the electrons and the nuclei) whose motions are governed by the laws of quantum mechanics. By invoking the Born-Oppenheimer approximation (see Section 1.2), we substantially reduce the complexity of this picture. The electron problem is briefly outlined, and then set aside. Instead, we turn our attention to the motions of the nuclei on some energy landscape. These motions can be addressed with three levels of theory: classical mechanics (Section 1.3), quantum mechanics (Section 1.4), and a hybrid of these two, the *semiclassical* methods (Section 1.5). Finally, in Section 1.6, we introduce the concept of reducing the dimensionality of the model used to describe a particular molecular system. These *reduced dimensionality techniques* are of extreme value to the theoretical chemist, since they enable more complex systems to be addressed for a given computational cost.

1.2 The Born-Oppenheimer Approximation

The Born-Oppenheimer (BO) approximation, which allows for the separation of the electronic and nuclear degrees of freedom, is one of the most important ideas in Chemistry. According to Struve [1], *without it, electronic and nuclear motions would be scrambled in complicated molecular Hamiltonians and extensive numerical calculations would be necessary to extract even the most qualitative features of vibrational and rotational structure.* The underlying idea is that the electrons bound to a molecule travel so much faster than do the nuclei, that we may consider the nuclei to move in the field of the averaged electronic charge density.

A brief summary begins with the molecular Hamiltonian, an object of fundamental importance in molecular spectroscopy. For a molecule with '*nuc*' atoms and '*el*' electrons, the Hamiltonian is: [1]

$$\begin{aligned}\hat{H} &= \sum_{N=1}^{nuc} -\frac{\hbar^2}{2m_N}\hat{\nabla}_N^2 + \sum_{n=1}^{el}\frac{-\hbar^2}{2m_e}\hat{\nabla}_n^2 + \sum_{m=1}^{el}\sum_{n>m}^{el}\frac{e^2}{4\pi\epsilon_0|\mathbf{r}_m-\mathbf{r}_n|} \\ &\quad - \sum_{n=1}^{el}\sum_{N>n}^{nuc}\frac{Z_N e}{4\pi\epsilon_0|\mathbf{r}_n-\mathbf{R}_N|} + \sum_{M=1}^{nuc}\sum_{N>M}^{nuc}\frac{Z_M Z_N}{4\pi\epsilon_0|\mathbf{R}_M-\mathbf{R}_N|} \,. \end{aligned} \tag{1.1}$$

The electronic and nuclear coordinates are $\mathbf{r}$ and $\mathbf{R}$, respectively. The mass of nucleus N is m_N, and Z_N is its charge. We have accounted for, in order, nuclear kinetic energy, electronic kinetic energy, electronic repulsion, electron-nuclear attraction, and nuclear repulsion. The corresponding time-independent Schrödinger equation (TISE) [2] is

$$\hat{H}|\Psi_n(\mathbf{r},\mathbf{R})\rangle = E_n|\Psi_n(\mathbf{r},\mathbf{R})\rangle \,. \tag{1.2}$$

Neglecting nuclear motion (*i.e.* omitting the nuclear kinetic energy operator) leads us to the *electronic* Hamiltonian:

$$\begin{aligned}\hat{H}^{el} &= \sum_{n=1}^{el}\frac{-\hbar^2}{2m_e}\hat{\nabla}_n^2 + \sum_{m=1}^{el}\sum_{n>m}^{el}\frac{e^2}{4\pi\epsilon_0|\mathbf{r}_m-\mathbf{r}_n|} \\ &\quad - \sum_{n=1}^{el}\sum_{N>n}^{nuc}\frac{Z_N e}{4\pi\epsilon_0|\mathbf{r}_n-\mathbf{R}_N|} + \sum_{M=1}^{nuc}\sum_{N>M}^{nuc}\frac{Z_M Z_N}{4\pi\epsilon_0|\mathbf{R}_M-\mathbf{R}_N|} \,, \end{aligned} \tag{1.3}$$

in which a particular (fixed) nuclear configuration enters only parametrically. The resulting *electronic problem*,

$$\hat{H}^{el}|\psi_n(\mathbf{r};\mathbf{R})\rangle = \varepsilon_n(\mathbf{R})|\psi_n(\mathbf{r};\mathbf{R})\rangle \,, \tag{1.4}$$

is overwhelmingly less difficult to solve. In principle, we could endeavour to solve (1.4) for all possible $\mathbf{R}$, and this would give the *Born-Oppenheimer Potential Energy Surface* (BO-PES), $\varepsilon_0(\mathbf{R})$. The global minimum on this surface indicates the *equilibrium structure.*

[1] Recall that our electrons and nuclei are taken as point charges, and all nuclear spin effects are neglected. Spin-orbit coupling is ignored for the electrons, but antisymmetry (*i.e.* the Pauli Principle) is accounted for in order to get proper electronic structure.

The study of electronic structure has commanded much attention in recent years owing to the development of computer software which has made practical *ab initio* calculations an accessible and indispensable tool to Chemists of a variety of disciplines. This has been acknowledged with the 1998 Nobel Prize in Chemistry going to Kohn and Pople for their work on this problem. [3] However, many classes of physico-chemical phenomena are governed by the dynamics of the nuclei - both within and between molecules - and these comprise the field of molecular dynamics. Examples which are found as subjects of frequent theoretical investigation include vibronic spectroscopy, molecular photodissociation, and the study of chemical reaction rates (*i.e.* kinetics). Processes are studied in the gas phase (elastic, inelastic or reactive scattering problems, for example), in solution (transport properties, fluid dynamics, docking of biomolecules, protein folding), and in the solid phase (molecular crystal growth and fracture, plastic mechanical properties, defect formation). Equilibrium properties can be calculated using ensemble averages, and transport properties and spectra are obtained from appropriate time correlation functions using linear response theory. [4, 5]

Although electronic structure programs support normal mode analysis, in which nuclear degrees of freedom are investigated to harmonic approximation about the equilibrium structure, this is adequate only for small amplitude oscillations. There is often the need to characterise broader regions of the potential energy landscape, and the development of molecular potentials has for a long time been an active area of research. These potentials can be carefully parameterised[2] analytical expressions, defined over full configuration space, or can be calculated "on the fly" using the semiempirical force fields of Molecular Mechanics (MM) or *ab initio* programs (Quantum Chemistry - Molecular Dynamics, QCMD - presently a rapidly growing area of research).

With a PES in hand, it is now decided whether the nuclear dynamics are going to be calculated according to the laws of classical or quantum mechanics.

1.3 Classical MD

Classical molecular dynamics (MD) is based on classical mechanics. From a particular set of initial conditions (configuration, momenta) for a molecular system, one solves Newtons equation, $F = ma$, to obtain the corresponding trajectory. Historically, MD is what theoretical chemists first employed for small systems in the context of reactive scattering. Because of the relatively small computational cost associated with determining these trajectories, MD is routinely used today for large biological systems, condensed phase reactions, and the study of materials, for example. Numerous methodological developments have been made in the past forty years [4, 6] and one of the objectives of the research presented here is to develop a framework that would allow one to reuse this resource to study quantum dynamics.

[2]Potentials can be parameterised to reproduce spectroscopic data, or the results of electronic structure calculations.

1.4 Quantum MD

Although it is true that *for many systems it is only because we ask quantum questions (such as energy specific transition probabilities between two quantum states) that we need to invoke quantum mechanics at all* [7], it is these laws which nature ultimately obeys. When quantum phenomena such as coherence, tunneling, or the quantisation of bounded motion are significant, classical MD is doomed to failure. Only quantum methods can address problems involving nonadiabatic electronic degrees of freedom (essential for certain problems in photochemistry), or be used to predict the selection rules for transitions involving identical particle symmetry, for example. Quantum effects become especially significant for hydrogen atom motion, which is consequential for solvation, hydrogen-bonding and proton transfer.

In quantum molecular dynamics (QMD), molecular motions are governed by the time-dependent Schrödinger equation (TDSE):

$$i\hbar\frac{\partial\Psi(\mathbf{R})}{\partial t} = \hat{H}\Psi(\mathbf{R}) \ , \tag{1.5}$$

where, here our Hamiltonian accounts for nuclear motion:

$$\hat{H}^{nuc} = \sum_{N=1}^{nuc} -\frac{\hbar^2}{2m_N}\hat{\nabla}_N^2 + V(\mathbf{R}) \ . \tag{1.6}$$

The potential term, $V(\mathbf{R})$, is the BO-PES from Section 1.2.

In earlier years, Chemists tended to focus primarily on the energy form of the Schrödinger equation, $\hat{H}\Psi_n = E_n\Psi_n$, but this has since given way to some extent to the time-dependent version due to the short-time nature of the "essential physics" of a number of problems. [8] Regardless of which route is taken, the variational method is normally used, in which the Hamiltonian is represented in some basis set. The computational effort lies in diagonalising the Hamiltonian matrix and this procedure is susceptible to poor scaling: the size of the Hamiltonian matrix goes as n^N where N is the number of degrees of freedom and n is the number of basis functions used to represent each of these (typically 10 - 20). Diagonalisation routines scale as the cube of this size. Presently, the "state of the art" in QMD calculations involve models which are limited to fewer than 10 effective degrees of freedom. [9] Therefore, new scalable approximate schemes are presently being sought.

These alternative schemes can be grouped into three categories. The first involves the use of mixed quantum-classical models in which select degrees of freedom are subjected to QMD, while the rest are handled classically. Although this is an intuitively simple strategy, it leads to inconsistencies, especially at the boundary separating the two subsystems. In effective potential methods, classical-like equations of motion are solved, but the force is derived from a potential which has been modified to accommodate quantum effects. This thesis is concerned with the third class, in which all degrees of freedom are treated *semiclassically* (*i.e.* on the same footing).

1.5 Semiclassical Methods

Semiclassical methods are characterised by their use of classical trajectories in order to obtain quantum information about a system. This feature has immediate appeal: an intuitively classical quality is preserved which facilitates physical interpretation of the results. Development of these methods experienced a dramatic revival in the early 1970's, and they have since been demonstrated to capture quantum effects such as tunneling, quantum coherence, and zero point energy, at least qualitatively.

The origins of these methods can be traced back to Dirac and the correspondence principle. In his book [10], Dirac demonstrated that the Hamilton-Jacobi equations of classical dynamics could be recovered from the Schrödinger equation in the limit $\hbar \to 0$ (this is presented in Section 2.3). On a historical note, this line of reasoning inspired Feynmann to develop his path integral formulation of quantum mechanics [11], a paradigm from which the various semiclassical schemes are most naturally derived.

As with pure quantum dynamics, of central importance in various semiclassical schemes is Green's function, which determines the amplitude connecting coordinate space at two distinct times. Green's function is a *propagator* - that is, it directs the evolution of some arbitrary wavefunction, Ψ, from one time to another under the influence of the Hamiltonian (this is discussed in more detail in Section 2.1). Modern semiclassical methods endeavour to provide an approximate form for the quantum Green's function. The archetype for the semiclassical propagator is due to Van Vleck [12] (see Section 2.5). Because it is difficult to implement, save for a couple of exceptions, it is not used directly. The chief difficulties with it arise from the notorious *root-search* problem, in which all possible classical trajectories connecting two points in coordinate-space by a certain time-interval must be located. Computationally practical semiclassical propagators side-step this problem by going to an ***initial-value representation*** (IVR) [8, 13, 14], a change of variables whereby final-time position is exchanged for initial-time momentum. The propagator used in this thesis is the initial-value version of the Herman-Kluk (HK) propagator (HK-IVR). [15, 16, 17, 18, 19, 20]

The genealogy of the HK-IVR begins with a paper by Heller [7], in which he identified a novel approach to semiclassical dynamics based on Gaussian wavepackets (GWP - this is presented in Section 2.6.1).[7] A specific GWP form of the wavefunction (*ansatz*) is imposed, defined by four time-dependent parameters. These parameters define the centre of the wavepacket, and its associated momentum, the width of the wavepacket and its phase. Expanding the potential to second order, he found analytic expressions for the time-evolution of these four parameters (according to the TDSE), and discovered that the centre of the GWP follows a classical trajectory. Later, Heller discovered that even if the width parameter is fixed to some constant value, the wavepackets perform surprisingly

well (see Section 2.6.2).[21] Even the evolution of position-momentum correlation is captured at least qualitatively by a "swarm" of these *frozen* Gaussians (FG) about some central trajectory. Using the so-called *frozen Gaussian approximation* (FGA), in which an overcomplete set of FG's is used as a representation, the HK-IVR propagator was born. This propagator has since received the lion's share of recent attention (see Section 2.7).

Papers continue to appear which are devoted to the efficient evaluation of individual parts of the HK-IVR integral [22, 23], and a number of conditioning techniques have been developed to facilitate its integration.[24, 25, 26]

1.6 Reduced Dimensionality Techniques

No matter how efficient emerging semiclassical propagators become, there will always be a desire to tackle problems which are beyond feasible size limits. The simplest and most straightforward way to substantially reduce the computational effort required for a particular problem is to reduce the complexity of the model used to describe it.[3] The dimensionality of a model is reduced according to the timescale of the motions which are of principal interest. By eliminating undesirable modes, complex molecular motions can be effectively described by a reduced number of coordinates.

The principle, like that of the BO approximation, is that motions of different timescales couple only weakly to each other. Eliminating undesirable, high frequency modes (by fixing them to mean values) greatly facilitates calculation: larger timesteps may be taken when integrating the classical equations of motion, thereby allowing longer simulations for a given amount of CPU time.

Traditionally, this procedure involves first finding and changing to a new coordinate of lower dimension which naturally describes the motion of interest. For any system more complicated than, say butane, defining this new coordinate (and its derivatives) is either nontrivial or not feasible. Furthermore, if this new coordinate is curvilinear, an ordering problem arises in the kinetic energy operator. According to Schulman [27], *if you like excitement, conflict, and controversy, especially when nothing very serious is at stake, then you will love the history of quantisation on curved spaces.*

Forthcoming studies employing the HK-IVR are at the level of complexity where implementing the traditional procedure is becoming increasingly difficult. Therefore, the potential value of an alternate, more general way of reducing the dimensionality of a problem is becoming increasingly apparent. We would hope for such a method to be easy to implement and general. A desire for generality is keeping with the spirit of potentially integrating this method with existing MD codes. Also, we hope that, even if this method has a higher associated computational cost than the alternatives, that it at least scales as well with the effective number of degrees of freedom.

[3] Of course I do not mean to imply that the development of new models by theorists is trivial. For my purposes, it is enough that countless models have been cataloged, and so to make use of them, or to introduce holonomic bond constraints, is straightforward.

In this work, we propose a novel method which meets the above criteria. It evolved from the viewpoint that things would be much simpler if calculations remained in Cartesian coordinates with the reduction in dimension being accomplished through the application of holonomic (bond) constraints.

Chapter 2

Theory and Methods

This section begins with a discussion of the importance and utility of the quantum mechanical propagator and then proceeds to briefly outline what it means to seek a classical limit in QM. This follows with a summary of some important features of a few of the more fundamental semiclassical schemes. This is intended to be a survey of the historical development for the framework of semiclassical theory which is relevant to the Herman-Kluk initial-value representation.

I should emphasise that the semiclassical propagator is the central entity in this thesis. It is what we evaluate in order to obtain results which may be compared with experiment or exact quantum calculations. I conclude with a justification for the precise form of the HK-IVR and a brief description of the computational approach employed here.

2.1 The Importance of the Propagator in Quantum MD

The fundamental question of quantum dynamics is: "how does a state ket change in time?" To address this question, let us define an operator, $\hat{K}(t_2, t_1)$, which will take a ket at time, t_1, and transform it into the corresponding ket some time later, $t_2 > t_1$, as it evolves under the influence of the Hamiltonian, (Equation (1.6)),

$$|\Psi(t_2)\rangle = \hat{K}(t_2, t_1)|\Psi(t_1)\rangle \ . \tag{2.1}$$

We want to ensure that $\hat{K}$ is unitary, since we want it to preserve the norm of our state (*i.e.* preserve probability), and we know that a wavefunction evolves in time according to the TDSE (Equation 1.5). [2]

Before we proceed, let us ask a simpler question: how does a *stationary state* (an eigenstate of the Hamiltonian) evolve in time? This is worked out easily enough:

$$i\hbar\frac{\partial}{\partial t}|n\rangle = \hat{H}|n\rangle = E_n|n\rangle \ .$$

Now we just need to solve a separable ordinary differential equation

$$\begin{aligned}
\frac{\mathrm{d}|n\rangle}{|n\rangle} &= -\frac{iE_n}{\hbar}\mathrm{d}t \\
\ln||n(t)\rangle| &= -\frac{iE_nt}{\hbar} + C \\
|n(t)\rangle &= e^{-iE_nt/\hbar}e^C \\
|n(0)\rangle &= e^C \\
\therefore |n(t)\rangle &= e^{-iE_nt/\hbar}|n(0)\rangle \ . \qquad (2.2)
\end{aligned}$$

This is not surprising. The term, *stationary state* alludes to the fact that there is no time dependence in an arbitrary observable calculated for these states (the phase terms cancel). If we are not in a stationary state, we are left with an operator in an exponent

$$\hat{K}(t,0) = e^{-i\hat{H}t/\hbar} \ . \qquad (2.3)$$

Exponentiating an operator properly is an important problem in quantum dynamics - there is no simple solution which does not involve first solving an eigenvalue problem. The best we can do at this point is decompose our state ket in terms of the stationary states:

$$|\Psi\rangle = \sum_n |n\rangle c_n \ , \qquad (2.4)$$

which leads us to

$$|\Psi(t)\rangle = \sum_n |n\rangle c_n e^{-iE_nt/\hbar} \ . \qquad (2.5)$$

This is not terribly useful, however, since it presupposes that we have already solved the TISE, $\hat{H}|n\rangle = E_n|n\rangle$.

Potential utility aside, Equation (2.3) does provide us with our starting point for further discussion of the propagator. We begin by taking it in the coordinate representation:

$$\begin{aligned}
\Psi_t(\mathbf{x}') &= \langle \mathbf{x}'|\Psi(t)\rangle \\
&= \langle \mathbf{x}'|e^{-i\hat{H}t/\hbar}|\Psi(0)\rangle \\
&= \int \mathrm{d}\mathbf{x}\langle \mathbf{x}'|e^{-i\hat{H}t/\hbar}|\mathbf{x}\rangle\langle \mathbf{x}|\Psi(0)\rangle \\
&= \int \mathrm{d}\mathbf{x}K_t(\mathbf{x}',\mathbf{x})\Psi_0(\mathbf{x}) \ . \qquad (2.6)
\end{aligned}$$

On the second last line, we have inserted a complete set of position states ($\mathbf{1} = \int \mathrm{d}\mathbf{x}|\mathbf{x}\rangle\langle\mathbf{x}|$). This coordinate representation of $\hat{K}$ is usually called the "kernel of the propagator", however in this thesis, to lighten the language we will simply call it *the* propagator,

$$K_t^{QM}(\mathbf{x}',\mathbf{x}) = \langle \mathbf{x}'|e^{-i\hat{H}t/\hbar}|\mathbf{x}\rangle \ . \qquad (2.7)$$

We will use it as the starting point for developing much of the forthcoming theory in the next chapter.

To summarise, Equation (2.7) gives the QM amplitude of a transition from a point $\mathbf{x}$ to $\mathbf{x}'$ in time, t. What makes it so fundamental is that it can be used to transform a wavefunction $|\Psi_0\rangle$ to $|\Psi_t\rangle$. Computing the time-dependence of a wavefunction is equivalent to solving the TDSE, and therefore, once the propagator is known, solving for *any* observable of the system is trivial.

Other uses for the propagator

The imaginary time version of the propagator ($t \to -i\hbar\beta$) is an important quantity in statistical mechanics as it represents the equilibrium density operator. In turn, the trace of this operator yields the central quantity of statistical mechanics, the partition function, which is defined as:

$$Z = \mathrm{Tr}\, \mathrm{e}^{-\beta \hat{\mathrm{H}}} \,, \tag{2.8}$$

where β is related to the temperature as $\beta = \frac{1}{k_B T}$. [28] The density operator is also be used to calculate the ensemble average for a given observable, represented by the operator, $\hat{O}$:

$$\langle \hat{O} \rangle = \frac{1}{Z}\, \mathrm{Tr}\, \mathrm{e}^{-\beta \hat{\mathrm{H}}}\, \hat{O} \,. \tag{2.9}$$

This expression can be extended to the treatment of dynamical quantities through the use of time correlation functions:

$$\langle \hat{O}\hat{O}(t) \rangle = \frac{1}{Z}\, \mathrm{Tr}\, \mathrm{e}^{-\beta \hat{\mathrm{H}}}\, \hat{O}\, \hat{O}(\mathrm{t}) \,, \tag{2.10}$$

where $\hat{O}(t)$ is the Heisenberg representation of $\hat{O}$, and is given by:

$$\hat{O}(t) = e^{+i\hat{H}t/\hbar}\, \hat{O}\, e^{-i\hat{H}t/\hbar} \,. \tag{2.11}$$

Here, we have made use of the *real time* version of the propagator. By invoking the ***fluctuation-dissipation theorem***, which connects the spontaneous fluctuations of a system to its relaxation following a perturbation, one can use time correlation functions to study the various transport and spectral properties. For instance, the velocity-velocity correlation function can be connected to the diffusion coefficient (D) of a particular particle in a gas or a liquid:

$$D \propto \int_0^t \mathrm{d}t' \langle \hat{v}\, \hat{v}(t') \rangle \,, \tag{2.12}$$

and similarly, the dipole-dipole correlation can be connected to the infra-red absorption spectrum.[5]

2.2 The Classical Limit of Quantum Mechanics

A fundamental question of quantum mechanics is: "which conditions must be met so that classical concepts may be assumed to apply?" The set of these conditions is referred to as the *classical*

limit of quantum mechanics. We should clarify an issue here: quantum mechanics assumes that classical mechanics is correct. That is, quantum mechanics proceeds by constructing the Hamiltonian operator from classical energy considerations and then replacing Poisson brackets with commutators, etc. Even the path integral approach assumes that the classical expression for the action is correct. In this sense, we do not hope to *derive* the classical laws of motion as a limiting case of quantum mechanics, even though quantum mechanics *is* more fundamental.

Three limits are commonly considered: (1) vanishing Planck's constant ($\hbar \to 0$), (2) high energy / quantum number ($n \to \infty$), and (3) short de Broglie wavelength / large mass ($m \to \infty$). In this thesis, we focus our attention on the first limit. A comment: $\hbar$ is not necessarily small; its value depends on the system of units being used. Instead it is important only that it be negligibly small when compared to other quantities of the same dimension (*e.g.* action). In the following sections, we will present some of the most fundamental and important of these semiclassical schemes.

2.3 Dirac's "Crude" Semiclassical Approximation

I present Dirac's semiclassical approximation (as it appears in his famous book, [10]) not only because it was one of the first to appear, but also because it offers qualitative physical arguments.

By casting the wavefunction in polar form, Dirac examined how this so-called *wavepacket* varied in time, according to the TDSE. *For any dynamical system with a classical analogue, a state for which the classical description is valid as an approximation is represented in quantum mechanics by a wave packet.*[10] The hope is to find some classical-like equations of motion corresponding to the centre of the wavepacket. Of course, the accuracy in our knowledge of the coordinates and momenta of this point are limited by Heisenberg's Uncertainty Principle.

For simplicity, we consider the one-dimensional case, taking the (time-dependent) wavefunction as

$$\psi(x,t) = A(x,t)e^{iS(x,t)/\hbar} \,, \tag{2.13}$$

where $A(x,t)$ and $S(x,t)$ are real functions of position and time. Inserting into the TDSE with the Hamiltonian,

$$\hat{H} = -\frac{\hbar^2}{2m}\frac{\partial^2}{\partial x^2} + V(x) \,, \tag{2.14}$$

we obtain

$$i\hbar\frac{\partial A}{\partial t} - A\frac{\partial S}{\partial t} = e^{-iS/\hbar}\hat{H}e^{iS/\hbar}A \,. \tag{2.15}$$

Dirac notices that $e^{-iS/\hbar}\hat{H}e^{iS/\hbar}$ is a unitary transformation with

$$e^{-iS/\hbar}\hat{x}e^{iS/\hbar} = x \tag{2.16}$$

$$e^{-iS/\hbar}\hat{p}e^{iS/\hbar} = \hat{p} + \frac{\partial S}{\partial x} \,. \tag{2.17}$$

The first expression holds since $\hat{x}$ and $e^{-iS/\hbar}$ commute in the coordinate representation. The second follows from

$$\begin{aligned} e^{-iS/\hbar}\hat{p}e^{iS/\hbar}|f\rangle &= e^{-iS/\hbar}\left(-i\hbar\frac{\partial}{\partial x}\right)e^{iS/\hbar}|f\rangle \\ &= -i\hbar\left(\frac{i}{\hbar}\frac{\partial S}{\partial x}+\frac{\partial}{\partial x}\right)|f\rangle \\ &= \left(\frac{\partial S}{\partial x}+\hat{p}\right)|f\rangle\ . \end{aligned} \tag{2.18}$$

Therefore,

$$e^{-iS/\hbar}\hat{H}(\hat{p},\hat{x})e^{iS/\hbar} = \hat{H}(\frac{\partial S}{\partial x}+\hat{p},x). \tag{2.19}$$

With this, (2.15) becomes

$$i\hbar\frac{\partial A}{\partial t} - A\frac{\partial S}{\partial t} = \hat{H}(\frac{\partial S}{\partial x}+\hat{p},x)A\ . \tag{2.20}$$

We now take the classical limit $\hbar \to 0$. The vanishing terms of Equation (2.20) are $i\hbar\partial A/\partial t$ and $\hat{p} = -i\hbar\partial/\partial x$, leaving us with a partial differential equation for the phase of the wavepacket (we have divided $A(x,t)$ out):

$$\begin{aligned} 0 &= \hat{H}(\frac{\partial S}{\partial x},x)+\frac{\partial S}{\partial t} \\ &= \frac{1}{2m}\left(\frac{\partial S}{\partial x}\right)^2+V(x)+\frac{\partial S}{\partial t}\ . \end{aligned} \tag{2.21}$$

Equation (2.21) exactly resembles the Hamilton-Jacobi equation in classical mechanics [29] where $S(x,t)$ is the classical action:[1]

$$S(x,t) = \int_0^t \mathrm{d}t'\left\{p_{t'}\dot{x}_{t'} - H(p_{t'},x_{t'})\right\}\ . \tag{2.22}$$

What remains now is to find an equation for the amplitude of our wavepacket, $A(x,t)$. To do this, we consider a generic Hermitian operator, $\hat{f}(x)$. We go to Dirac's notation and multiply Equation (2.20) by $\langle A|\hat{f}|$:

$$\langle A|\hat{f}|i\hbar\frac{\partial A}{\partial t} - A\frac{\partial S}{\partial t}\rangle = \langle A|\hat{f}\hat{H}(\frac{\partial S}{\partial x}+p,x)|A\rangle\ . \tag{2.23}$$

Taking the transpose of each side, we obtain

$$\langle -i\hbar\frac{\partial A}{\partial t} - A\frac{\partial S}{\partial t}|\hat{f}|A\rangle = \langle A|\hat{H}(\frac{\partial S}{\partial x}+p,x)\hat{f}|A\rangle\ . \tag{2.24}$$

Subtracting (2.24) from (2.23) gives

$$\begin{aligned} \langle A|\hat{f}|2i\hbar\frac{\partial A}{\partial t}\rangle &= \langle A|\hat{f}\hat{H}-\hat{H}\hat{f}|A\rangle \\ 2\langle A|\hat{f}|\frac{\partial A}{\partial t}\rangle &= \langle A|\frac{1}{i\hbar}\left(\hat{f}\hat{H}-\hat{H}\hat{f}\right)|A\rangle \\ \langle f\frac{\partial}{\partial t}(A^2)\rangle &= \langle A|\left\{\hat{f},\hat{H}\right\}|A\rangle\ , \end{aligned} \tag{2.25}$$

[1]The notation used here may be ambiguous. It should clarify things to indicate that S is a ***functional*** of the time-dependent variables, p_t and x_t, which depend explicitly on time and parametrically on the boundary conditions, x_0 and x (final position, as it appears on the left-hand-side of the equation).

where $\left\{\hat{f},\hat{H}\right\}$ denotes a Poisson Bracket (PB). [29] To evaluate this PB, we take advantage of the fact that $\hbar$ will be considered small, so that we may expand $\hat{H}$ about $\hat{p}=\frac{\partial S}{\partial x}$ for small $\delta\hat{p}$

$$\begin{aligned}\hat{H}(\hat{p},x)\Big|_{\hat{p}=\frac{\partial S}{\partial x}} &= \sum_{k=0}^{\infty}\frac{1}{k!}\hat{H}^{(k)}(\frac{\partial S}{\partial x},x)\left(\hat{p}-\frac{\partial S}{\partial x}\right)^{k}\\ &\approx \hat{H}(\frac{\partial S}{\partial x},x)+\frac{\partial}{\partial p}\left[\hat{H}(\hat{p},x)\right]_{\hat{p}=\frac{\partial S}{\partial x}}\left(\hat{p}-\frac{\partial S}{\partial x}\right)\\ &= \hat{H}(\frac{\partial S}{\partial x},x)+\frac{1}{m}\frac{\partial S}{\partial x}\left(\hat{p}-\frac{\partial S}{\partial x}\right)\ . \end{aligned} \tag{2.26}$$

Therefore

$$\begin{aligned}\left\{\hat{f},\hat{H}(\hat{p}+\frac{\partial S}{\partial x},x)\right\} &\approx \left\{\hat{f},\hat{H}(\frac{\partial S}{\partial x},x)\right\}+\frac{1}{m}\frac{\partial S}{\partial x}\left\{\hat{f},\hat{p}\right\}-\frac{1}{m}\frac{\partial S}{\partial x}\left\{\hat{f},\frac{\partial S}{\partial x}\right\}\\ &= \frac{1}{m}\frac{\partial S}{\partial x}\left\{\hat{f},\hat{p}\right\}\ , \end{aligned} \tag{2.27}$$

since functions of x commute with $\hat{f}$. We now use the definition of a PB in 1D [10] to evaluate the final PB:

$$\left\{\hat{f},\hat{p}\right\}=\frac{\partial\hat{f}}{\partial x}\frac{\partial\hat{p}}{\partial p}-\frac{\partial\hat{f}}{\partial p}\frac{\partial\hat{p}}{\partial x}=\frac{\partial\hat{f}}{\partial x}\ . \tag{2.28}$$

So we have

$$\begin{aligned}\langle f\frac{\partial}{\partial t}\left(A^{2}\right)\rangle &= \langle A|\frac{1}{m}\frac{\partial S}{\partial x}\frac{\partial f}{\partial x}|A\rangle\\ &= \langle A^{2}\frac{\partial f}{\partial x}\frac{\partial}{\partial p}\hat{H}(p,x)\Big|_{\hat{p}=\frac{\partial S}{\partial x}}\rangle\ . \end{aligned} \tag{2.29}$$

Next, we exploit a property of the derivatives of brackets,

$$\begin{aligned}\frac{\mathrm{d}}{\mathrm{d}x}\langle a(x)b(x)\rangle &= \langle a'(x)b(x)\rangle+\langle a(x)b'(x)\rangle\ =\ 0\\ \therefore\langle a(x)b'(x)\rangle &= -\langle a'(x)b(x)\rangle\ , \end{aligned} \tag{2.30}$$

to finally arrive at

$$\begin{aligned}\langle\hat{f}\frac{\partial}{\partial t}\left(A^{2}\right)\rangle &= \langle A^{2}\frac{\partial\hat{f}}{\partial x}\frac{\partial}{\partial p}\hat{H}(\hat{p},x)\Big|_{\hat{p}=\frac{\partial S}{\partial x}}\rangle\\ &= -\langle\hat{f}\frac{\partial}{\partial x}\left(A^{2}\right)\frac{\partial}{\partial p}\hat{H}(\hat{p},x)\Big|_{\hat{p}=\frac{\partial S}{\partial x}}\rangle\\ &= -\langle\hat{f}\frac{\partial}{\partial x}\left(A^{2}\frac{\partial}{\partial p}\hat{H}(\hat{p},x)\Big|_{\hat{p}=\frac{\partial S}{\partial x}}\right)\rangle\\ \frac{\partial}{\partial t}\left(A^{2}\right) &= -\frac{\partial}{\partial x}\left(A^{2}\frac{\partial}{\partial p}\hat{H}(\hat{p},x)\Big|_{\hat{p}=\frac{\partial S}{\partial x}}\right)\ . \end{aligned} \tag{2.31}$$

The second last step is made by observing that

$$\frac{\partial}{\partial x}\left(\frac{\partial}{\partial p}\hat{H}(\hat{p},x)\Big|_{\hat{p}=\frac{\partial S}{\partial x}}\right)=0\ ,$$

and the last step holds since $\hat{f}(x)$ is an arbitrary (and Hermitian) function of x. Equation (2.31) also resembles a classical equation: it is just the equation of conservation for a fluid with density, A^2, at position, x, and time, t. Taking the velocity of the fluid to be

$$\frac{\partial x}{\partial t} = \frac{\partial}{\partial p}\hat{H}(\hat{p}, x)\Big|_{\hat{p}=\frac{\partial S}{\partial x}} , \tag{2.32}$$

the dynamics of the fluid can be found by solving

$$H\left(\frac{\partial S}{\partial x}, x\right) + \frac{\partial S}{\partial t} = 0 ,$$

where H is the classical Hamiltonian. Next, we turn our attention to the validity of this semiclassical limit. We would like to localise our 'fluid' so that the density (A^2) vanishes outside some small region; the size of this region being restricted by the Uncertainty Principle. Dropping the terms with $\hbar$ of orders of 2 or greater is justified if [10]

$$\frac{1}{A(x,t)}\frac{\partial}{\partial x}A(x,t) \ll \frac{1}{\hbar}\frac{\partial}{\partial x}S(x,t) . \tag{2.33}$$

That is, the localised region must contain a large number of wavelengths of $\psi(x,t)$ in order for the approximation to be valid.

Finally, if we take $S(x,t)$ to be the action evaluated along some classical trajectory, *i.e.* so that

$$p = \frac{\partial S}{\partial x} , \tag{2.34}$$

then

$$\begin{aligned} \frac{\partial p}{\partial t} &= \frac{\partial}{\partial t}\frac{\partial S}{\partial x} \\ &= \frac{\partial}{\partial x}\frac{\partial S}{\partial t} \\ &= -\frac{\partial}{\partial x}\left(H(p,x)\right) . \end{aligned} \tag{2.35}$$

This result, taken with (2.32) are just Hamilton's classical equations of motion. Therefore, so long as (2.33) holds, we observe classical mechanics as a limiting case of quantum mechanics.

2.4 The WKB Semiclassical Approximation

As seen in Section 2.3, wave mechanics and the Hamilton-Jacobi (HJ) formalism of classical mechanics seem to be intimately related. This is no surprise: Schrödinger was guided by the HJ equation when he formulated his wave equation. Here, a semiclassical approximation is shown, due to Wigner, Kramers, and Brillouin (WKB) [30], which follows naturally from HJ theory. The WKB approximation is also one of the earliest[2] and most fundamental of the semiclassical approximations, and is very successful in integrable problems with a separable Hamiltonian. [31]

[2] *c.a.* 1926.

The basic idea is that reflection, or scattering, of a particle occurs in regions where the potential varies sharply. Because reflection leads to quantum interference, a semiclassical regime can be proposed for systems in which the potential is comparatively smooth.

Again, the 1D case is considered for simplicity, and we restrict ourselves to stationary states with positive kinetic energy (*i.e.* $E \geq V$). We take the (time-independent) wavefunction to be of the form[3]

$$\psi(x) = e^{i\phi(x)/\hbar} , \tag{2.36}$$

and we assume that the phase term, $\phi(x)$, can be expanded in powers of $\hbar$ (hoping, of course, that this series will converge):

$$\phi(x) = \phi_0(x) + \hbar\phi_1(x) + \hbar^2\phi_2(x) + \cdots . \tag{2.37}$$

As in Section 2.3, we consider only up to single powers of $\hbar$, and insert the resulting wavefunction into the TISE. Collecting like powers of $\hbar$, we obtain

$$\begin{aligned} 0 &= \hbar^2\Big(\phi_1'(x)^2 - i\phi_1''(x)\Big) \\ &+ \hbar\Big(2\phi_0'(x)\phi_1'(x) - i\phi_0''(x)\Big) \\ &+ \Big(\phi_0'(x)^2 + 2m(V(x) - E)\Big) . \end{aligned} \tag{2.38}$$

Assuming that all dependence on $\hbar$ is explicit, each of these terms will be 0. Starting with the $\hbar^0$ term, we arrive at an expression for $\phi_0(x)$:

$$\begin{aligned} \phi_0'(x)^2 &= 2m(E - V(x)) \\ \therefore\ \phi_0(x) &= \pm\int_{x_0}^{x} \mathrm{d}x' \sqrt{2m(E - V(x'))} . \end{aligned} \tag{2.39}$$

Using this result, we proceed to solve the $\hbar^1$ term for $\phi_1(x)$:

$$\begin{aligned} \phi_1'(x) &= \frac{i}{2}\left(\frac{\phi_0''(x)}{\phi_0'(x)}\right) \\ &= \frac{i}{2}\left(-\frac{mV'(x)}{\sqrt{2m(E - V(x))}}\right)\left(\frac{1}{\sqrt{2m(E - V(x))}}\right) \\ &= -\frac{imV'(x)}{2}\left(\frac{1}{2m(E - V(x))}\right) \\ \therefore\ \phi_1(x) &= \frac{i}{4}\ln\big[2m(E - V(x))\big] . \end{aligned} \tag{2.40}$$

Before combining Equations (2.39) and (2.40) to form the WKB wavefunction, we look at the condition to ignore the $\hbar^2$ term in our expansion: [30]

$$\frac{m\hbar|V'(x)|}{[2m(E - V(x))]^{3/2}} \ll 1 . \tag{2.41}$$

[3] We may leave out the amplitude term, since we are not requiring that our phase be real, anymore.

Here, we are comparing the de Broglie wavelength,

$$\lambda = \frac{h}{\sqrt{2m(E - V(x))}} , \tag{2.42}$$

to the "smoothness" of the potential

$$\lambda^3 \ll \frac{2\pi h^2}{m|V'(x)|} . \tag{2.43}$$

Or, to express this limit in a different way, we notice that

$$\frac{\mathrm{d}\lambda}{\mathrm{d}x} = \frac{mhV'(x)}{[2m(E - V(x))]^{3/2}} . \tag{2.44}$$

Comparing this with (2.41), we alternatively say that the WKB approximation is valid when

$$\left|\frac{\mathrm{d}\lambda}{\mathrm{d}x}\right| \ll 2\pi . \tag{2.45}$$

This condition is met provided that $V(x)$ varies slowly with respect to x, or if $|E - V(x)|$ is not too small.

We now construct our WKB wavefunction, using our approximation for $\phi(x)$:

$$\begin{aligned}
\psi_{\pm}^{WKB}(x) &= \exp\left\{\frac{i}{\hbar}\Big[\phi_0(x) + \hbar\phi_1(x)\Big]\right\} \\
&= \exp\left\{\pm\frac{i}{\hbar}\int_{x_0}^{x} \mathrm{d}x' \sqrt{2m(E - V(x'))}\right\} \\
&\quad \times \exp\left\{\ln\Big|2m(E - V(x))\Big|^{\frac{1}{4}}\right\} \\
&= \Big|2m(E - V(x))\Big|^{-\frac{1}{4}} \exp\left\{\pm\frac{i}{\hbar}\int_{x_0}^{x} \mathrm{d}x' \sqrt{2m(E - V(x'))}\right\} .
\end{aligned} \tag{2.46}$$

Because we obtained (2.46) from the TISE, it is an approximation to a stationary state. Therefore, including time dependence involves only including the (trivial) phase factor, $\exp(-iEt/\hbar)$, where E is the (conserved) energy of the trajectory. So, our final expression for the time-dependent WKB wavefunction is:

$$\psi_{\pm}^{WKB}(x,t) = \Big|2m(E - V(x))\Big|^{-\frac{1}{4}} \exp\left\{\pm\frac{i}{\hbar}\int_{x_0}^{x} \mathrm{d}x' \sqrt{2m(E - V(x'))} - \frac{i}{\hbar}Et\right\} . \tag{2.47}$$

Now, comparing this to Dirac's result (which uses the same level of approximation), we propose that the phase is calculated as the action, $S(x,t)$, along the classical trajectory, where

$$\begin{aligned}
S(x,t) &= \int_0^t \mathrm{d}t' \Big\{p_{t'}\dot{x}_{t'} - E\Big\} \\
&= \int_{x_0}^{x} \mathrm{d}x' p(x') - \int_0^t \mathrm{d}t' E .
\end{aligned} \tag{2.48}$$

Noticing that the classical expression for momentum is

$$p(x) = \sqrt{2m(E - V(x))} ,$$

we observe that

$$\psi_{\pm}^{WKB}(x,t) = \left|2m(E-V(x))\right|^{-\frac{1}{4}} e^{\pm iS(x,t)/\hbar} , \tag{2.49}$$

where $\psi_{+}^{WKB}(x,t)$ is called the "classical wavefunction". It satisfies the classical equations of motion exactly, and the quantum equations of motion approximately. Again, the approximation holds so long as the potential varies smoothly with x. This is not a universal criterion for obtaining the semiclassical limit: the WKB conditions are not always sufficient, nor are they exclusive. For example, scattering problems involving sharp potentials will never satisfy the WKB conditions for approximation. Therefore, other schemes are necessary for certain scenarios.

2.5 The Van Vleck Propagator

Here, I will present the first semiclassical expression for the propagator, (2.7); an expression which Van Vleck provided as early as 1928. [12] It is widely considered to be the most fundamental semiclassical propagator, and is generally used as a starting point when more advanced forms are proposed (as is the case for the HK-IVR).

Van Vleck arrived at this propagator after considering a classical form which satisfied the TDSE in the limit $\hbar \to 0$. More recent and more rigorous derivations are available [32], but are beyond the scope of this thesis. (Certainly, Van Vleck's original paper is far too arcane for me to decipher - so the "quasi-derivation" that follows was taken from [31]).

2.5.1 Quasi-derivation of the Van Vleck propagator

Here, I present a justification for the form of the Van Vleck propagator, taking the N-dimensional free particle as an instructive example. We begin with the exact propagator for this model system:

$$K_t^{FP}(\mathbf{x}',\mathbf{x}) = \langle \mathbf{x}'| \exp\left(-\frac{it}{2\hbar m}\hat{\mathbf{p}}^2\right)|\mathbf{x}\rangle . \tag{2.50}$$

Inserting a complete set of (N-dimensional) momentum states allows us to evaluate the operator by $\hat{\mathbf{p}}|\mathbf{p}\rangle = \mathbf{p}|\mathbf{p}\rangle$:

$$\begin{aligned} K_t^{FP}(\mathbf{x}',\mathbf{x}) &= \int d\mathbf{p} \langle \mathbf{x}'| \exp\left(-\frac{it}{2\hbar m}\hat{\mathbf{p}}^2\right)|\mathbf{p}\rangle\langle\mathbf{p}|\mathbf{x}\rangle \\ &= \int d\mathbf{p} \exp\left(-\frac{it}{2\hbar m}\mathbf{p}^2\right)\langle \mathbf{x}'|\mathbf{p}\rangle\langle\mathbf{p}|\mathbf{x}\rangle . \end{aligned} \tag{2.51}$$

Using the definition of the overlaps above:

$$\langle \mathbf{x}|\mathbf{p}\rangle = \left(\frac{1}{2\pi\hbar}\right)^{N/2} \exp\left(\frac{i}{\hbar}\mathbf{p}\cdot\mathbf{x}\right) , \tag{2.52}$$

leads us to a multidimensional Gaussian integral which we evaluate analytically (see Appendix A)

$$\begin{aligned} K_t^{FP}(\mathbf{x}',\mathbf{x}) &= \left(\frac{1}{2\pi\hbar}\right)^N \int d\mathbf{p} \exp\left[-\left(\frac{it}{2\hbar m}\right)\mathbf{p}^2\right] \exp\left[\frac{i}{\hbar}\left(\mathbf{p}\cdot\mathbf{x}' - \mathbf{p}\cdot\mathbf{x}\right)\right] \\ &= \left(\frac{1}{2\pi\hbar}\right)^N \int d\mathbf{p} \exp\left[-\left(\frac{it}{2\hbar m}\right)\mathbf{p}^2 + \frac{i}{\hbar}\mathbf{p}\cdot(\mathbf{x}'-\mathbf{x})\right] \\ &= \left(\frac{1}{2\pi\hbar}\right)^N \left(\frac{2\pi\hbar m}{it}\right)^{N/2} \exp\left[\left(\frac{i}{\hbar}\right)^2 \frac{(\mathbf{x}'-\mathbf{x})^2}{4}\left(\frac{2\hbar m}{it}\right)\right] \\ &= \left(\frac{m}{2\pi i\hbar t}\right)^{N/2} \exp\left\{\frac{i}{\hbar}\left[\frac{m}{2t}(\mathbf{x}'-\mathbf{x})^2\right]\right\} . \end{aligned} \tag{2.53}$$

Since we might expect an action term to appear somewhere in the propagator, we shall work out an expression for the action of a free particle. Noticing that a free particle's momentum is constant and that potential energy is zero,

$$\begin{aligned} S_t(\mathbf{x}) &= \int_{\mathbf{x}_0}^{\mathbf{x}} d\mathbf{x}'\mathbf{p} - \int_0^t dt' E \\ &= \mathbf{p}\cdot(\mathbf{x}-\mathbf{x}_0) - \left(\frac{t}{2m}\right)\mathbf{p}\cdot\mathbf{p} . \end{aligned} \tag{2.54}$$

Because momentum is constant, we may replace it with

$$\mathbf{p} = m\frac{\Delta\mathbf{x}}{\Delta t} ,$$

to arrive at

$$\begin{aligned} S_{\Delta t}(\Delta\mathbf{x}) &= \left(m\frac{\Delta\mathbf{x}}{\Delta t}\right)\Delta\mathbf{x} - \frac{1}{2m}\left(m\frac{\Delta\mathbf{x}}{\Delta t}\right)^2 \Delta t \\ &= \frac{m}{2\Delta t}\Delta\mathbf{x}^2 . \end{aligned}$$

Therefore,

$$S_t(\mathbf{x}',\mathbf{x}) = \frac{m}{2t}(\mathbf{x}'-\mathbf{x})^2 \tag{2.55}$$

is the classical action calculated along a trajectory which connects points $\mathbf{x}$ and $\mathbf{x}'$ in time, t. This is precisely what appears in (2.53), the way we have suggestively written it. Now, we turn our attention to second derivatives of this action term,

$$\begin{aligned} \left(\frac{\partial^2 S_t(\mathbf{x}',\mathbf{x})}{\partial\mathbf{x}'\partial\mathbf{x}}\right)_{ij} &= \frac{\partial}{\partial x_i'}\left[\frac{m}{2t}\frac{\partial}{\partial x_j}(\mathbf{x}'-\mathbf{x})^2\right] \\ &= \frac{m}{2t}\frac{\partial}{\partial x_i'}\left[2(x_j'-x_j)(-1)\right] \\ &= \left(-\frac{m}{t}\right)\frac{\partial x_j'}{\partial x_i'} \\ &= \left(-\frac{m}{t}\right)\delta_{ij} . \end{aligned} \tag{2.56}$$

In a leap of faith, we propose that the determinant of this matrix will enter into our expression for the propagator. It is evaluated easily enough as the product of diagonal elements (our matrix is diagonal due to the δ_{ij} term)

$$\det\left(-\frac{\partial^2 S_t(\mathbf{x}',\mathbf{x})}{\partial \mathbf{x}'\partial \mathbf{x}}\right) = \left(\frac{m}{t}\right)^N . \tag{2.57}$$

Now, by inspection of Equations (2.53),(2.55) and (2.57), we propose the following general form for the propagator:

$$K_t(\mathbf{x}',\mathbf{x}) = \left(\frac{1}{2\pi i\hbar}\right)^{N/2}\left[\det\left(-\frac{\partial^2 S_t}{\partial \mathbf{x}'\partial \mathbf{x}}\right)\right]^{1/2}\exp\left[\frac{i}{\hbar}S_t(\mathbf{x}',\mathbf{x})\right] . \tag{2.58}$$

Van Vleck obtained (2.58) using rigorous and outmoded methods in asymptotic analysis, in an effort to connect classical mechanics to the early transformation theory of Dirac [33] and Jordan [34] in the limit $\hbar \to 0$. As mentioned earlier, Gutzwiller re-derived this result using Feynman path integrals and the *stationary-phase approximation*. This approximation is presented in Appendix B since it is used later to arrive at the HK-IVR. The underlying principle is simple enough, though. The phase term, $\exp(iS/\hbar)$, causes the integrand to be highly oscillatory (when $S >> \hbar$). Therefore, integration should mostly cancel (positive areas match with a corresponding negative area). The main contribution to the overall integral will occur in places where the phase is *stationary*, *i.e.* where $\delta S = 0$. By Hamilton's variational principal, this region of stationary phase corresponds to the classical trajectory. So, we just need to evaluate the integral along a classical path and we may use steepest descent [35] for the region in the immediate vicinity of this path. This prescription leads to "Fresnel integrals", which have discrete phase changes which occur at the *conjugate points*: points where the determinant goes to infinity or through zero. This phase change was determined to be $(-\pi v/2)$, where the so-called Maslov index, v, keeps track of the number of conjugate points encountered along a trajectory. So we would like to define a subtlety in our notation[4],

$$\left[\det\left(-\frac{\partial^2 S_t}{\partial \mathbf{x}'\partial \mathbf{x}}\right)\right]^{1/2} = \sqrt{\det\left(-\frac{\partial^2 S_t}{\partial \mathbf{x}'\partial \mathbf{x}}\right)}e^{-iv\pi/2} , \tag{2.59}$$

and propose

$$K_t(\mathbf{x}',\mathbf{x}) = \left(\frac{1}{2\pi i\hbar}\right)^{N/2}\sqrt{\det\left(-\frac{\partial^2 S_t}{\partial \mathbf{x}'\partial \mathbf{x}}\right)}\exp\left[\frac{i}{\hbar}S_t(\mathbf{x}',\mathbf{x}) - \frac{iv\pi}{2}\right] . \tag{2.60}$$

Since there is not necessarily a unique solution to the equations of motion when solved as a boundary-value problem, we must sum over all possible trajectories.

$$K_t^{VV}(\mathbf{x}',\mathbf{x}) = \left(\frac{1}{2\pi i\hbar}\right)^{N/2}\sum_{traj.}\sqrt{\det\left(-\frac{\partial^2 S_t}{\partial \mathbf{x}'\partial \mathbf{x}}\right)}\exp\left[\frac{i}{\hbar}S_t(\mathbf{x}',\mathbf{x}) - \frac{iv\pi}{2}\right] . \tag{2.61}$$

[4]On the right-hand side, we take the positive root always; the correct branch is determined by the phase term ($e^{-iv\pi/2} = \pm 1$).

This is our final result; the nature of the determinant here will be discussed in more detail in Section 2.7.

Save for a few exceptions, (2.61) is not normally used directly. Two main factors are usually identified as the prime culprits for prohibiting direct evaluation. First is the root search problem. Since the roots of the classical equations of motion (when phrased as a boundary-value problem) are multiple, in general, we must conduct a search for all such roots where $\psi_t(\mathbf{x}')$ is significant. Especially at long times, the number of these roots can become quite large.

The second drawback is that (2.61) is not valid at the conjugate points (also called *caustics*). At these points, the propagator becomes undefined. Therefore, motivation exists for alternate schemes which are capable of bypassing these problems. Such schemes are found with the initial-value methods.

2.6 Heller's Gaussian Wavepackets

Here, we present the development of certain semiclassical methods based on Gaussian wavepackets (GWP). All of the GWP's encountered in this thesis are commonly called *coherent states* in the literature. This term originally arose with reference to optical coherence (in lasers, for example), but now is used to describe any state which minimises the uncertainty relation for the harmonic oscillator. It turns out that such states are also eigenfunctions of the *annihilation operator*, $\hat{a}$ [2], and this is often used as an alternative definition.

Between the appearance of Dirac's mysterious remark concerning wavepackets as a classical analogue (see Section 2.3) and the early 1970's, a large literature on semiclassical dynamics accumulated employing the principal of expansion in $\hbar$. In 1975, a paper by Heller [7] appeared, in which he set out to *examine an alternative avenue of approach to the semiclassical limit of quantum mechanics. The approximations involved in the theory presented below differ significantly from those of the semiclassical techniques mentioned above. It is hoped that the present theory will provide an alternative framework which may be valid in certain regimes which are complementary to existing techniques.* This "avenue", discussed in Section 2.6.1, led, in 1981, to his *frozen Gaussian approximation*[5] (FGA). [21] In Section 2.6.2, we introduce the FGA and use it to arrive at our first initial value representation for the propagator. Again, the most appealing feature of the initial value methods is the evasion of the root-search problem and difficulties at caustics encountered with the Van Vleck propagator. It is also interesting that the appearance of these papers was accompanied by a dramatic revival of interest in the semiclassical methods.

[5] By "frozen", we mean that the width of the wavepacket is prevented from changing. In this context, GWP's used prior to the FGA are commonly called *thawed Gaussians*.

2.6.1 Dynamics with "thawed" Gaussians

Heller [7] begins with Dirac's derivation for the semiclassical amplitude and phase of the wavefunction and points out that for a harmonic oscillator, these equations are valid regardless of how big or small $\hbar$ is. It is here that he breaks with the usual line of reasoning in order to investigate the dynamics of Gaussian wavefunctions in harmonic potentials.

Gaussian wavepackets evolving in a harmonic potential stay Gaussian, and undergo periodic motion with $\langle p \rangle$ and $\langle x \rangle$ following a classical trajectory and its width "refocusing" to the same value once per period. The motion of the centre of the wavepacket follows from Ehrenfest's Theorem which states that

$$\frac{\mathrm{d}\langle p \rangle}{\mathrm{d}t} = -\frac{\partial H(\langle p \rangle, \langle x \rangle)}{\partial \langle x \rangle} + C \ , \tag{2.62}$$

where C is an error term

$$C \sim d^2 \left[\frac{\partial^3 V}{\partial x^3} \left(\frac{\partial V}{\partial x} \right)^{-1} \right]_{x=\langle x \rangle} , \tag{2.63}$$

and d is the diameter of the wavepacket. Notice that the error is zero when there is no anharmonicity in the potential. The idea for his semiclassical approximation is this: as long as a GWP is sufficiently localised so that it can be considered to "feel" only up to quadratic terms of the potential, then it will stay Gaussian. Therefore we can hope to find analytic expressions for the time-evolution of the various parameters which define the GWP.

So, Heller's reasoning begins with the selection of a convenient form (*ansatz*) for the GWP in one dimension,

$$\psi(x,t) = \exp\left\{ \frac{i}{\hbar} \left[\alpha_t (x - x_t)^2 + p_t (x - x_t) + \gamma_t \right] \right\} \ , \tag{2.64}$$

where x_t and p_t are the position and momentum associated with the centre of the GWP, and α_t and γ_t are the time-dependent width and phase parameters, respectively. This form is "convenient" since it can be verified that

$$\begin{aligned} \langle p \rangle_\psi &= p_t \\ \langle x \rangle_\psi &= x_t \ . \end{aligned} \tag{2.65}$$

Now, the principal approximation involved in this method is to replace the potential in the Hamiltonian with an approximate potential which is harmonic everywhere:

$$\begin{aligned} \hat{H} &= -\frac{\hbar^2}{2m}\frac{\partial^2}{\partial x^2} + V(x) \\ &\approx -\frac{\hbar^2}{2m}\frac{\partial^2}{\partial x^2} + V(x_t) + V'(x_t)(x - x_t) + \frac{1}{2}V''(x_t)(x - x_t)^2 \ . \end{aligned} \tag{2.66}$$

Inserting (2.64) and (2.66) into the TDSE (Equation (1.5)), we obtain

$$\left\{ \begin{array}{l} [-\dot{\alpha}_t](x - x_t)^2 \\ +[2\alpha_t \dot{x}_t - \dot{p}_t](x - x_t) \\ +[p_t \dot{x}_t - \dot{\gamma}_t] \end{array} \right\} \psi(x,t) = \left\{ \begin{array}{l} [\frac{2}{m}\alpha_t^2 + \frac{1}{2}V''(x_t)](x - x_t)^2 \\ +[\frac{2}{m}\alpha_t p_t + V'(x_t)](x - x_t) \\ +[V(x_t) - \frac{i\hbar}{m}\alpha_t + \frac{1}{2m}p_t^2] \end{array} \right\} \psi(x,t) \ . \tag{2.67}$$

Comparing like powers of $(x - x_t)$ leads to three equations:

$$\dot{\alpha}_t = -\frac{2}{m}\alpha_t^2 - \frac{1}{2}V''(x_t) \tag{2.68}$$

$$2\alpha_t \dot{x}_t - \dot{p}_t = \frac{2}{m}\alpha_t p_t + V'(x_t) \tag{2.69}$$

$$p_t \dot{x}_t - \dot{\gamma}_t = V(x_t) - \frac{i\hbar}{m}\alpha_t + \frac{1}{2m}p_t^2 \ . \tag{2.70}$$

Equation (2.69) suggests that we should define

$$\dot{x}_t = \left.\frac{\partial H}{\partial p}\right|_{p=p_t} = \frac{1}{m}p_t \tag{2.71}$$

$$\dot{p}_t = -\left.\frac{\partial H}{\partial x}\right|_{x=x_t} = -V'(x_t) \ . \tag{2.72}$$

Noticing (in Equation (2.70)) that $H(p_t, x_t) = p_t^2/2m + V(x_t) = E$ is a conserved quantity, we arrive at differential equations specifying the time-dependence of the other two quantities parameterising our wavepacket:

$$\dot{\alpha}_t = -\frac{2}{m}\alpha_t^2 - \frac{1}{2}V''(x_t) \tag{2.73}$$

$$\dot{\gamma}_t = p_t \dot{x}_t + \frac{i\hbar}{m}\alpha_t - E \ . \tag{2.74}$$

In principle, we are done. All we need to do for arbitrary potentials in one dimension is integrate Equations (2.73) and (2.74) as our wavepacket executes its classical motion. Given the simplicity of this method, it works surprisingly well. Although Heller provides an analogous recipe for two-dimensional wavepackets, it is not easy to generalise to problems of increased dimensionality. Still it is perhaps the most intuitive of the semiclassical approaches outlined so far.

2.6.2 The frozen Gaussian approximation

In the time after the appearance of the "thawed" GWP paper, subsequent research demonstrated that *rather astoundingly, quantitative agreement between exact and semiclassical wave functions can be obtained by surrounding the point -like classical trajectories conventionally used to semiclassically quantise a given potential by a rigid or "frozen" Gaussian wavepacket.*[21] Although it is true that the width of a GWP distorts as it travels and furthermore, for anharmonic potentials, it won't even remain Gaussian, it was proven that *a Fourier transformed frozen Gaussian is an eigenfunction of an arbitrary system in the limit* $\hbar \to 0$. Freezing the width parameter frees us from integrating (2.73). Furthermore, guided by (2.61), and recognising the similarity between (2.74) and the expression for classical action, (2.22), we anticipate that we might be able to avoid integrating (2.74), too. If we could, then all that would remain would be the computation of classical trajectories.

Suppose we expand our initial wavefunction in a set of frozen GWP's,

$$|\psi_0\rangle = \sum_n |g^{\gamma}_{np_iq_i}\rangle c_n \ , \tag{2.75}$$

where the coefficients, c_n, define the phase and amplitude of each wavepacket. The form of the wavepackets has been modified slightly compared to (2.64):

$$\langle x|g^{\gamma}_{np_iq_i}\rangle = \left(\frac{\gamma}{\pi}\right)^{N/4} \exp\left[-\frac{\gamma}{2}(x-q_{ni})^2 + \frac{i}{\hbar}p_{ni}(x-q_{ni})\right] . \tag{2.76}$$

Notice that the width has been redefined ($\gamma = -\frac{2i}{\hbar}\alpha_t$) and it is assumed to be real and positive. Now, the time dependence of our wavefunction is made by the so-called *Frozen Gaussian Approximation*:

$$\begin{aligned} |\psi_t\rangle &= \sum_n e^{-i\hat{H}t/\hbar}|g^{\gamma}_{np_iq_i}\rangle c_n \\ &\overset{FGA}{\approx} \sum_n e^{+i\Gamma_{nt}/\hbar}|g^{\gamma}_{np_tq_t}\rangle c_n , \end{aligned} \tag{2.77}$$

where

$$\langle x|g^{\gamma}_{np_tq_t}\rangle = \left(\frac{\gamma}{\pi}\right)^{N/4} \exp\left[-\frac{\gamma}{2}(x-q_{nt})^2 + \frac{i}{\hbar}p_{nt}(x-q_{nt})\right] \tag{2.78}$$

$$\Gamma_{nt} = \int_0^t \mathrm{d}t' \{p_{nt'}\dot{q}_{nt'} - \langle E\rangle_{nt}\} \tag{2.79}$$

$$\langle E\rangle_{nt} = \langle g^{\gamma}_{np_tq_t}|\hat{H}|g^{\gamma}_{np_tq_t}\rangle . \tag{2.80}$$

Again, the potential has been approximated as Equation (2.66). Notice how closely Γ_{nt} now resembles a classical action, (2.22). Also, it should be noted that the subscripts on the wavepacket have been changed to indicate that its centre follows a classical trajectory.

Heller proceeds to test the FG method by computing a semiclassical vibronic absorption spectrum for a Henon-Heiles potential [21] and reports *surprisingly good* agreement with the corresponding quantum mechanical results. The error observed was attributed to the FG's being frozen (superposition error is much less of a problem since our set of GWP's is overcomplete). To explain how such a simple method could yield such accurate results, Heller provides his *collective correlation* picture, rather than rigorous derivation. In this picture, a "swarm" of FG's is capable of capturing position-momentum correlation (*i.e.* it can distort), even though individually, they cannot.

For future comparison (in Section 2.7) it is convenient to also introduce an even simpler propagator which is similar to Equation (2.77), except that Γ_{nt} is replaced with the classical action. This propagator makes use of the following "statement of completeness" for the GWP's of Equation (2.76):

$$\left(\frac{1}{2\pi\hbar}\right)^N \iint \mathrm{d}\mathbf{p}\mathrm{d}\mathbf{q}|g^{\gamma}_{\mathbf{pq}}\rangle\langle g^{\gamma}_{\mathbf{pq}}| = \mathbf{1} . \tag{2.81}$$

This equation has been generalised to N dimensions, with $\{\mathbf{p},\mathbf{q}\}$ being N-dimensional vectors, so that

$$\langle \mathbf{x}|g^{\gamma}_{\mathbf{pq}}\rangle = \left(\frac{\gamma}{\pi}\right)^{N/4} \exp\left[-\frac{\gamma}{2}(\mathbf{x}-\mathbf{q})^2 + \frac{i}{\hbar}\mathbf{p}(\mathbf{x}-\mathbf{q})\right] . \tag{2.82}$$

Inserting this expression into the QM propagator, (2.7), gives

$$K_t^{QM}(\mathbf{x}',\mathbf{x}) = \left(\frac{1}{2\pi\hbar}\right)^N \iint \mathrm{d}\mathbf{p}_i\mathrm{d}\mathbf{q}_i \langle \mathbf{x}'|e^{-i\hat{H}t/\hbar}|g^\gamma_{\mathbf{p}_i\mathbf{p}_i}\rangle\langle g^\gamma_{\mathbf{p}_i\mathbf{p}_i}|\mathbf{x}\rangle \ . \tag{2.83}$$

Now, making the "crude" FGA approximation mentioned above leads to Heller's *primitive* initial value representation,

$$K_t^{EJH}(\mathbf{x}',\mathbf{x}) = \left(\frac{1}{2\pi\hbar}\right)^N \iint \mathrm{d}\mathbf{p}_i\mathrm{d}\mathbf{q}_i e^{iS_{\mathbf{p}_i\mathbf{q}_i t}/\hbar}\langle \mathbf{x}'|g^\gamma_{\mathbf{p}_i\mathbf{q}_i}\rangle\langle g^\gamma_{\mathbf{p}_i\mathbf{q}_i}|\mathbf{x}\rangle \ . \tag{2.84}$$

This particular appearance of the propagator will be used again in subsequent sections to allow for easy comparison. Notice that we have not accounted for the coefficients of Equation (2.77). This is an issue which will arise later on, when the specific form of the coefficients will be determined. The consequence of this is that $K_t^{EJH}(\mathbf{x}',\mathbf{x})$ fails to capture the quantum effect of zero point energy.

2.7 The Herman-Kluk Initial Value Representation

Herman and Kluk proposed their frozen Gaussian approximation in 1984 [15] in a paper where they offered a more substantial analysis of the collective correlation idea of Heller. They demonstrated that the divergence of adjacent classical trajectories does, in fact, account for the distortion of Ψ_t. Their propagator is unitary within the stationary-phase approximation and includes a pre-exponential factor, which is now commonly referred to as the *Herman-Kluk prefactor*. The HK-IVR is free from caustics, satisfies the TDSE to first order in $\hbar$, and reduces to the Van Vleck propagator when the integrals are evaluated by stationary-phase methods.

In 1994, Kay [18, 19] derived a general formula for a broad class of IVR's, and related specific instances of it to established semiclassical wave propagation techniques.

2.7.1 The coherent state approximation: Arriving at the HK-IVR propagator

The form of the propagator which is to be developed herein will be made with analogy to Section 2.6.2. Again, our initial wavefunction, Ψ_0, is decomposed in terms of frozen GWP's of Equation (2.76). The potential will be approximated quadratically (ensuring that our GWP's are sufficiently localised to justify this), and the parameters specifying the centres of the wavepackets follow classical trajectories.

In this derivation, our starting point will be taken as Equation (2.83), in which an (overcomplete) set of coherent states is inserted into the quantum propagator,

$$K_t^{QM}(\mathbf{x}',\mathbf{x}) = \left(\frac{1}{2\pi\hbar}\right)^N \iint \mathrm{d}\mathbf{p}_i\mathrm{d}\mathbf{q}_i \langle \mathbf{x}'|e^{-i\hat{H}t/\hbar}|g^\gamma_{\mathbf{p}_i\mathbf{q}_i}\rangle\langle g^\gamma_{\mathbf{p}_i\mathbf{q}_i}|\mathbf{x}\rangle \ . \tag{2.85}$$

Now, instead of making Heller's primitive FGA, we propose another form which contains a pre-exponential factor to be determined later (this will be done by comparison to the Van Vleck propagator):

$$e^{-i\hat{H}t/\hbar}|g^{\gamma}_{\mathbf{p}_i\mathbf{q}_i}\rangle \approx R_{\mathbf{p}_i\mathbf{q}_i t}e^{+i\hat{S}_{\mathbf{p}_i\mathbf{q}_i t}/\hbar}|g^{\gamma}_{\mathbf{p}_i\mathbf{q}_i}\rangle \; . \tag{2.86}$$

Recall that $S_{\mathbf{p}_i\mathbf{q}_i t}$ is the classical action and N is the dimensionality of the system. In principal, γ is an arbitrary real positive width parameter. Inserting this into (2.85) gives

$$\begin{aligned} K_t(\mathbf{x}',\mathbf{x}) &\approx \left(\frac{1}{2\pi\hbar}\right)^N \iint \mathrm{d}\mathbf{p}_i\mathrm{d}\mathbf{q}_i R_{\mathbf{p}_i\mathbf{q}_i t}e^{+iS_{\mathbf{p}_i\mathbf{q}_i}/\hbar}\langle\mathbf{x}'|g^{\gamma}_{\mathbf{p}_i\mathbf{q}_i}\rangle\langle g^{\gamma}_{\mathbf{p}_i\mathbf{q}_i}|\mathbf{x}\rangle \\ &= \left(\frac{1}{2\pi\hbar}\right)^N \left(\frac{\gamma}{\pi}\right)^{N/2} \iint \mathrm{d}\mathbf{p}_i\mathrm{d}\mathbf{q}_i R_{\mathbf{p}_i\mathbf{q}_i t}e^{+i\Phi_{\mathbf{p}_i\mathbf{q}_i t}/\hbar} \; , \end{aligned} \tag{2.87}$$

where we have made use of Equation (2.82) to evaluate the overlap terms. The term in the exponent is

$$\Phi_{\mathbf{p}_i\mathbf{q}_i t} = S_{\mathbf{p}_i\mathbf{q}_i t} + \left[\mathbf{p}_t(\mathbf{x}'-\mathbf{q}_t) - \mathbf{p}_i(\mathbf{x}-\mathbf{q}_i)\right] + \frac{i\hbar\gamma}{2}\left[(\mathbf{x}'-\mathbf{q}_t)^2 + (\mathbf{x}-\mathbf{q}_i)^2\right] \; . \tag{2.88}$$

We now make the stationary-phase approximation (see Appendix B) to arrive at

$$\begin{aligned} \iint \mathrm{d}\mathbf{p}_i\mathrm{d}\mathbf{q}_i R_{\mathbf{p}_i\mathbf{q}_i t}e^{+i\Phi_{\mathbf{p}_i\mathbf{q}_i t}/\hbar} &\approx (2\pi i\hbar)^N \sum_k^{st.pts} R_{\mathbf{p}_i\mathbf{q}_i t}\det\left[\Phi''_{\mathbf{p}_i\mathbf{q}_i t}\right]^{-1/2} \\ &\quad \times e^{+i\Phi_{\mathbf{p}_i\mathbf{q}_i t}/\hbar} \; . \end{aligned} \tag{2.89}$$

This leads us to a new semiclassical propagator, which is accurate to both the FGA and the stationary-phase approximation:

$$\begin{aligned} K_t^{FG-SP}(\mathbf{x}',\mathbf{x}) &= \left(\frac{1}{2\pi\hbar}\right)^N \left(\frac{\gamma}{\pi}\right)^{N/2} (2\pi i\hbar)^N \\ &\quad \times \sum_k^{st.pts} R_{\mathbf{p}_i\mathbf{q}_i t}\det\left[\Phi''_{\mathbf{p}_i\mathbf{q}_i t}\right]^{-1/2} e^{+i\Phi_{\mathbf{p}_i\mathbf{q}_i t}/\hbar} \\ &= i^N\left(\frac{\gamma}{\pi}\right)^{N/2} \sum_k^{st.pts} R_{\mathbf{p}_i\mathbf{q}_i t}\det\left[\Phi''_{\mathbf{p}_i\mathbf{q}_i t}\right]^{-1/2} e^{+i\Phi_{\mathbf{p}_i\mathbf{q}_i t}/\hbar} \; . \end{aligned} \tag{2.90}$$

Since we are evaluating the sum in (2.90) at stationary points,

$$\Phi'_{\mathbf{p}_i\mathbf{q}_i t} = \begin{pmatrix} \frac{\partial\Phi_{\mathbf{p}_i\mathbf{q}_i t}}{\partial\mathbf{p}_i} \\ \frac{\partial\Phi_{\mathbf{p}_i\mathbf{q}_i t}}{\partial\mathbf{q}_i} \end{pmatrix} = \mathbf{0} \; , \tag{2.91}$$

and

$$\Phi''_{\mathbf{p}_i\mathbf{q}_i t} = \begin{pmatrix} \frac{\partial^2\Phi_{\mathbf{p}_i\mathbf{q}_i t}}{\partial\mathbf{p}_i^2} & \frac{\partial^2\Phi_{\mathbf{p}_i\mathbf{q}_i t}}{\partial\mathbf{p}_i\partial\mathbf{q}_i} \\ \frac{\partial^2\Phi_{\mathbf{p}_i\mathbf{q}_i t}}{\partial\mathbf{q}_i\partial\mathbf{p}_i} & \frac{\partial^2\Phi_{\mathbf{p}_i\mathbf{q}_i t}}{\partial\mathbf{q}_i^2} \end{pmatrix} \tag{2.92}$$

is some Hessian matrix. Note that $R_{\mathbf{p}_i\mathbf{q}_i t}$ must be evaluated at all stationary points. Now, we compare this expression to the Van Vleck propagator (Equation (2.61)) to determine the exact form

of the Herman-Kluk prefactor. To do this, we begin by evaluating the two terms of (2.91):

$$\frac{\partial \Phi_{\mathbf{p}_i\mathbf{q}_i t}}{\partial \mathbf{p}_i} = \frac{\partial S_{\mathbf{p}_i\mathbf{q}_i t}}{\partial \mathbf{p}_i} + \left(\frac{\partial \mathbf{p}_t}{\partial \mathbf{p}_i}\right)^T (\mathbf{x}' - \mathbf{q}_t) - \left(\frac{\partial \mathbf{q}_t}{\partial \mathbf{p}_i}\right)^T \mathbf{p}_t$$
$$-(\mathbf{x} - \mathbf{q}_i) - i\gamma\hbar \left(\frac{\partial \mathbf{q}_t}{\partial \mathbf{p}_i}\right)^T (\mathbf{x}' - \mathbf{q}_t) \tag{2.93}$$

$$\frac{\partial \Phi_{\mathbf{p}_i\mathbf{q}_i t}}{\partial \mathbf{q}_i} = \frac{\partial S_{\mathbf{p}_i\mathbf{q}_i t}}{\partial \mathbf{q}_i} + \left(\frac{\partial \mathbf{p}_t}{\partial \mathbf{q}_i}\right)^T (\mathbf{x}' - \mathbf{q}_t) - \left(\frac{\partial \mathbf{q}_t}{\partial \mathbf{q}_i}\right)^T \mathbf{p}_t + \mathbf{p}_i$$
$$-i\gamma\hbar \left[\left(\frac{\partial \mathbf{q}_t}{\partial \mathbf{q}_i}\right)^T (\mathbf{x}' - \mathbf{q}_t) + (\mathbf{x} - \mathbf{q}_i)\right] . \tag{2.94}$$

It can be shown that the partial derivatives of the classical action with respect to $\mathbf{p}_i$ and $\mathbf{q}_i$ can be written equivalently as:

$$\frac{\partial S_{\mathbf{p}_i\mathbf{q}_i t}}{\partial \mathbf{p}_i} = \left(\frac{\partial \mathbf{q}_t}{\partial \mathbf{p}_i}\right)^T \mathbf{p}_t \tag{2.95}$$

$$\frac{\partial S_{\mathbf{p}_i\mathbf{q}_i t}}{\partial \mathbf{q}_i} = \left(\frac{\partial \mathbf{q}_t}{\partial \mathbf{q}_i}\right)^T \mathbf{p}_t - \mathbf{p}_i . \tag{2.96}$$

These expressions are obtained by differentiating the definition of the classical action with respect to $\mathbf{p}_i$ and $\mathbf{q}_i$, and then using Hamilton's equations of motion to cancel terms in the integral over t. Before continuing, we simplify our result by defining two matrices,

$$\mathbf{V} = \left[\frac{\partial \mathbf{p}_t}{\partial \mathbf{p}_i} - i\gamma\hbar \frac{\partial \mathbf{q}_t}{\partial \mathbf{p}_i}\right] \tag{2.97}$$

$$\mathbf{W} = \left[\frac{\partial \mathbf{p}_t}{\partial \mathbf{q}_i} - i\gamma\hbar \frac{\partial \mathbf{q}_t}{\partial \mathbf{q}_i}\right] , \tag{2.98}$$

and notice that Equations (2.93) and (2.94) can be rewritten as:

$$\frac{\partial \Phi_{\mathbf{p}_i\mathbf{q}_i t}}{\partial \mathbf{p}_i} = \mathbf{V}^T(\mathbf{x}' - \mathbf{q}_t) - (\mathbf{x} - \mathbf{q}_i) \tag{2.99}$$

$$\frac{\partial \Phi_{\mathbf{p}_i\mathbf{q}_i t}}{\partial \mathbf{q}_i} = \mathbf{W}^T(\mathbf{x}' - \mathbf{q}_t) - i\gamma\hbar(\mathbf{x} - \mathbf{q}_i) . \tag{2.100}$$

It is these equations which determine the stationary-phase points. We may now rewrite (2.91) more compactly in matrix form:

$$\begin{pmatrix} \mathbf{V}^T & -\mathbf{1} \\ \mathbf{W}^T & -i\gamma\hbar\mathbf{1} \end{pmatrix} \begin{pmatrix} \mathbf{x}' - \mathbf{q}_t \\ \mathbf{x} - \mathbf{q}_i \end{pmatrix} = \begin{pmatrix} \mathbf{0} \\ \mathbf{0} \end{pmatrix} . \tag{2.101}$$

Now, to investigate the nature of the solution to (2.101), we turn our attention to the determinant of the matrix:

$$\det \begin{pmatrix} \mathbf{V}^T & -\mathbf{1} \\ \mathbf{W}^T & -i\gamma\hbar\mathbf{1} \end{pmatrix} = \det \left(\mathbf{V}^T \cdot (-i\gamma\hbar\mathbf{1}) + \mathbf{1} \cdot \mathbf{W}^T\right) . \tag{2.102}$$

Since we may take the transpose of the matrix on the right-hand side without affecting the determinant,

$$\begin{aligned}
\det\left(-i\gamma\hbar\mathbf{V}^T+\mathbf{W}^T\right) &= \det\left(\mathbf{W}-i\gamma\hbar\mathbf{V}\right) \\
&= \det\left[\frac{\partial\mathbf{p}_t}{\partial\mathbf{q}_i}-i\gamma\hbar\frac{\partial\mathbf{q}_t}{\partial\mathbf{q}_i}-i\gamma\hbar\left(\frac{\partial\mathbf{p}_t}{\partial\mathbf{p}_i}-i\gamma\hbar\frac{\partial\mathbf{q}_t}{\partial\mathbf{p}_i}\right)\right] \\
&= (-2i\gamma\hbar)^N\det\left\{\frac{1}{2}\left[\frac{\partial\mathbf{q}_t}{\partial\mathbf{q}_i}+\frac{\partial\mathbf{p}_t}{\partial\mathbf{p}_i}-\frac{1}{i\gamma\hbar}\frac{\partial\mathbf{p}_t}{\partial\mathbf{q}_i}-i\gamma\hbar\frac{\partial\mathbf{q}_t}{\partial\mathbf{p}_i}\right]\right\} \\
&= (-2i\gamma\hbar)^N\det\mathcal{R}\,, \qquad (2.103)
\end{aligned}$$

with

$$\mathcal{R}=\frac{1}{2}\left[\frac{\partial\mathbf{q}_t}{\partial\mathbf{q}_i}+\frac{\partial\mathbf{p}_t}{\partial\mathbf{p}_i}-\frac{1}{i\gamma\hbar}\frac{\partial\mathbf{p}_t}{\partial\mathbf{q}_i}-i\gamma\hbar\frac{\partial\mathbf{q}_t}{\partial\mathbf{p}_i}\right]\,. \qquad (2.104)$$

It can be shown that $\det\mathcal{R}\neq 0$. Therefore, only the trivial solution of (2.101) remains:

$$\begin{aligned}
\mathbf{x}' &= \mathbf{q}_t \\
\mathbf{x} &= \mathbf{q}_i\,. \qquad (2.105)
\end{aligned}$$

Therefore, each stationary point corresponds to a classical trajectory which satisfies the boundary conditions of (2.105) (*i.e.* we may replace "*st.pts*" in (2.90) with "*traj.*"). We must find each of these trajectories since they will all contribute to our propagator (as Equation (2.90)). Equation (2.105) greatly simplifies our expression for the phase term:

$$\Phi_{\mathbf{p}_i\mathbf{q}_i t}=S_{\mathbf{x}'\mathbf{x}t}\,. \qquad (2.106)$$

Notice that the matrix $\Phi''_{\mathbf{p}_i\mathbf{q}_i t}$ can be written equivalently as

$$\Phi''_{\mathbf{p}_i\mathbf{q}_i t}=\begin{pmatrix}\left(\frac{\partial\mathbf{q}_t}{\partial\mathbf{p}_i}\right)^T & \mathbf{0}\\ \left(\frac{\partial\mathbf{q}_t}{\partial\mathbf{q}_i}\right)^T & \mathbf{1}\end{pmatrix}\begin{pmatrix}-\mathbf{V} & -\mathbf{W}\\ \mathbf{1} & i\gamma\hbar\mathbf{1}\end{pmatrix}\,. \qquad (2.107)$$

Using the relation $\det(\mathbf{AB})=\det(\mathbf{A})\det(\mathbf{B})$, we find that

$$\begin{aligned}
\det\Phi''_{\mathbf{p}_i\mathbf{q}_i t} &= \det\left(\frac{\partial\mathbf{q}_t}{\partial\mathbf{p}_i}\right)\det\left(\mathbf{W}-i\gamma\hbar\mathbf{V}\right) \\
&= (-2i\gamma\hbar)^N\det\left(\frac{\partial\mathbf{x}'}{\partial\mathbf{p}_i}\right)\det\mathcal{R}\,. \qquad (2.108)
\end{aligned}$$

For the last step, we used the result of (2.103) and (2.105).

Now, we apply this result to our equation for the propagator (2.90):

$$\begin{aligned}
K_t^{FG-SP}(\mathbf{x}',\mathbf{x}) &= i^N\left(\frac{\gamma}{\pi}\right)^{\frac{N}{2}}\sum_k^{st.pts}R_{\mathbf{p}_i\mathbf{q}_i t}\det\left[\Phi''_{\mathbf{p}_i\mathbf{q}_i t}\right]^{-\frac{1}{2}}e^{+i\Phi_{\mathbf{p}_i\mathbf{q}_i t}/\hbar} \\
&= i^N\left(\frac{\gamma}{\pi}\right)^{\frac{N}{2}}\left(-\frac{1}{2i\gamma\hbar}\right)^{\frac{N}{2}}\sum_{traj.}R_{\mathbf{p}_i\mathbf{q}_i t}\left[\det\left(\frac{\partial\mathbf{x}'}{\partial\mathbf{p}_i}\right)\det\mathcal{R}\right]^{-\frac{1}{2}}e^{iS_{\mathbf{x}'\mathbf{x}t}/\hbar} \\
&= \left(\frac{1}{2\pi i\hbar}\right)^{\frac{N}{2}}\sum_{traj.}R_{\mathbf{p}_i\mathbf{q}_i t}\left[\det\left(\frac{\partial\mathbf{x}'}{\partial\mathbf{p}_i}\right)\det\mathcal{R}\right]^{-\frac{1}{2}}e^{iS_{\mathbf{x}'\mathbf{x}t}/\hbar}\,. \qquad (2.109)
\end{aligned}$$

Comparing this result to the equivalent Van Vleck expression,

$$K_t^{VV}(\mathbf{x}',\mathbf{x}) = \left(\frac{1}{2\pi i\hbar}\right)^{\frac{N}{2}} \sum_{traj.} \left[\det\left(\frac{\partial \mathbf{x}'}{\partial \mathbf{p}_i}\right)\right]^{-\frac{1}{2}} e^{iS_{\mathbf{x}'\mathbf{x}t}/\hbar} , \tag{2.110}$$

Herman and Kluk proposed their final form of the prefactor:

$$\begin{aligned} R_{\mathbf{p}_i\mathbf{q}_i t} &= \det \mathcal{R}^{1/2} \\ &= \det\left\{\frac{1}{2}\left[\frac{\partial \mathbf{q}_t}{\partial \mathbf{q}_i} + \frac{\partial \mathbf{p}_t}{\partial \mathbf{p}_i} - \frac{1}{i\gamma\hbar}\frac{\partial \mathbf{p}_t}{\partial \mathbf{q}_i} - i\gamma\hbar\frac{\partial \mathbf{q}_t}{\partial \mathbf{p}_i}\right]\right\}^{1/2} . \end{aligned} \tag{2.111}$$

We now recall the FGA proposed in (2.86) and write our final result for the HK-IVR:

$$K^{HK}(\mathbf{x}',\mathbf{x}) = \left(\frac{1}{2\pi\hbar}\right)^N \iint \mathrm{d}\mathbf{p}_i \mathrm{d}\mathbf{q}_i R_{\mathbf{p}_i\mathbf{q}_i t} e^{iS_{\mathbf{p}_i\mathbf{q}_i t}/\hbar} \langle \mathbf{x}'|g^\gamma_{\mathbf{p}_t\mathbf{q}_t}\rangle\langle g^\gamma_{\mathbf{p}_i\mathbf{q}_i}|\mathbf{x}\rangle . \tag{2.112}$$

2.7.2 Application of the HK-IVR

For the remainder of this thesis, we will concern ourselves with the *autocorrelation function*(ACF), which is defined as

$$C(t) = \langle \Psi_0|\Psi_t\rangle . \tag{2.113}$$

In particular, we are interested in the HK-IVR approximation to $C(t)$:

$$C^{HK}(t) = \left(\frac{1}{2\pi\hbar}\right)^N \iint \mathrm{d}\mathbf{p}_i \mathrm{d}\mathbf{q}_i R_{\mathbf{p}_i\mathbf{q}_i t} e^{iS_{\mathbf{p}_i\mathbf{q}_i t}/\hbar} \langle \Psi_0|g^\gamma_{\mathbf{p}_t\mathbf{q}_t}\rangle\langle g^\gamma_{\mathbf{p}_i\mathbf{q}_i}|\Psi_0\rangle . \tag{2.114}$$

The ACF is a useful quantity since it is related to the spectrum of energy levels (the *power spectrum*) by a Fourier transform (see Appendix C). We restrict ourselves to a Gaussian initial wavefunction with the same form as our coherent states: $|\Psi_0\rangle = |g^\gamma_{\mathbf{p}_0\mathbf{q}_0}\rangle$. To further simplify the overlap terms of (2.114), we choose our width parameters, γ, to be the same also:

$$\langle \mathbf{x}|\Psi_0\rangle = \left(\frac{\gamma}{\pi}\right)^{N/4} \exp\left[-\frac{\gamma}{2}(\mathbf{x}-\mathbf{q}_0)^2 + \frac{i}{\hbar}\mathbf{p}_0(\mathbf{x}-\mathbf{q}_0)\right] . \tag{2.115}$$

In general, the widths for each degree of freedom do not have to be the same. Instead, we place the values for each in a diagonal matrix and evaluate the appropriate term in (2.115) as:

$$-\frac{\gamma}{2}(\mathbf{x}-\mathbf{q}_0)^2 = -\frac{1}{2}[\gamma\cdot(\mathbf{x}-\mathbf{q}_0)]\cdot(\mathbf{x}-\mathbf{q}_0) . \tag{2.116}$$

Selecting appropriate values for γ is an issue which is usually not mentioned in the literature. We employ a simple, yet physically justified scheme for choosing these based only on a single parameter (see Appendix E). Conveniently, the overlap terms of (2.114) are Gaussian integrals, and can be

evaluated analytically (see Appendix A):

$$\begin{aligned}
\langle g^{\gamma}_{\mathbf{p}_i\mathbf{q}_i}|\Psi_0\rangle &= \int \mathrm{d}\mathbf{x}\langle g^{\gamma}_{\mathbf{p}_i\mathbf{q}_i}|\mathbf{x}\rangle\langle\mathbf{x}|\Psi_0\rangle \\
&= \exp\left[-\frac{\gamma}{4}(\mathbf{q}_i-\mathbf{q}_0)^2-\frac{1}{4\gamma\hbar^2}(\mathbf{p}_i-\mathbf{p}_0)^2\right] \\
&\times \exp\left[+\frac{i}{2\hbar}(\mathbf{p}_i+\mathbf{p}_0)(\mathbf{q}_i-\mathbf{q}_0)\right] \qquad (2.117)\\
\langle\Psi_0|g^{\gamma}_{\mathbf{p}_t\mathbf{q}_t}\rangle &= \int \mathrm{d}\mathbf{x}\langle\Psi_0|\mathbf{x}\rangle\langle\mathbf{x}|g^{\gamma}_{\mathbf{p}_t\mathbf{q}_t}\rangle \\
&= \exp\left[-\frac{\gamma}{4}(\mathbf{q}_t-\mathbf{q}_0)^2-\frac{1}{4\gamma\hbar^2}(\mathbf{p}_t-\mathbf{p}_0)^2\right] \\
&\times \exp\left[-\frac{i}{2\hbar}(\mathbf{p}_i+\mathbf{p}_0)(\mathbf{q}_i-\mathbf{q}_0)\right] . \qquad (2.118)
\end{aligned}$$

Now, it is important to recognise that for any non-trivial molecular system, the $2N$-dimensional phase-space is *enormous*. Therefore, we cannot hope to hack the double integral over $\mathbf{p}_i$ and $\mathbf{q}_i$ using standard numerical techniques (*i.e.* by the trapezoid rule, for example). Instead, we use direct Monte Carlo sampling.[36] We are blessed with a natural Gaussian sampling function: namely, the Gaussian portion of (2.117):

$$\exp\left[-\frac{\gamma}{4}(\mathbf{q}_i-\mathbf{q}_0)^2-\frac{1}{4\gamma\hbar^2}(\mathbf{p}_i-\mathbf{p}_0)^2\right] .$$

Accordingly, this term is removed (along with the appropriate normalisation factor, $(4\pi)^{-N}$) from (2.114), and phase-space points, $(\mathbf{p}_i, \mathbf{q}_i)$, are selected using a Gaussian random number generator. By accumulating the integrand from each of these *initial conditions*, we can monitor the convergence of our integral, $C(t)$. Because the action term appears in the phase of the integrand, this integral can become highly oscillatory (especially at long time, when the action may become quite large when compared to $\hbar$). This can make convergence of this integral very slow, sometimes prohibitively so. This problem receives its own share of attention in the literature, where "smoothing" or "filtering" procedures are developed specifically for application to the HK-IVR.[8, 24, 25, 26] For the model systems discussed in this thesis, this was not a serious problem, however future work will certainly incorporate one of these.

Now, what remains is to evolve each such contribution of the integrand in time and compute our autocorrelation function over a time period which is sufficient to adequately resolve the portion of the energy spectrum we are interested in.

Computing the overlaps and classical action is straightforward. By integrating the classical equations of motion using your favourite integrator (*Velocity Verlet*, for example), we solve for the parameters defining the coherent states (recall that the width does not change), as well as keep track of our action, $S_{\mathbf{p}_i\mathbf{q}_i t}$, along this trajectory. The time-dependence of the Herman-Kluk prefactor,

$R_{\mathbf{p}_i\mathbf{q}_i t}$, is more involved and presents the computational bottleneck in this procedure.[6]

Accommodating a diagonal γ matrix, the prefactor is

$$R_{\mathbf{p}_i\mathbf{q}_i t} = \det\left\{\frac{1}{2}\left[\frac{\partial \mathbf{q}_t}{\partial \mathbf{q}_i} + \gamma^{-1}\frac{\partial \mathbf{p}_t}{\partial \mathbf{p}_i}\gamma - \frac{1}{i\hbar}\gamma^{-1}\frac{\partial \mathbf{p}_t}{\partial \mathbf{q}_i} - i\hbar\frac{\partial \mathbf{q}_t}{\partial \mathbf{p}_i}\gamma\right]\right\}^{1/2} . \tag{2.119}$$

In fact, the partial derivatives here are the elements of the *monodromy matrix*, which is defined as

$$\mathbf{M} = \begin{pmatrix} \mathbf{M}_{qq} & \mathbf{M}_{qp} \\ \mathbf{M}_{pq} & \mathbf{M}_{pp} \end{pmatrix} , \tag{2.120}$$

where

$$\begin{matrix} \mathbf{M}_{qq} = \frac{\partial \mathbf{q}_t}{\partial \mathbf{q}_i} & \mathbf{M}_{qp} = \frac{\partial \mathbf{q}_t}{\partial \mathbf{p}_i} \\ \mathbf{M}_{pq} = \frac{\partial \mathbf{p}_t}{\partial \mathbf{q}_i} & \mathbf{M}_{pp} = \frac{\partial \mathbf{p}_t}{\partial \mathbf{p}_i} \end{matrix} . \tag{2.121}$$

Each of these elements is an $N \times N$ matrix, so the full monodromy matrix is $2N \times 2N$. In practice, these partial derivatives are not evaluated explicitly, but rather, auxiliary equations are integrated along with the classical trajectory itself. Notation is simplified if we go to mass-weighted Cartesian coordinates such that[7]

$$\begin{aligned} \mathbf{p}^{mw} &= m^{-\frac{1}{2}}\,\mathbf{p} \\ \mathbf{q}^{mw} &= m^{+\frac{1}{2}}\,\mathbf{q} . \end{aligned} \tag{2.122}$$

We now drop the superscript, and it is assumed that $\mathbf{p}$ and $\mathbf{q}$ are as (2.122). This new coordinate is convenient, since the equations of motion are now

$$\begin{aligned} \dot{\mathbf{p}}_t &= -\frac{\partial V}{\partial \mathbf{q}_t} \\ \dot{\mathbf{q}}_t &= \mathbf{p}_t . \end{aligned} \tag{2.123}$$

So, the auxiliary equations are

$$\dot{\mathbf{M}}_{qq} = \frac{\partial \dot{\mathbf{q}}_t}{\partial \mathbf{q}_i} = \frac{\partial \mathbf{p}_t}{\partial \mathbf{q}_i} = \mathbf{M}_{pq} \tag{2.124}$$

$$\dot{\mathbf{M}}_{qp} = \frac{\partial \dot{\mathbf{q}}_t}{\partial \mathbf{p}_i} = \frac{\partial \mathbf{p}_t}{\partial \mathbf{p}_i} = \mathbf{M}_{pp} \tag{2.125}$$

$$\begin{aligned} \dot{\mathbf{M}}_{pq} &= \frac{\partial \dot{\mathbf{p}}_t}{\partial \mathbf{q}_i} = \frac{\partial}{\partial \mathbf{q}_i}\left(-\frac{\partial V}{\partial \mathbf{q}_t}\right) \\ &= \left(\frac{\partial \mathbf{q}_t}{\partial \mathbf{q}_i}\frac{\partial}{\partial \mathbf{q}_t}\right)\left(-\frac{\partial V}{\partial \mathbf{q}_t}\right) = \left(-\frac{\partial^2 V}{\partial \mathbf{q}_t^2}\right)\mathbf{M}_{qq} \end{aligned} \tag{2.126}$$

$$\begin{aligned} \dot{\mathbf{M}}_{pp} &= \frac{\partial \dot{\mathbf{p}}_t}{\partial \mathbf{p}_i} = \frac{\partial}{\partial \mathbf{p}_i}\left(-\frac{\partial V}{\partial \mathbf{q}_t}\right) \\ &= \left(\frac{\partial \mathbf{q}_t}{\partial \mathbf{p}_i}\frac{\partial}{\partial \mathbf{q}_t}\right)\left(-\frac{\partial V}{\partial \mathbf{q}_t}\right) = \left(-\frac{\partial^2 V}{\partial \mathbf{q}_t^2}\right)\mathbf{M}_{qp} . \end{aligned} \tag{2.127}$$

[6] Actually, in more complex systems, or those exhibiting chaotic behavior, the convergence of the integral is the bottleneck.

[7] Here, our mass is also a diagonal matrix.

This can be written compactly in matrix form:

$$\frac{\mathrm{d}}{\mathrm{d}t}\begin{pmatrix} \mathbf{M}_{qq} & \mathbf{M}_{qp} \\ \mathbf{M}_{pq} & \mathbf{M}_{pp} \end{pmatrix} = \begin{pmatrix} \mathbf{0} & \mathbf{1} \\ -\frac{\partial^2 V}{\partial \mathbf{q}_i^2} & \mathbf{0} \end{pmatrix}\begin{pmatrix} \mathbf{M}_{qq} & \mathbf{M}_{qp} \\ \mathbf{M}_{pq} & \mathbf{M}_{pp} \end{pmatrix}. \tag{2.128}$$

Therefore, to compute $R_{\mathbf{p}_i\mathbf{q}_i t}$, we propagate the monodromy matrix (initially set to unity) according to (2.128). This, in turn, requires computing the second derivative of the potential in mass-weighted coordinates at each timestep. In this thesis, it is not in fact (2.128) which is used, but rather a log-derivative formulation which was proposed by Miller [23] and is discussed in Appendix F. The advantage of this alternative scheme is that it sidesteps the need to solve a matrix of coupled differential equations, while simultaneously avoiding the *branch-cut* problem associated with taking the square-root of the complex quantity of Equation (2.119).

Note that throughout this work, multiplicative factors in the autocorrelation function were not included since the goal was to assess the validity of our new approach for the calculation of energy levels. For this purpose, the function $C(t)$ was renormalised so that $C(0) = 1$. For applications where the absolute value of the correlation function is required (such as in the calculation of reaction rate constants), one should include all the proper multiplicative factors. Such applications are beyond the scope of this thesis and will be the subject of future work.

Chapter 3

Results and Discussion

The purpose of this present work is to establish a general method for computing the semiclassical propagator in Cartesian coordinates which allows for the inclusion of holonomic constraints. As outlined in Section 2.7.2, the principal difficulties encountered in the evaluation of the HK-IVR are the oscillatory nature of the integrand and the slow convergence of the integral by Monte Carlo methods.

It is our point of view that the elimination of high frequency modes can be thought of as an integral conditioning technique. High frequency modes are undesirable primarily because they contribute to the accumulation of classical action in the phase of Equation (2.112), leading to a rapid oscillation of the integrand. By reducing the frequency of this oscillation, we are able to evaluate our autocorrelation functions using larger timesteps. Furthermore, the convergence of the ACF is improved: because oscillations are diminished, and because the time-dependent dynamical variables will vary more smoothly with initial conditions[1], fewer Monte Carlo trajectories are necessary. Again, introducing our constraints is justified so long as the motion of the bonds to be frozen is not significantly coupled to the motions of primary interest. Again, we remain in Cartesian coordinates throughout so that our scheme is completely general - *i.e.* the evaluation of the derivatives of a curvilinear coordinate is not necessary.

To establish our method, we address a model system: a water bender with one effective degree of freedom. We compute the power spectrum using both exact quantum methods (Section 3.2.1) and the "traditional" application of the HK-IVR for a constrained system (Section 3.2.2). This will establish for us a basis of comparison for the results of the novel method we shall present in Section 3.2.3. Prior to our discussion of the water bender, however, we shall provide a *proof of principle* for our method: a constrained harmonic oscillator model problem. Any novel means of computing the various components of (2.112) will be presented as they arise, for simplicity and flow.

[1]This leads to smaller values for the elements of the monodromy matrix, and therefore, smaller values for the HK-prefactor.

3.1 Proof of Principle: A Harmonic Oscillator Model

In order to establish some confidence that our approach is theoretically justified, we introduce a model which possesses the essential elements of a typical constrained problem, yet is simple enough that both exact quantum and semiclassical procedures can be carried out analytically. This model consists of two particles of mass, m located at points x_1 and x_2 in a one dimensional harmonic trap with force constant, ω^2. The relative distance between these two particles is constrained such that $x_1 - x_2$ is constant. The potential is given by

$$V(x_1, x_2) = \frac{1}{2}m\omega^2(x_1^2 + x_2^2) \; . \tag{3.1}$$

We begin by solving for the exact quantum energy levels, and proceed to illustrate the methods for solving the problem semiclassically.

3.1.1 The quantum energy levels

Before the constraint connecting the two particles is applied, the Hamiltonian for our system, in coordinates x_1 and x_2 is

$$\hat{H}(x_1, x_2) = \left(-\frac{\hbar^2}{2m}\frac{\partial^2}{\partial x_1^2} + \frac{1}{2}m\omega^2 x_1^2 \right) + \left(-\frac{\hbar^2}{2m}\frac{\partial^2}{\partial x_2^2} + \frac{1}{2}m\omega^2 x_2^2 \right) . \tag{3.2}$$

Here, the simplest way to apply the constraint is to change to centre-of-mass and relative distance coordinates defined by

$$\begin{aligned} r &= x_1 - x_2 \\ R &= \frac{1}{2}(x_1 + x_2) \; , \end{aligned} \tag{3.3}$$

where the Jacobian associated with this change of variables is unity. The Hamiltonian becomes

$$\hat{H}(R, r) = \left(-\frac{\hbar^2}{2M}\frac{\partial^2}{\partial R^2} + \frac{1}{2}M\omega^2 R^2 \right) + \left(-\frac{\hbar^2}{2\mu}\frac{\partial^2}{\partial r^2} + \frac{1}{2}\mu\omega^2 r^2 \right) , \tag{3.4}$$

where $M = 2m$ is the total mass, and $\mu = \frac{1}{2}m$ is the reduced mass of the two particles. We introduce the constraint by fixing r to a constant value, r_0, and by removing the kinetic energy operator associated with the motion along this coordinate. This yields a one dimensional Hamiltonian which has harmonic oscillator eigenfunctions:

$$\hat{H}(R; r_0)\psi_n(R; r_0) = \left(\hbar\omega(n + \frac{1}{2}) + \frac{1}{2}\mu\omega^2 r_0^2 \right)\psi_n(R; r_0) \; . \tag{3.5}$$

It is $E_n = \hbar\omega(n + \frac{1}{2}) + \frac{1}{2}\mu\omega^2 r_0^2$ which we hope to reproduce semiclassically. Because our model is so simple, we may integrate (2.112) both analytically and numerically in order to investigate the error associated with the numerical implementation of our approach. Because our potential is harmonic, we may expect the HK-IVR to be formally exact.

3.1.2 The semiclassical energy levels

Here, we would like to evaluate the semiclassical autocorrelation function for our model harmonic oscillator system without introducing the change of coordinate, (3.3). The HK-IVR ACF is:

$$C(t) = (2\pi)^{-2} \iint \mathrm{d}\mathbf{p}_i \, \mathrm{d}\mathbf{q}_i \, R_{\mathbf{p}_i\mathbf{q}_i t} \, e^{iS_{\mathbf{p}_i\mathbf{q}_i t}} \langle \Psi_0 | g^{\gamma}_{\mathbf{p}_t\mathbf{q}_t} \rangle \langle g^{\gamma}_{\mathbf{p}_i\mathbf{q}_i} | \Psi_0 \rangle \ , \tag{3.6}$$

where $\mathbf{p}$, $\mathbf{q}$ are two-dimensional vectors. To evaluate this expression analytically, we must first find the solutions to the constrained equations of motion: $\mathbf{p}_t(\mathbf{p}_i, \mathbf{q}_i)$ and $\mathbf{q}_t(\mathbf{p}_i, \mathbf{q}_i)$. Using these equations, we will find explicit expressions for each of the terms in the integrand. Finally, the integration will be performed analytically over the subspace of initial conditions which satisfy the constraints to yield an expression for $C(t)$.

The constrained equations of motion

Our task here is to solve Newton's equations of motion for the two particles whose positions and momenta are connected by two constraints:

$$\begin{aligned} g_1 &= (x_1 - x_2)^2 - r_0^2 = 0 \\ g_2 &= p_1 - p_2 = 0 \, . \end{aligned} \tag{3.7}$$

The equations of motion are to be solved by the method of Lagrange multipliers:

$$\begin{aligned} m\ddot{x_1} &= -\frac{\partial}{\partial x_1} V^c(x_1, x_2; \lambda_1, \lambda_2, r_0) \\ m\ddot{x_2} &= -\frac{\partial}{\partial x_2} V^c(x_1, x_2; \lambda_1, \lambda_2, r_0) \ , \end{aligned} \tag{3.8}$$

where

$$V^c(x_1, x_2; \lambda_1, \lambda_2, r_0) = \frac{1}{2} m\omega^2 (x_1^2 + x_2^2) - \lambda_1 g_1 - \lambda_2 g_2 \ . \tag{3.9}$$

Evaluating this expression leads to

$$\begin{aligned} \ddot{x_1} + \omega^2 x_1 + 2\lambda_1 (x_1 - x_2) &= 0 \\ \ddot{x_2} + \omega^2 x_2 - 2\lambda_1 (x_1 - x_2) &= 0 \, . \end{aligned} \tag{3.10}$$

These equations are decoupled by taking their sum and difference and making substitutions, $u_1 = \frac{1}{2}(x_1 + x_2)$ and $u_2 = x_1 - x_2$:

$$\begin{aligned} \ddot{u_1} + \omega^2 u_1 &= 0 \\ \ddot{u_2} + (\omega^2 + \frac{4\lambda_1}{m}) u_2 &= 0 \, . \end{aligned} \tag{3.11}$$

These differential equations can now be solved independently, yielding the solutions

$$\begin{aligned} u_1(t) &= c_1 \sin(\omega t) + c_2 \cos(\omega t) \\ u_2(t) &= c_3 \sin\left(\sqrt{\omega^2 + \frac{4\lambda_1}{m}}\, t\right) + c_4 \cos\left(\sqrt{\omega^2 + \frac{4\lambda_1}{m}}\, t\right) , \end{aligned}$$

so that, finally,

$$\begin{aligned}
x_1(t) &= c_1\sin(\omega t) + c_2\cos(\omega t) + \frac{1}{2}c_3\sin\left(\sqrt{\omega^2+\frac{4\lambda_1}{m}}t\right) + \frac{1}{2}c_4\cos\left(\sqrt{\omega^2+\frac{4\lambda_1}{m}}t\right)\\
x_2(t) &= c_1\sin(\omega t) + c_2\cos(\omega t) - \frac{1}{2}c_3\sin\left(\sqrt{\omega^2+\frac{4\lambda_1}{m}}t\right) - \frac{1}{2}c_4\cos\left(\sqrt{\omega^2+\frac{4\lambda_1}{m}}t\right)\\
p_1(t) &= m\dot{x_1}(t)\\
p_2(t) &= m\dot{x_2}(t)\,. \qquad (3.12)
\end{aligned}$$

Notice that our constraint connecting the momenta is redundant. We solve for $\{c_1, c_2, c_3, c_4\}$ using the initial values, $\{x_1(0) = x_{1i}\ ,\ x_2(0) = x_{2i}\ ,\ p_1(0) = p_{1i}\ ,\ p_2(0) = p_{2i}\}$, and λ_1 is evaluated using (3.7), giving $\lambda_1 = -(\omega^2 m/4)$. Our final equations of motion are:

$$\begin{aligned}
x_1(t) &= \left(\frac{1}{2m\omega}\right)p_{Ri}\sin(\omega t) + R_i\cos(\omega t) + \frac{1}{2}r_0\\
x_2(t) &= \left(\frac{1}{2m\omega}\right)p_{Ri}\sin(\omega t) + R_i\cos(\omega t) - \frac{1}{2}r_0\\
p_1(t) &= \frac{1}{2}p_{Ri}\cos(\omega t) - R_i m\omega\sin(\omega t)\\
p_2(t) &= \frac{1}{2}p_{Ri}\cos(\omega t) - R_i m\omega\sin(\omega t)\,, \qquad (3.13)
\end{aligned}$$

where the substitutions $p_{Ri} = p_{1i} + p_{2i}$, $R_i = \frac{1}{2}(x_{1i} + x_{2i})$, and $r_0 = x_{1i} - x_{2i}$ have been made for brevity only. Now that we have explicit analytical expressions for the positions and momenta of our system, we can work out the constituents of the integrand of Equation (3.6).

The semiclassical autocorrelation function

Here, we will develop a final expression for (3.6) and then perform integration analytically to obtain an expression for the ACF. We begin by writing (3.6) in more detail, where integration is restricted to the region of phase space where the initial conditions obey the constraints through the inclusion of delta functions:

$$\begin{aligned}
C(t) &= (2\pi)^{-2}\int \mathrm{d}x_{1i}\int \mathrm{d}x_{2i}\ \ \delta\big((x_{1i}-x_{2i})^2 - r_0^2\big)\\
&\quad \int \mathrm{d}p_{1i}\int \mathrm{d}p_{2i}\ \ \delta(p_{1i}-p_{2i})\\
&\quad R_t(x_{1i},x_{2i},p_{1i},p_{2i})\ \times \exp\left(\frac{i}{\hbar}S_t(x_{1i},x_{2i},p_{1i},p_{2i})\right)\\
&\quad \langle\Psi_0|g_t^\gamma(x_{1i},x_{2i},p_{1i},p_{2i})\rangle\langle g_i^\gamma(x_{1i},x_{2i},p_{1i},p_{2i})|\Psi_0\rangle\,. \qquad (3.14)
\end{aligned}$$

First we shall evaluate the Hermann-Kluk prefactor, $R_t(x_{1i}, x_{2i}, p_{1i}, p_{2i})$. Recall that it is defined as equation (2.119) of Section (2.7.2). As it turns out, the derivatives of (2.121) conveniently do not depend on initial conditions. Therefore, the prefactor may be moved outside the integrals. It comes

out:

$$R_t = \sqrt{\det\left\{\frac{1}{2}\left(\mathbf{M_{pp}} + \mathbf{M_{qq}} - i\gamma\mathbf{M_{qp}} + \frac{i}{\gamma}\mathbf{M_{pq}}\right)\right\}}$$
$$= \sqrt{\cos(\omega t) - \frac{i}{2m\omega\gamma}(\gamma^2 + m^2\omega^2)\sin(\omega t)}\ . \tag{3.15}$$

Notice that (3.15) involves taking the square root of a complex number. This leads to a branch cut problem which normally requires that you keep track of the kernel of the square root along a particular trajectory. Since our R-factor is independent of initial conditions (and therefore only needs to be evaluated once), we found it simpler to pre-calculate it and remove the discontinuities by inspection.

The phase term, $e^{iS_t/\hbar}$, involves the classical action, S_t, which evaluates to

$$S_t = \int_0^t d\tau\left[T(p_{x1\tau}, p_{x2\tau}) - V(x_{1\tau}, x_{2\tau})\right]$$
$$= \left(\frac{1}{4m\omega}p_{Ri}^2 - m\omega R_i^2\right)\sin(\omega t)\cos(\omega t)$$
$$+ p_{Ri}R_i\sin^2(\omega t) - \frac{m\omega^2}{4}r_0^2 t\ . \tag{3.16}$$

All that remains is to select a width parameter, γ (we chose a value of 1.0), substitute in the expression for the overlaps and evaluate Gaussian integrals (the Dirac delta functions are taken in the Fourier representation) using the computer algebra program, *Maple* [37]. Although this prescription is straightforward, the algebraic results are cumbersome and are not presented. Because our system is harmonic, we expect our results to exact. That is, we expect any discrepancies in the results to reflect errors in the numerical implementation only. In fact, no significant discrepancies were observed, so we do not show this result (*i.e.* so far, so good ...).

Another semiclassical ACF is computed: one where integration is not carried out analytically, but by the Monte Carlo procedure described in Section 2.7.2. The constrained equations of motion are integrated numerically, using the *Rattle* algorithm developed by Ryckaert [38] and Anderson [39]. Rattle is an integrator for the classical equations of motion which is based on the Velocity Verlet algorithm, but allows for the systematic inclusion of holonomic constraints. A more thorough investigation of the performance of Rattle appears in Section 3.2.3. Here, the motivation is to determine the error introduced simply by going to a fully numerical scheme - a scheme which will closely resemble the one used with the water bender. The results appear in Figures 3.1 - 3.4, the upshot being that our approach yields an ACF which is indistinguishable from the corresponding quantum result. Note that the power spectra presented have been conditioned with a Gaussian window function prior to Fourier transforming (see Appendices C and D). This gives a preferred line-shape, allowing for accurate determination of peak positions. The numerical positions of the

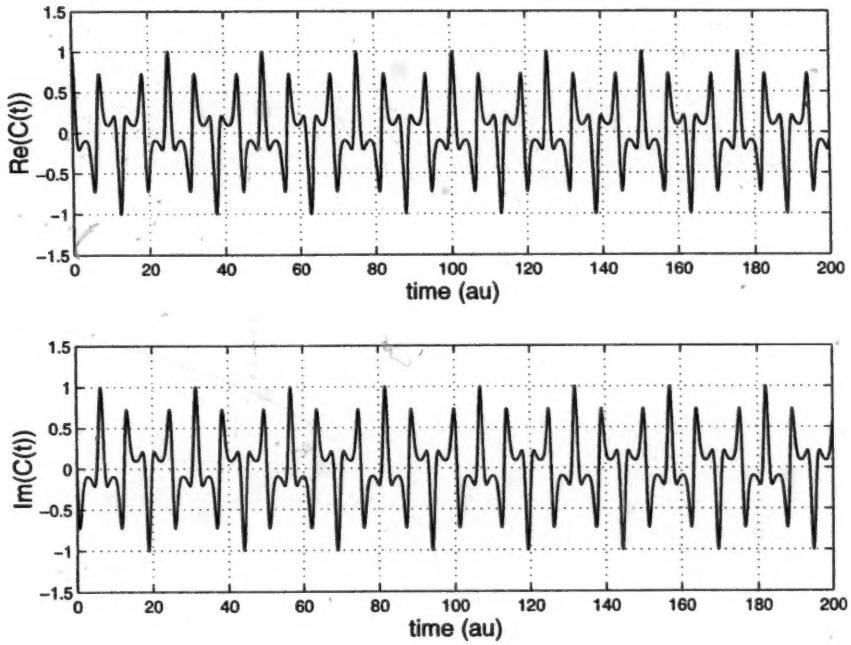

Figure 3.1: The quantum autocorrelation function for two particles in a harmonic well.

energy levels predicted by quantum mechanics and those computed by the HK-IVR are presented in Table 3.1.

3.2 A Physical Example: A Water Bender

In this section, we consider a simple constrained molecular system: a stationary (*i.e.* no centre-of-mass motion) water molecule with rigid O-H bonds. This model (see Figure 3.5) will provide the testing grounds for the development of our general method for evaluating the HK-IVR for arbitrary

Table 3.1: The calculated energy levels for the two particles in a harmonic trap. Values are given in E_h. The numbers in brackets indicate the uncertainty on the last digit.

peak	QM	SC-IVR
0	0.750(2)	0.750(2)
1	1.750(2)	1.750(2)
2	2.750(2)	2.750(2)
3	3.750(2)	3.750(2)
4	4.750(2)	4.750(2)

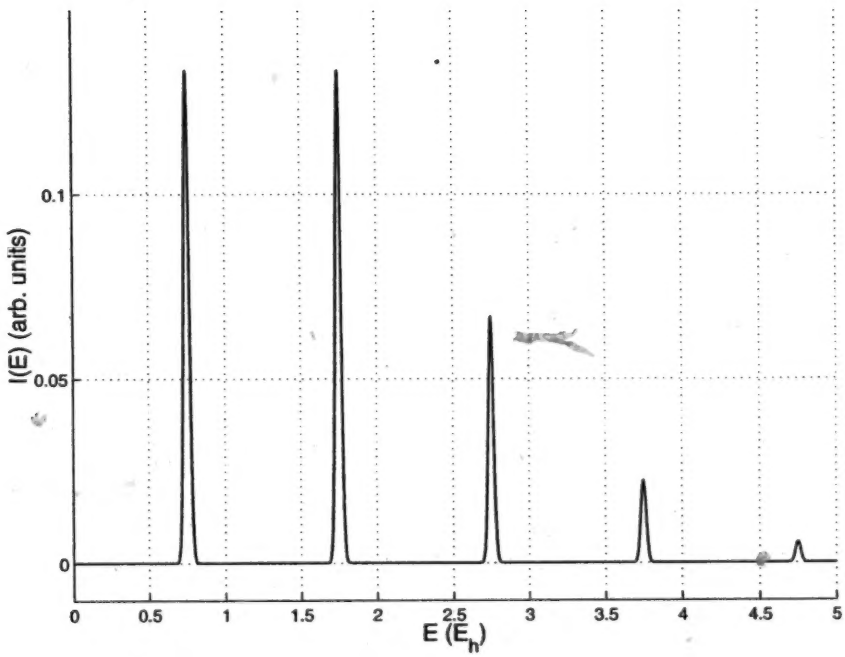

Figure 3.2: The quantum power spectrum for two particles in a harmonic well taken as the Fourier transform of the windowed autocorrelation function.

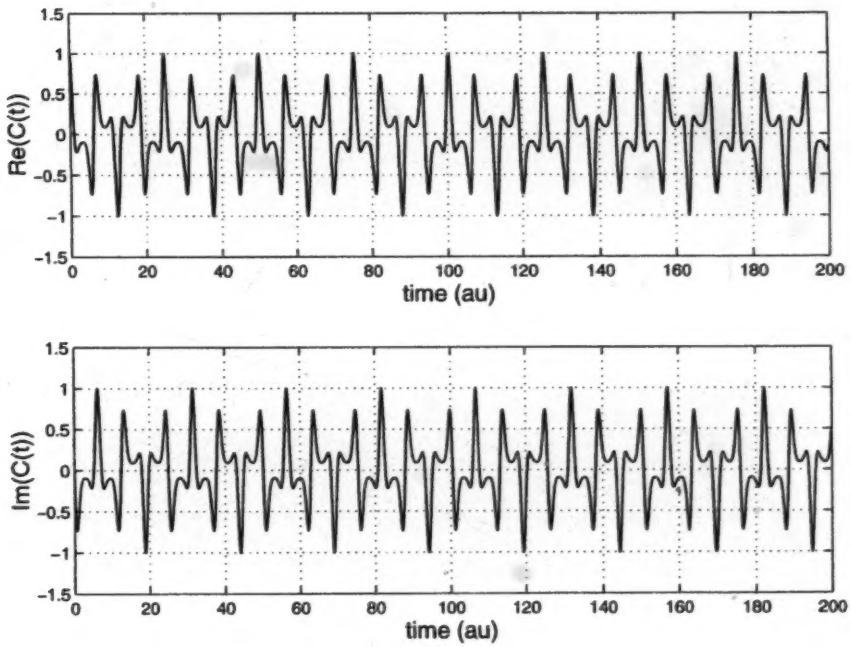

Figure 3.3: The HK-IVR autocorrelation function for two particles in a harmonic well.

molecular systems.

We begin by computing the exact quantum ACF for this system in the *bend* coordinate: the angle, θ, and its associated momentum, p_θ (Section 3.2.1). We proceed by establishing the HK-IVR in this coordinate (Section 3.2.2). Recall that this would be the "traditional" semiclassical procedure for this model. Finally, in Section 3.2.3, we will compute the HK-IVR ACF in Cartesian coordinates and compare results with the preceding two sections.

We use the potential of Polyansky, Jensen and Tennyson [40], implemented by the FORTRAN routine provided by the authors. It is a full potential defined over all configuration space, defined in terms of the curvilinear coordinates: $V(\theta, r_1, r_2)$. Figure 3.6 shows the relevant cross-section for the single dimension of our constrained subspace.

3.2.1 Exact quantum results

Exact quantum mechanical calculations were performed using the following Hamiltonian [41]:

$$\hat{H}(\theta; r_0) = -\frac{\hbar^2}{2}\frac{d}{d\theta}\left[\frac{2}{r_0^2}\left(\frac{1}{m_H} + \frac{1-\cos\theta}{m_O}\right)\right]\frac{d}{d\theta} + V(\theta; r_0)\ , \tag{3.17}$$

where m_O and m_H are the masses of oxygen and hydrogen, respectively. This has been adapted from the Eckart bond coordinates of [41] by setting r_1 and r_2 to their equilibrium value, r_0. The problem

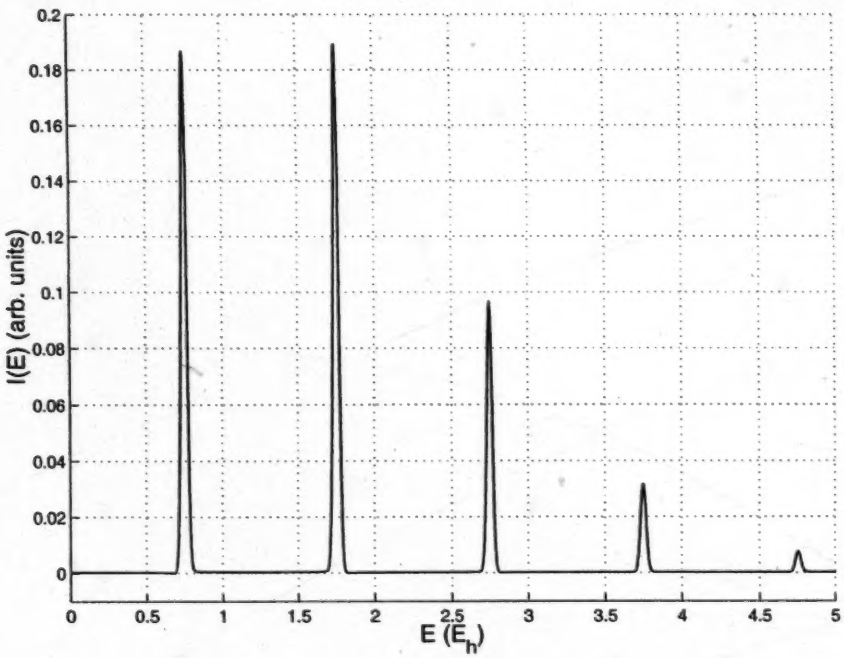

Figure 3.4: The HK-IVR power spectrum for two particles in a harmonic well.

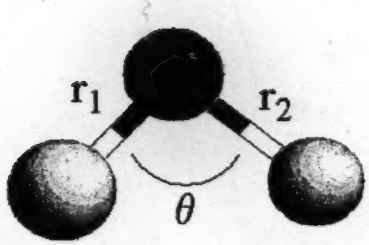

Figure 3.5: The curvilinear coordinate for water. The O-H bonds will be frozen by setting $r_1 = r_2 = r_0$.

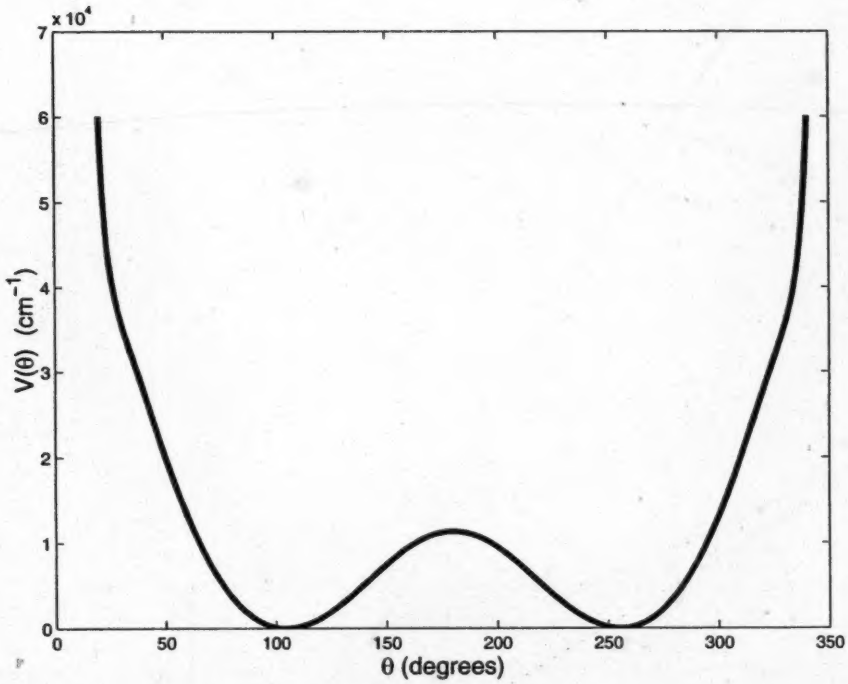

Figure 3.6: The 1D potential for the water-bender. O-H bonds are fixed at the equilibrium value, $r_0 = 0.958$ Å.

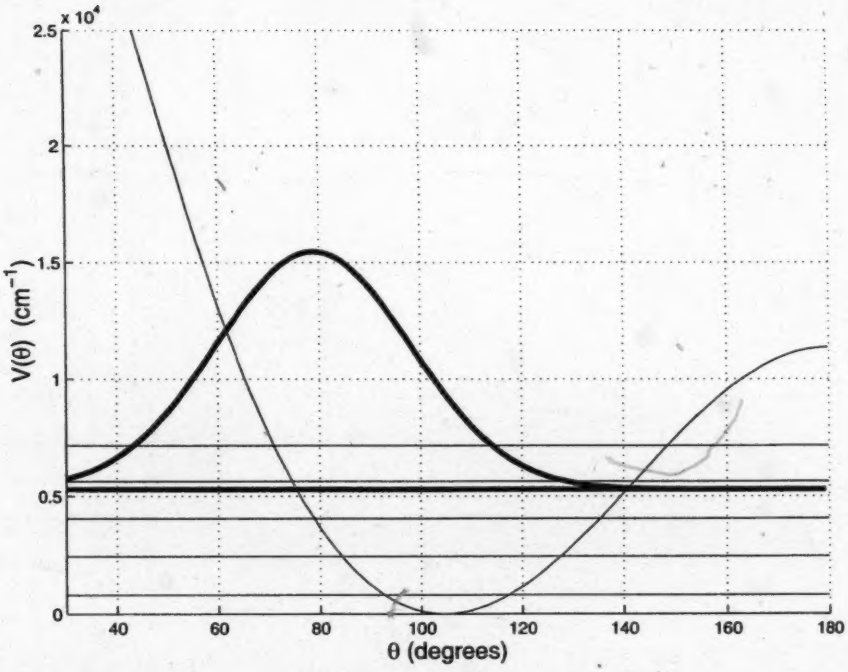

Figure 3.7: The 1D potential with first 5 energy levels. $|\Psi_0(\theta)|$ is shown as the bold curve, superimposed at a height $\langle\Psi_0|\hat{H}|\Psi_0\rangle = 5295.8\text{cm}^{-1}$.

is represented on a grid following the prescriptions of Wei and Carrington. [42] The Schrödinger equation is solved variationally in this representation to obtain energy levels and their associated wavefunctions. Various autocorrelation functions can subsequently be constructed. We chose our initial wavefunction, $|\Psi_0\rangle$, to be a coherent state of the form $|g^{\gamma}_{p_{e0}\theta_0}\rangle$ (this notation is used with reference to Equation 3.23).

Figure 3.7 shows the first 5 energy levels superimposed on our potential energy surface. The boldface curve indicates the GWP we have selected to represent the $t = 0$ state. The quantum ACF appears in Figure 3.8, and its corresponding power spectrum in Figure 3.9. The vertical lines in the power spectrum represent the computed eigenvalues and will be included in subsequent figures for assessing results visually. The numerical positions of the peaks are not presented until Section 3.2.3, where all results are summarised in Table 3.2. Notice that the energy spectrum for our water bender appears similar to the progression of a harmonic oscillator. The zero point energy is 808.0 cm^{-1}, and anharmonicity can be observed as a contraction of the peak spacing at higher energy levels.

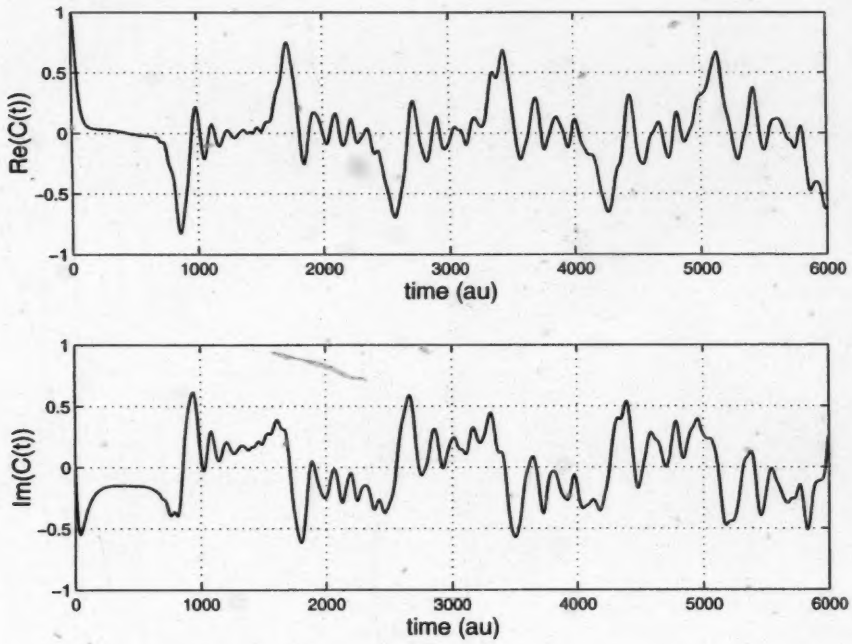

Figure 3.8: The quantum autocorrelation function for the 1D water-bender.

3.2.2 HK-IVR in curvilinear coordinates

Here, I present the approach for obtaining the ACF for our constrained water molecule in the "good" coordinates. This serves two purposes: first, to establish the level of accuracy for the HK-IVR in its usual implementation, and second, as an illustrative sample problem for how the HK-IVR is normally used. This will provide a lucent context for understanding how our method differs. The basic steps taken in the approaches of the following two sections are similar, and are enumerated here:

1. Get classical dynamics with constraints working:
   - choose a value for the timestep and ensure that energy is conserved.
   - choose a finite difference value for computing force.
   - ensure that the constrained bond lengths have numerically fixed values.
2. Select wavepacket width values (see Appendix E):
   - the width parameter is chosen small enough so that $C(t)$ has sufficient structure, yet large enough that the GWP's are well localised for accurate results.

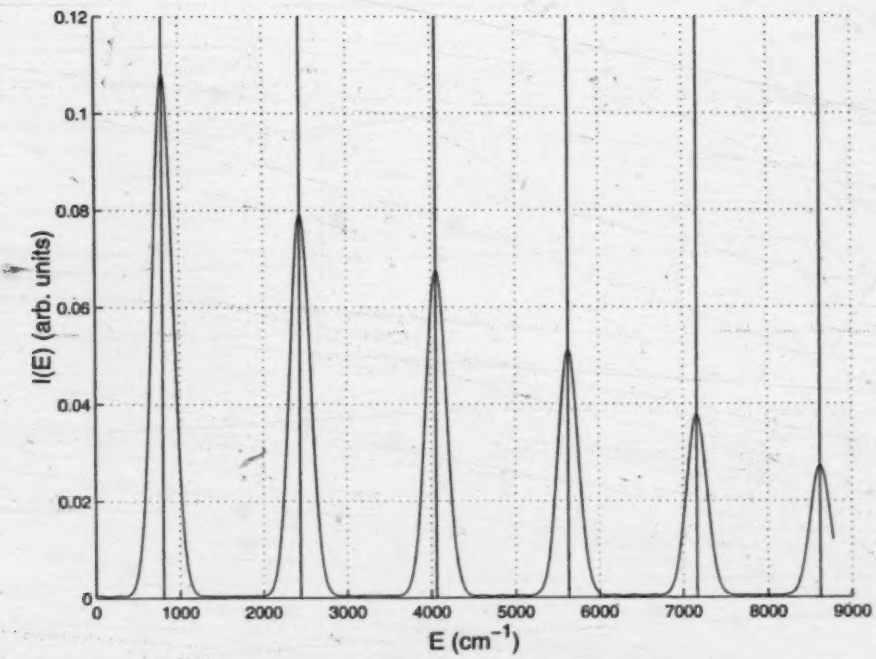

Figure 3.9: The quantum power spectrum for the 1D water-bender.

3. Get sampling procedure for initial conditions working:

   - initial conditions are written to file to be read in later as needed.
   - apply any measures to adjust initial conditions (*e.g.* placing centre of mass at origin, removing centre of mass translations, etc.).
   - inspect the distributions of $\mathbf{p}_i$ and $\mathbf{q}_i$.

4. Make sure that the overlaps of Equation (2.114) are computed correctly.

5. Make sure that the second derivatives of the potential are computed appropriately (recall that these are used in the evaluation of the HK-prefactor):

   - choose a suitable finite difference.
   - ensure that the Hessian matrix is properly mass-weighted.

6. Calculate $C(t)$ and its Fourier transform, $I(E)$:

   - make sure we are going for long enough times that accurate peak positions can be obtained.
   - make sure that our Monte Carlo average has converged.
   - apply a Gaussian window function to $C(t)$ prior to transforming.
   - obtain an accurate determination of the peak positions (*i.e.* the energy levels).

Equations of motion in curvilinear coordinates

It is trivial to obtain a classical Hamiltonian, once the quantum form is worked out. We simply replace $-i\hbar\frac{d}{d\theta}$ with the classical momentum, p_θ, in Equation (3.17) (the ordering in the kinetic energy operator is no longer an issue). Our classical Hamiltonian is therefore

$$H(p_\theta, \theta; r_0) = \frac{1}{2}\left[\frac{2}{r_0^2}\left(\frac{1}{m_H} + \frac{1-\cos\theta}{m_O}\right)\right] p_\theta^2 + V(\theta; r_0). \tag{3.18}$$

We would like to define the quantity in square brackets as $G(\theta)$[2],

$$G(\theta) = \frac{2}{r_0^2}\left(\frac{1}{m_H} + \frac{1-\cos\theta}{m_O}\right) . \tag{3.19}$$

G is, in general, a matrix of inverse masses in some curvilinear coordinate, as discussed in Wilson, Decius and Cross. [43] Its precise definition is complicated, however it is worked out for our water molecule in [43], and concurs with our present expression. Because we have only a single effective degree of freedom, our $G(\theta)$ is a scalar quantity.

[2]We are dropping the explicit reference to r_0 in our arguments

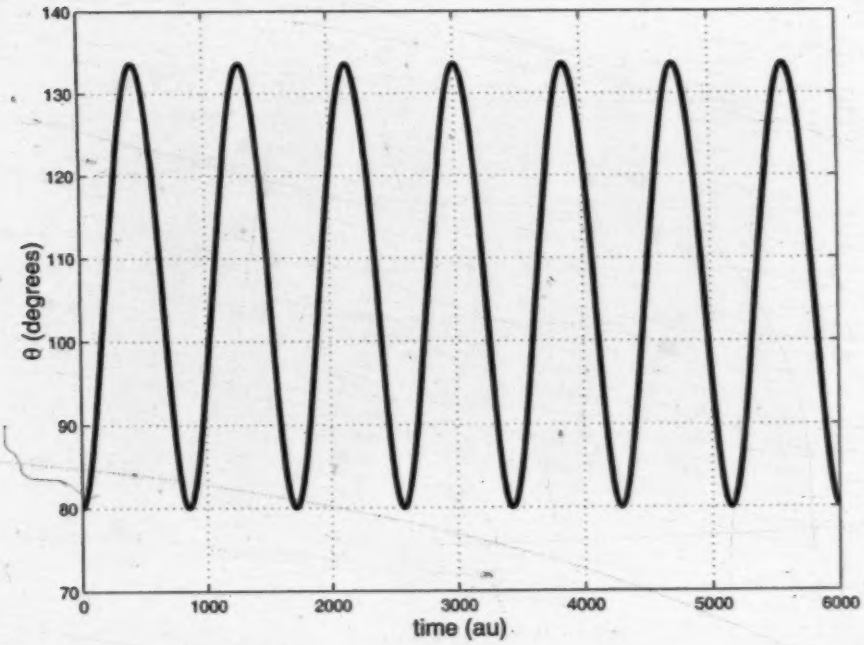

Figure 3.10: A sample trajectory of the water-bender with initial conditions, $(p_{\theta 0} = 0, \theta_0 = 80°)$.

The equations of motion can now be evaluated by Hamilton's laws:

$$\begin{aligned} \dot{p}_\theta &= -\frac{\partial H}{\partial \theta} \\ &= -\left(\frac{p_\theta^2}{2} G'(\theta) + V'(\theta)\right) \\ &= \left(-\frac{\sin\theta}{m_O r_0^2}\right) p_\theta^2 - V'(\theta) \qquad (3.20) \\ \dot{\theta} &= \frac{\partial H}{\partial p_\theta} \\ &= G(\theta) p_\theta \,. \qquad (3.21) \end{aligned}$$

Conservation of energy can be verified by taking the time derivative of the Hamiltonian. Equations (3.20) and (3.21) are integrated using the 4^{th} order Runge-Kutta method [36], while forces are computed from the potential by finite difference. A sample trajectory was computed with initial conditions ($\theta_0 = 80°, p_{\theta 0} = 0$) in order to get an idea for the timescale of the bend (see Figure 3.10). On the basis of this trajectory, we selected the total time for semiclassical wave propagation to be 6000 au. We proceed to determine a suitable timestep for our classical trajectories. In Figure 3.11, we show this same trajectory, but where a number of different timestep values were used, and observe whether total energy is conserved. Although a timestep of 10 au appears to be adequate,

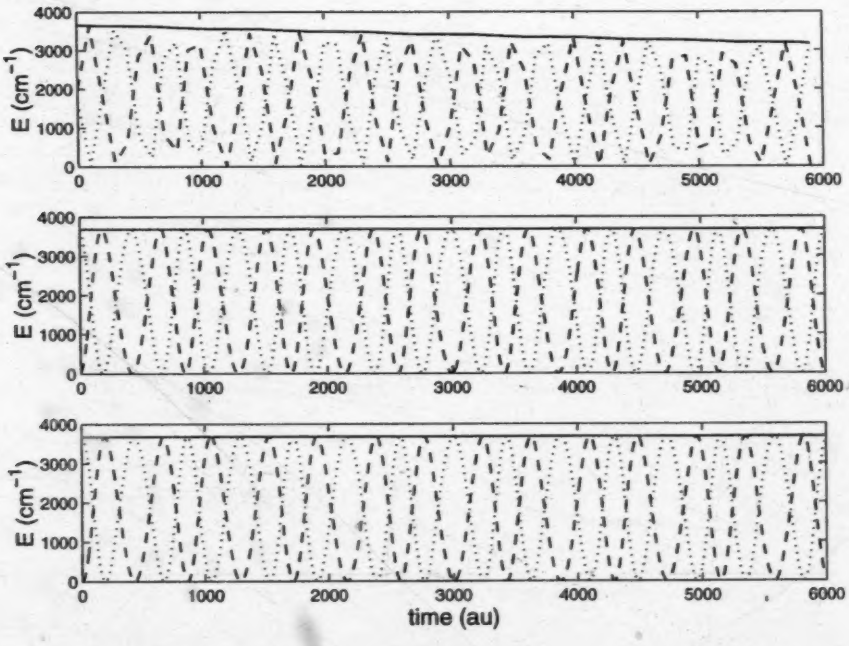

Figure 3.11: Determining a suitable timestep: looking at conservation of energy for a sample trajectory of the water-bender in 1D. In all figures, the dotted line is potential energy, the dashed line, kinetic energy, and the solid line is total energy. Top figure, dt = 100.0 au. Centre figure, dt = 10.0 au. Bottom figure, dt = 1.0 au. The timestep of the bottom figure was used for all trajectories computed subsequently.

a value of 1.0 au was used in subsequent calculations, "just to be safe". Conservation of energy can alternatively be observed from a *phase-space plot*. Here, the total energy is given by the area enclosed by the curve obtained when momentum is plotted against position. This plot (Figure 3.12) reassures us that this area is, in fact, constant as the water bender executes each period of its simple motion.

The semiclassical ACF

Now, we turn our attention to the precise form of the HK-IVR ACF for our one-dimensional problem:

$$C(t) = \int \mathrm{d}p_{\theta i} \int \mathrm{d}\theta_i e^{iS_t(p_{\theta i},\theta_i)/\hbar} R_t(p_{\theta i},\theta_i) \langle \Psi_0 | g^{\gamma}_{p_{\theta i},\theta_i} \rangle \langle g^{\gamma}_{p_{\theta i},\theta_i} | \Psi_0 \rangle \ . \tag{3.22}$$

Notice that we have not included a Jacobian factor in (3.22): we have not performed a change of variables, but instead simply use Equation (2.114) directly with our chosen coordinate. As outlined

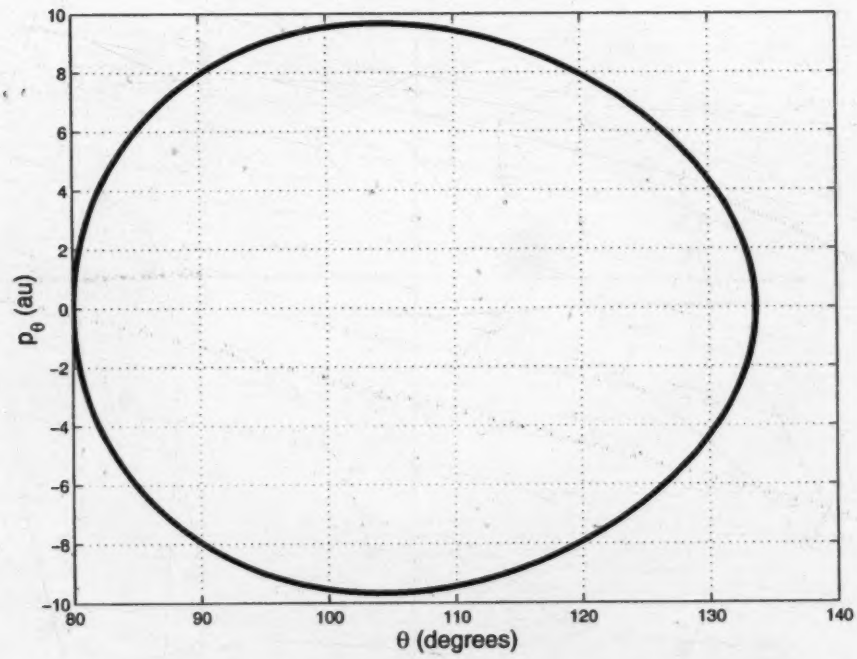

Figure 3.12: Phase-space plot for the water-bender in 1D.

in Section 2.7.2, we take our coherent states to be of the form

$$\langle\theta|g^{\gamma}_{p_{\theta i},\theta_i}\rangle = \left(\frac{\gamma}{\pi}\right)^{1/4} \exp\left[-\frac{\gamma}{2}(\theta-\theta_i)^2 + \frac{i}{\hbar}p_{\theta i}(\theta-\theta_i)\right] \tag{3.23}$$

$$\langle\theta|g^{\gamma}_{p_{\theta t},\theta_t}\rangle = \left(\frac{\gamma}{\pi}\right)^{1/4} \exp\left[-\frac{\gamma}{2}(\theta-\theta_t)^2 + \frac{i}{\hbar}p_{\theta t}(\theta-\theta_t)\right] . \tag{3.24}$$

Anticipating the Jacobian which will arise when evaluating the overlaps of (3.22), we take our initial wavefunction to be

$$\langle\theta|\Psi_0\rangle = \left(\frac{\gamma}{\pi}\right)^{1/4} \frac{1}{\sin\theta} \exp\left[-\frac{\gamma}{2}(\theta-\theta_0)^2 + \frac{i}{\hbar}p_{\theta 0}(\theta-\theta_0)\right] . \tag{3.25}$$

The overlap terms reduce to Gaussian integrals and are evaluated analytically:

$$\begin{aligned}
\langle g^{\gamma}_{p_\eta,\eta}|\Psi_0\rangle &= \int_0^{\pi} \sin\theta \mathrm{d}\theta \langle g^{\gamma}_{p_\eta,\eta}|\theta\rangle\langle\theta|\Psi_0\rangle \\
&\approx \int_{-\infty}^{+\infty} \sin\theta \mathrm{d}\theta \langle g^{\gamma}_{p_\eta,\eta}|\theta\rangle\langle\theta|\Psi_0\rangle \\
&= \sqrt{\frac{\gamma}{\pi}} \int_{-\infty}^{+\infty} \mathrm{d}\theta \exp\left\{-\frac{\gamma}{2}\left[(\theta-\eta)^2 + (\theta-\theta_0)^2\right] + \frac{i}{\hbar}\left[p_{\theta 0}(\theta-\theta_0) - p_\eta(\theta-\eta)\right]\right\} \\
&= \exp\left[-\frac{\gamma}{4}(\eta-\theta_0)^2 - \frac{1}{4\gamma}(p_\eta - p_{\theta 0})^2\right] \times \exp\left[\frac{i}{2\hbar}(p_\eta + p_{\theta 0})(\eta-\theta_0)\right] .
\end{aligned} \tag{3.26}$$

The approximation in the second step is justified so long as the GWP's are sufficiently localised in the interval $\theta \in (0,\pi)$. This may be verified, at least visually, by inspecting Figure 3.7. The wavefunction used in Figure 3.7 is identical to the one used here, except for the $(1/\sin\theta)$ term.

The first exponential in (3.26) is our Gaussian sampling function. It is removed from (3.22) (taking the appropriate normalisation factor with it), and is used to sample initial conditions from which the trajectories will be launched. The results of this sampling procedure are shown in Figures 3.13 and 3.14. An energy cutoff was then applied: initial conditions with energies larger than 10000cm^{-1} were discarded, as they tend to give rise to instability in the HK-prefactor propagation. This cutoff does not affect the results in a significant way. As our sampling function dictates, we obtain (roughly) Gaussian distributions in $p_{\theta i}$ and θ_i, with widths that are related by the reciprocal of the width, γ, in accordance with the Uncertainty Principle.

Heller's Primitive FGA

Before we describe the practical computation of the HK-prefactor, it is interesting to look at the energy levels calculated without it (*i.e.* with $R_t(p_{\theta i},\theta_i) = 1$). Recall that this is just Heller's ***primitive*** propagator, Equation (2.84). This ACF appears in Figure 3.15, and its transform in Figure 3.16. It is apparent that Heller's propagator fails utterly in capturing the quantum effect of zero point energy: the ground state energy is found to be 0. The spacing, however, seems to be acceptable when compared to the quantum results, although some of the anharmonicity in the progression is missed.

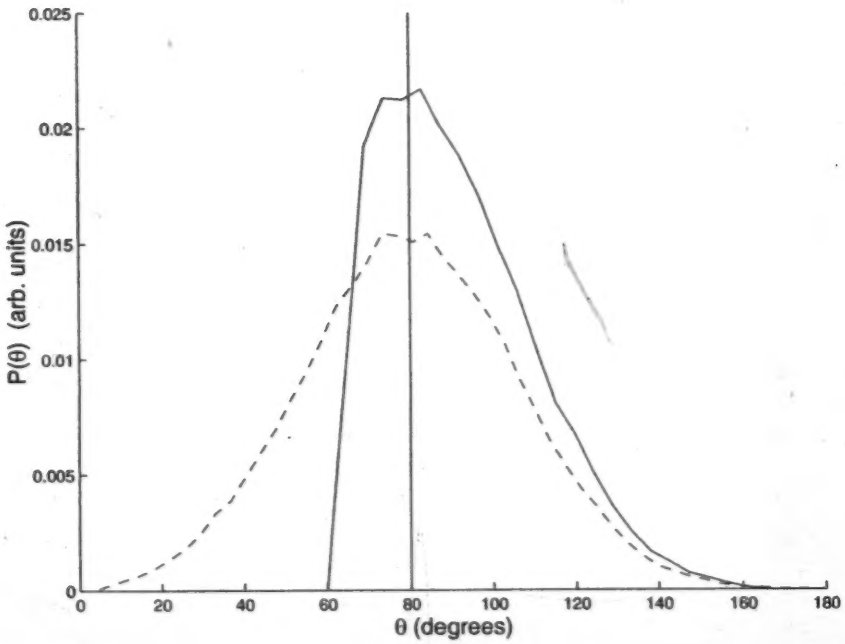

Figure 3.13: The distributions of θ sampled from $\theta_0 = 80°$ in angular coordinates using a wavepacket width, $\gamma = 10.0$. The solid line indicates the distribution when an energy cutoff was used ($E_{max} = 10000\text{cm}^{-1}$), while for the dashed line, there was no such cutoff. This figure was generated from 80000 sets of initial conditions.

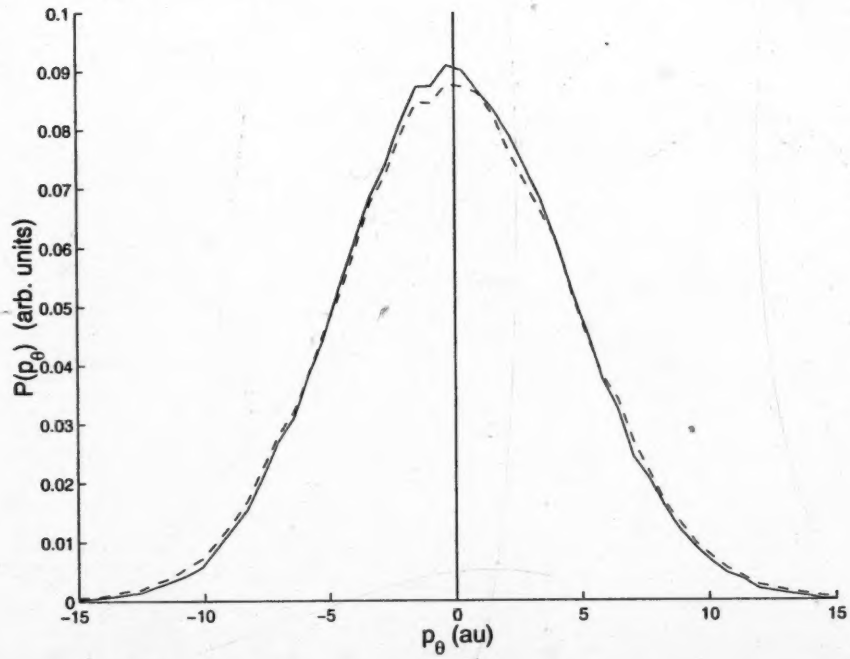

Figure 3.14: The distributions of p_θ sampled from $p_{\theta 0} = 0$ in angular coordinates using a wavepacket width, $\gamma = 10.0$. The solid line indicates the distribution when an energy cutoff was used ($E_{max} = 10000\text{cm}^{-1}$), while for the dashed line, there was no such cutoff. This figure was generated from 80000 sets of initial conditions.

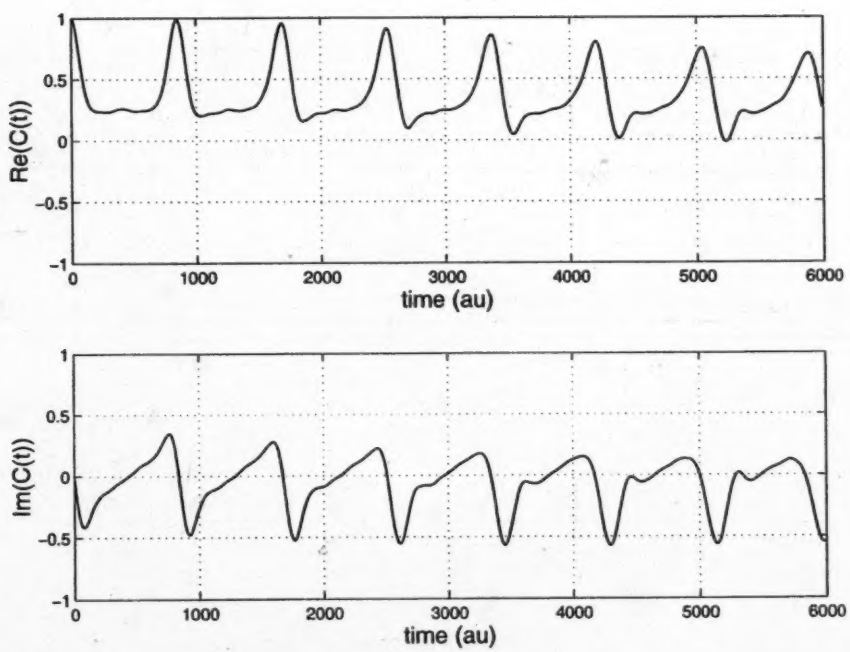

Figure 3.15: The primitive Heller autocorrelation function for the water-bender, calculated in 1D. This function was obtained from 4402 bound trajectories.

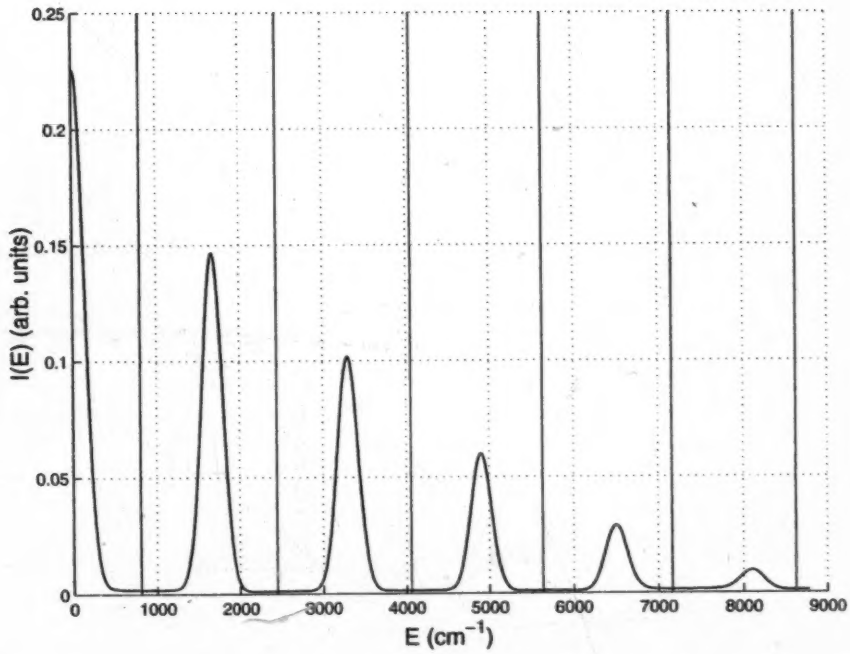

Figure 3.16: The primitive Heller power spectrum for the water-bender, calculated in 1D.

Evaluating the HK-prefactor

For the remainder of this section, we focus our attention on the evaluation of the HK-prefactor by two methods: one formally exact (Miller's log-derivative formulation [23], see Appendix F), and the other involving significant approximation to reduce computational cost (see Appendix F, also). These methods endeavour to solve (2.119), and I will leave the particulars to the appendix, except to say that they both require that the second derivative of the potential be computed in mass-weighted coordinates.

Now, recall that our potential depends on three internal coordinates: r_1, r_2 and θ. In our model, two of these have been frozen: $r_1 = r_2 = r_0$, and we must account for this in what is, in general, a 3×3 Hessian matrix. To do this, we turn to *projection methods*, *i.e.* the construction of a matrix which will remove modes of the Hessian matrix corresponding to motions along the frozen bonds. The projection matrix is used in conjunction with the mass-weighting procedure, so we will address this first.

In general, mass-weighting is coordinate-dependent (in Cartesian coordinates, it is trivial: see Equation 2.122). Here, we modify the Hessian matrix according to Wilson, Decius and Cross: by multiplication by the so-called *G-matrix* introduced near the beginning of this subsection. In our present coordinate, this matrix is: [43]

$$\mathbf{G} = \begin{pmatrix} \left(\frac{1}{m_H} + \frac{1}{m_O}\right) & \frac{1}{m_O}\cos\theta & -\frac{1}{m_O r_0}\sin\theta \\ \frac{1}{m_O}\cos\theta & \left(\frac{1}{m_H} + \frac{1}{m_O}\right) & -\frac{1}{m_O r_0}\sin\theta \\ -\frac{1}{m_O r_0}\sin\theta & -\frac{1}{m_O r_0}\sin\theta & \frac{2}{r_0^2}\left(\frac{1}{m_H} + \frac{1-\cos\theta}{m_O}\right) \end{pmatrix} . \tag{3.27}$$

We calculate our second derivative matrix, $\mathbf{F}$, as

$$\mathbf{F} = \frac{\partial^2 V}{\partial \mathbf{r} \partial \mathbf{r}} , \tag{3.28}$$

where $\mathbf{r} = (r_1, r_2, \theta)$. Mass weighting is then carried out:

$$\mathbf{F}^{mw} = \mathbf{G}\mathbf{F} . \tag{3.29}$$

In Figure 3.17, we present the three modes obtained by diagonalising $\mathbf{F}^{mw}$ (with $r_1 = r_2 = r_0$) for all possible values of θ. It is clear that the O-H stretches are generally much higher in energy than the bend. Furthermore, the bend mode becomes imaginary ($\omega^2 < 0$) for certain ranges of θ. This indicates the presence of a transition state near $\theta = 180°$, while the small "dip" around $\theta = 40°$ is a feature of the curvature of the potential (perhaps not physically relevant).

In the following section, the projection methods will be discussed in more detail. Here, it is enough to recognise that, because we are interested in the bend mode, and because this mode is precisely one of our present coordinates, projecting out r_1, r_2 motion simply involves picking off the

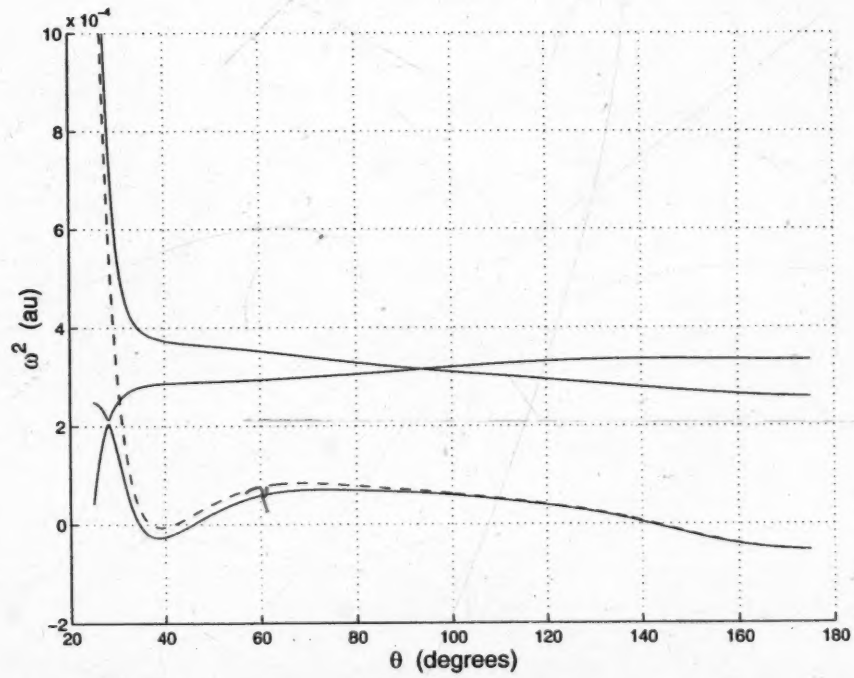

Figure 3.17: The square frequencies obtained by diagonalising **GF**. The dashed line corresponds to the bend mode in 1D, calculated as $G_{33}F_{33}$.

$(\mathbf{GF})_{33}$ term. It is easy to verify that an appropriate projection matrix, Δ, is

$$\Delta = \begin{pmatrix} 0 & 0 & 0 \\ 0 & 0 & 0 \\ 0 & 0 & 1 \end{pmatrix} . \tag{3.30}$$

That is, by diagonalising $(\Delta\mathbf{G}\Delta)\cdot(\Delta\mathbf{F}\Delta)$, we obtain the two zero-modes and our bend. In practice, it is of course simpler to obtain the square-frequency of this mode as

$$\kappa_t = G_{33}\left(\frac{\partial^2 V}{\partial\theta^2}\right) . \tag{3.31}$$

Now, we are ready to address the propagation of the HK-prefactor. We begin by using the formally exact log-derivative formulation, and proceed to investigate the cost to our accuracy associated with adopting a more approximate (*i.e.* less computationally demanding) form. In essence, the log-derivative formulation is equivalent to propagating the monodromy matrix by the auxiliary equations, (2.128), with initial conditions $\mathbf{M}_{t=0} = \mathbf{1}$, and computing the prefactor as (2.119). Although, in [23], Miller claims that his method avoids the ***branch-cut problem***, in which there is some ambiguity about choosing the correct sign when taking the root of a complex number, we found it necessary to keep track of the real and imaginary parts of the determinant of (2.119), in order to keep $R_t(p_{\theta i}, \theta_i)$ a continuous function of time.

The final expression

So, the prefactor is added to Heller's primitive ACF, giving the HK-IVR. Previously sampled initial conditions are propagated and the integrand, $I_t(\mathbf{p}_i, \mathbf{q}_i)$, is averaged into a current estimate for $C(t)$ at the end of each trajectory. Figure 3.18 shows the convergence of this average, made with comparison to the quantum ACF. The computation of $C(t)$ is halted when additional trajectories appear to be having no noticeable effect on the current result. This "converged" result and its corresponding spectrum are shown in Figures 3.19 and 3.20. Figures 3.21 and 3.22 contain the same results, but when the "Johnson's multichannel WKB approximation" [23] to the prefactor (of Appendix F) is employed. We draw the conclusion that this approximate form gives gives better line-shape, and no significant difference in accuracy in the energy levels. Therefore, from this point on, the prefactor is computed solely by this method.

3.2.3 HK-IVR in Cartesian coordinates

Finally, we are ready to present the development of our new method (*i.e.* so far we have done nothing novel). Again, our goal is to solve Equation (2.114) for a constrained system in Cartesian coordinates. We rewrite (2.114) here, and indicate that quantities are constrained by adding the superscript, c:

$$C(t) = \left(\frac{1}{2\pi\hbar}\right)^N \iint \mathrm{d}\mathbf{p}_i^c \mathrm{d}\mathbf{q}_i^c R_{\mathbf{p}_i^c\mathbf{q}_i^c t} \exp\left(\frac{i}{\hbar} S_{\mathbf{p}_i^c\mathbf{q}_i^c t}\right) \langle\Psi_0|g^\gamma_{\mathbf{p}_i^c\mathbf{q}_i^c}\rangle\langle g^\gamma_{\mathbf{p}_i^c\mathbf{q}_i^c}|\Psi_0\rangle . \tag{3.32}$$

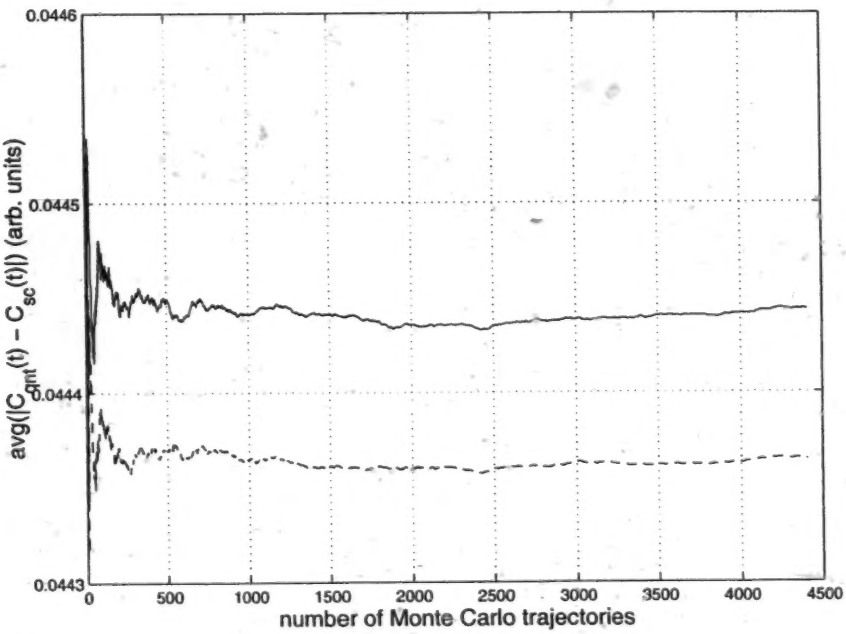

Figure 3.18: The convergence of the HK-IVR autocorrelation function for the water-bender in 1D. The origin of the vertical axis corresponds to exact agreement with the corresponding quantum results. The dashed line corresponds to the ACF with the exact expression for the HK-prefactor, while the solid line was produced by the ACF with the approximate prefactor.

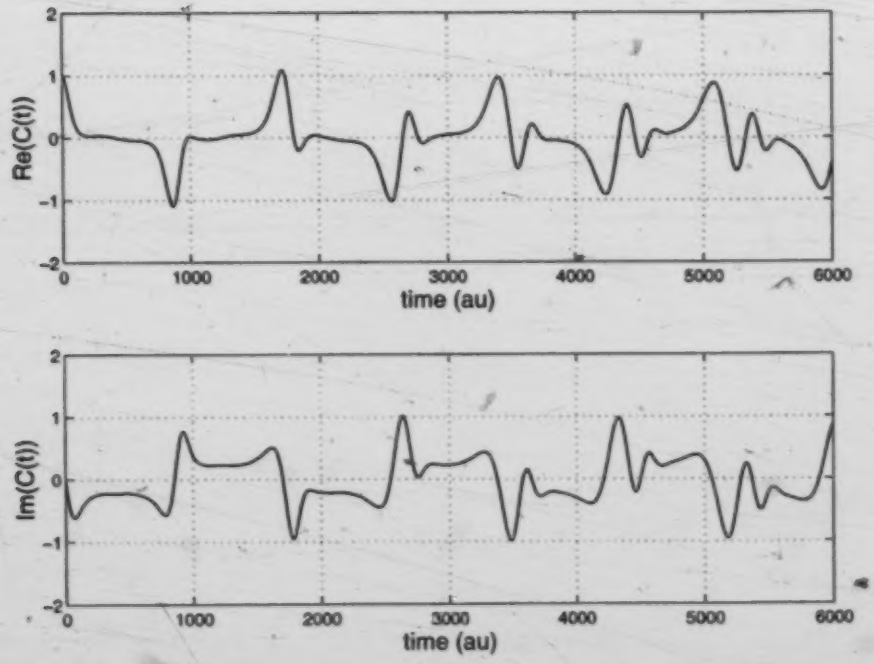

Figure 3.19: The HK-IVR autocorrelation function for the water-bender calculated in 1D using the exact expression for the prefactor. This function was obtained from 4402 bound trajectories.

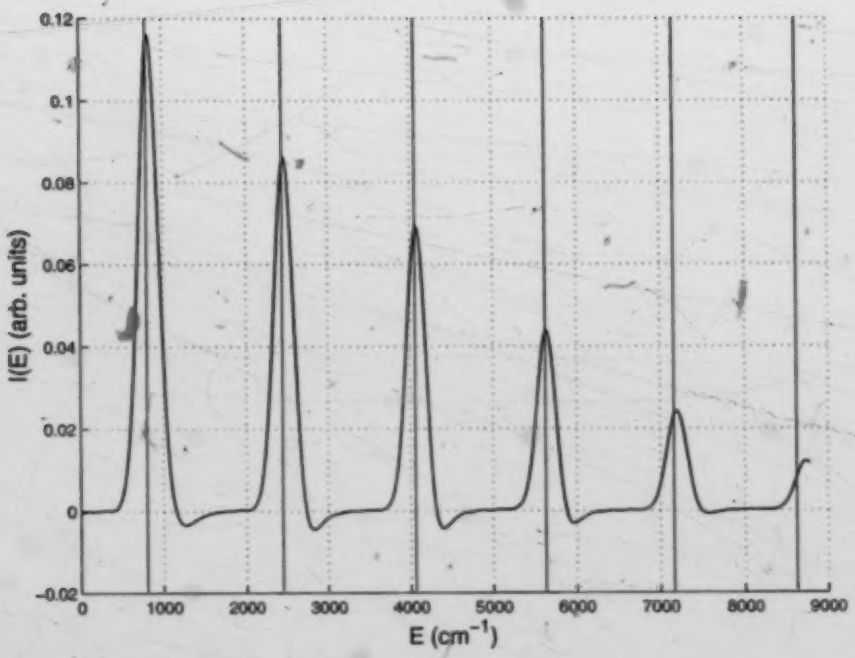

Figure 3.20: The HK-IVR power spectrum for the water-bender calculated in 1D using the exact expression for the prefactor.

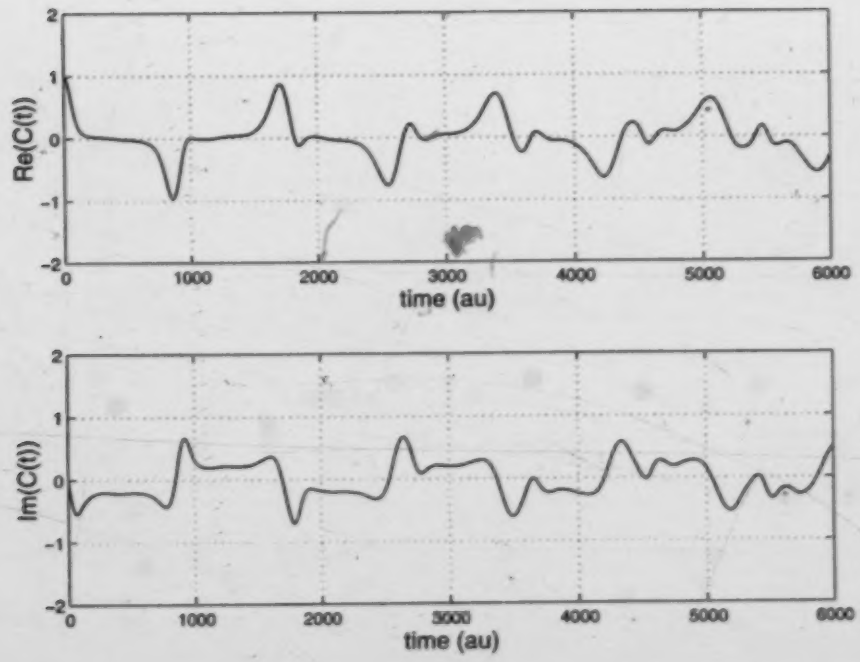

Figure 3.21: The HK-IVR autocorrelation function for the water-bender calculated in 1D using the "multichannel-WKB" approximation to the prefactor. This function was obtained from 4402 bound trajectories.

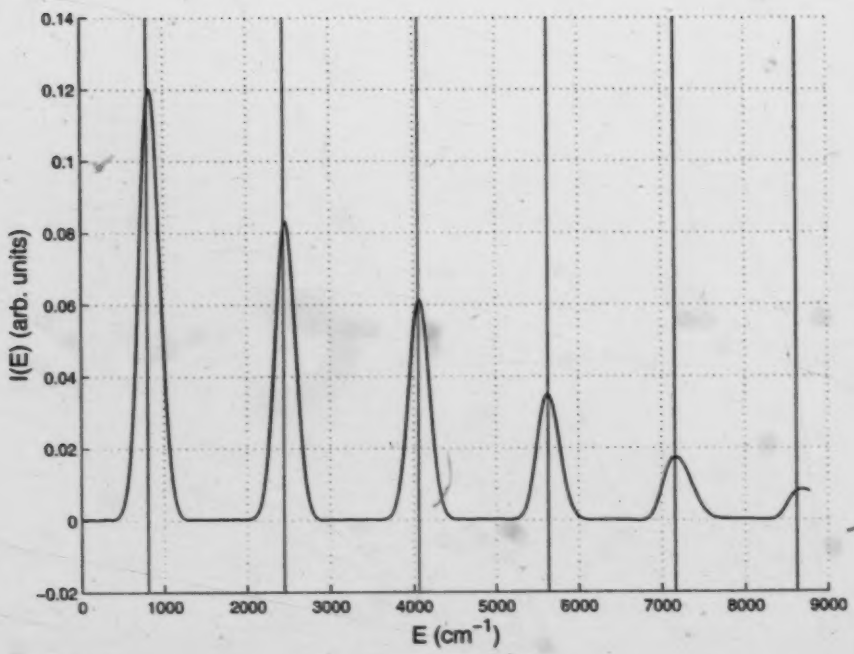

Figure 3.22: The HK-IVR power spectrum for the water-bender calculated in 1D using the "multichannel-WKB" approximation to the prefactor.

The presence of our constraints will certainly have an effect on the value of the normalisation for the set of coherent states, $(2\pi\hbar)^{-N}$. Because we do not actually compute this "pre-prefactor" anywhere (we instead renormalise $C(t)$), we have not worked out what it should be.

There are three principal challenges introduced by including the superscripts in (3.32). First, we must integrate the constrained classical equations of motion in Cartesian coordinates. This is handled by the Rattle algorithm and a discussion of the implementation and performance of this routine is discussed below. Second, we must modify the method for evaluating the HK-prefactor to account for our constraints. Again, this is done by constructing a projection matrix to remove all constrained motions from our Hessian, as it enters in Equation (2.128). Finally, we must be careful to integrate over the full region of phase-space in which the constraints are satisfied. That is, our implementation of the Monte Carlo sampling of initial conditions must be modified. Our initial wavefunction is chosen as $|\Psi_0\rangle = |g^{\gamma}_{\mathbf{p}_0\mathbf{q}_0}\rangle$.

The constrained equations of motion

Here we present the essence of the Rattle algorithm. [39] We want to solve Newton's law of motion,

$$m_i\ddot{\mathbf{q}}_i = \mathbf{F}_i \,, \tag{3.33}$$

for each atom as it executes its classical trajectory. Here, m_i is the mass of atom i, and $\mathbf{q}_i$ and $\mathbf{F}_i$ are its position and force in Cartesian coordinates (they are three-dimensional vectors). We want to apply "bond" constraints, that is, holonomic constraints of the form:

$$\sigma_k^{ij}(\mathbf{q}) = (\mathbf{q}_i - \mathbf{q}_j)^2 - d_{ij}^2 = 0 \,. \tag{3.34}$$

This constraint (labeled k) indicates that the distance between atoms i and j is fixed to d_{ij}. An additional force is needed in (3.33) to ensure that the complete set of these constraints, σ, is satisfied (*i.e.* $\sigma = 0$) at each timestep. We temporarily call this force $\mathbf{g}$, such that

$$\mathbf{m}\ddot{\mathbf{q}}^c = \mathbf{F} + \mathbf{g} \,. \tag{3.35}$$

Now, $\mathbf{m}$ is a diagonal matrix of masses (since we are in Cartesian coordinates), and $\mathbf{q}^c$ is the full configuration of the molecular system, subject to $\sigma = 0$. Deriving the Lagrangian equations of motion leads to the following particular form for $\mathbf{g}$: [4]

$$\mathbf{g} = \sum_{k=1}^{\text{constraints}} \left(-\lambda_k \frac{\partial \sigma_k}{\partial \mathbf{q}}\right) \,, \tag{3.36}$$

where λ_k is the (undetermined) Lagrangian multiplier corresponding to σ_k. These multipliers are calculated iteratively by the Rattle routine. Rattle combines the constraint force with the force derived from the potential, and integrates the classical trajectory by a method equivalent to Velocity

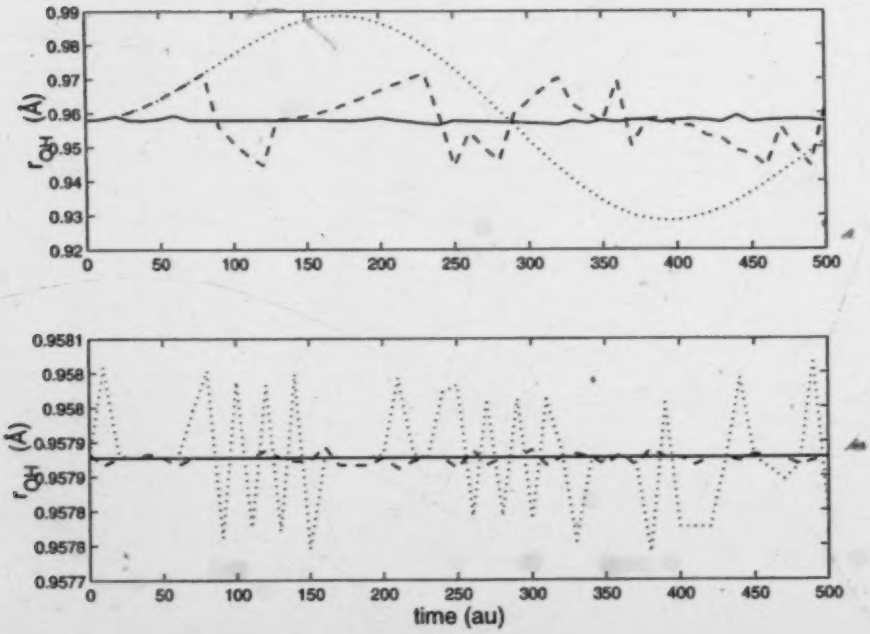

Figure 3.23: The effect of the value of the tolerance on Rattle's ability to hold the O-H bond length to the constrained value ($r_0 = 0.957927$ Å) over a sample trajectory. In the upper figure, the dotted line corresponds to a tolerance of 1.0, the dashed line, 0.1, and the solid line, 0.01. In the lower figure, the dotted line corresponds to a tolerance of 1×10^{-3}, the dashed line, 1×10^{-4}, and the solid line, 1×10^{-5}. A tolerance value of 1×10^{-6} was used in subsequent calculations.

Verlet, making sure that each element of $\sigma(\mathbf{q})$ is smaller than some *tolerance* at the end of each timestep. This is done in two stages. First, the constraint force is adjusted so that the constraints will be satisfied at the end of the timestep. Second, the momenta are adjusted to ensure that atomic motions are orthogonal to any rigid bonds connecting them.

Figure 3.23 shows the O-H bond distance as it fluctuates along a sample trajectory. It is observed that as the tolerance is made increasingly stringent, the closer this value is, on average, to r_0. A tolerance value of 1×10^{-6} was selected on this basis. That is, for each timestep, Rattle continues its iterations until

$$\begin{aligned} (r_1 - r_0)^2 &< 1 \times 10^{-6} \text{ au} , \\ \text{and } (r_2 - r_0)^2 &< 1 \times 10^{-6} \text{ au} . \end{aligned}$$

The number of iterations taken per timestep (over a short sample trajectory) is presented in Figure 3.24, and those performed to remove the undesirable components of the velocity, in Figure 3.25.

We can check to ensure that our implementation of the Rattle algorithm is, in fact, correct

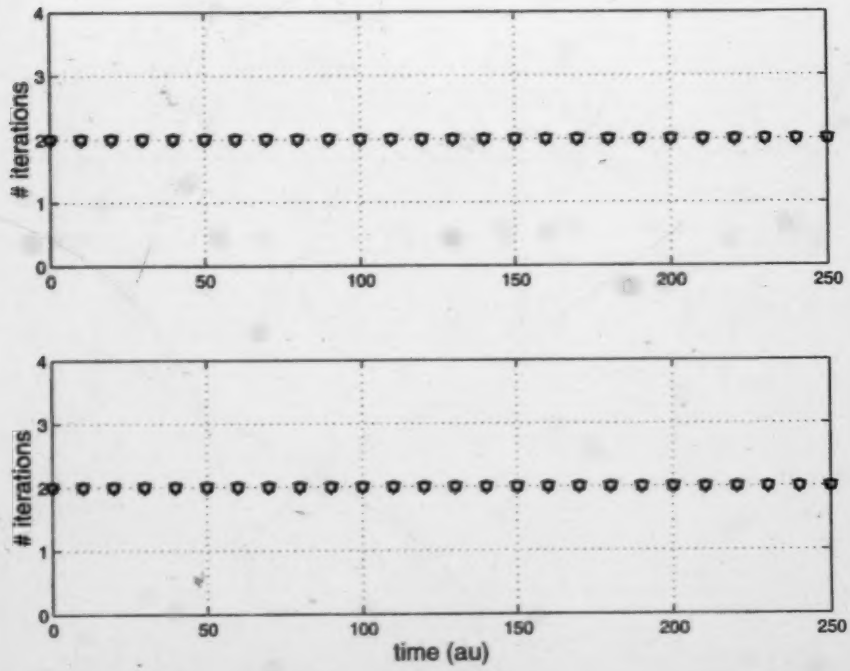

Figure 3.24: The number of iterations used by Rattle to apply the contraints to the molecular configuration as a function of time, over a short sample trajectory. This figure shows the relationship between the number of these iterations and the value of the tolerance. In the upper figure, the circles correspond to a tolerance of 1.0, the squares, 0.1, and the triangles, 0.01. In the lower figure, the circles correspond to a tolerance of 1×10^{-3}, the squares, 1×10^{-4}, and the triangles, 1×10^{-5}. Notice that as the tolerance is decreased, more iterations (on average) are required.

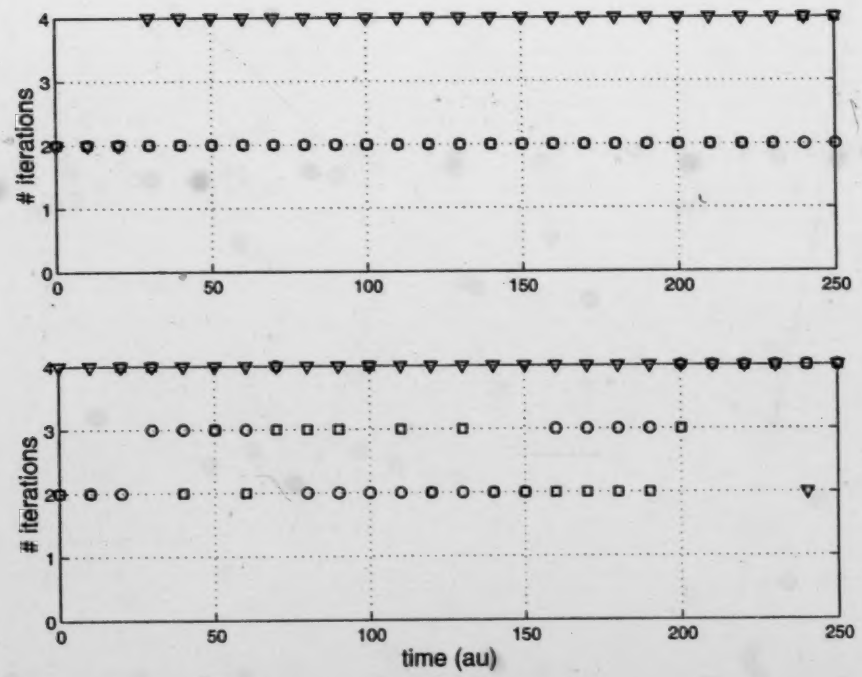

Figure 3.25: The number of iterations used by Rattle to apply the contraints to the velocities as a function of time, over a short sample trajectory. This figure shows the relationship between the number of these iterations and the value of the tolerance. The tolerance values and associated symbols match with the preceeding figure. Notice that as the tolerance is decreased, more iterations (on average) are required.

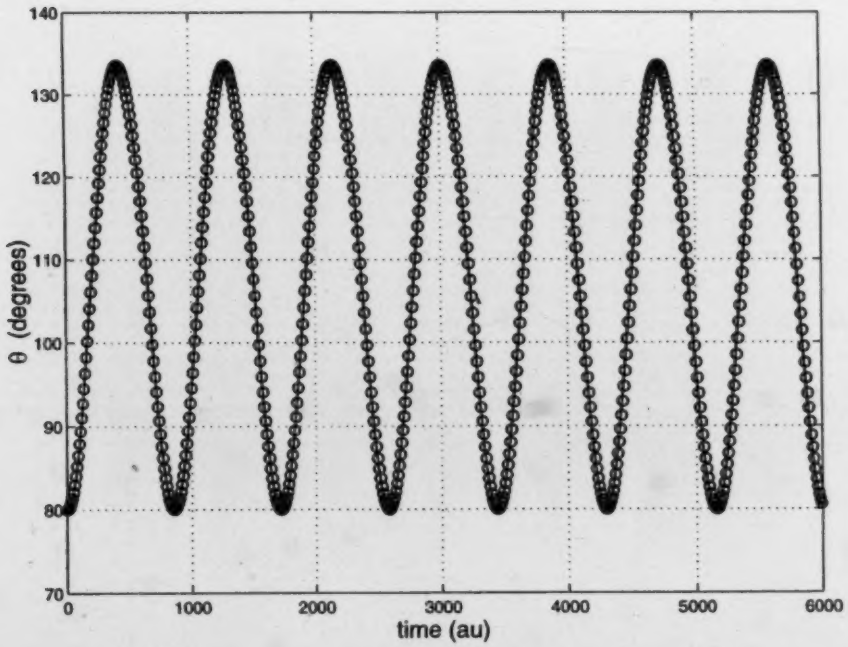

Figure 3.26: A comparison of a trajectory obtained by integrating the angular equations of motion (the solid line) with the corresponding trajectory calculated in Cartesian coordinates by Rattle (the circles). The initial conditions are ($p_{\theta 0} = 0, \theta_0 = 80°$) and a tolerance of 1×10^{-6} was used.

by comparing to the trajectories obtained in the previous section. Figure 3.26 confirms that no significant discrepancy is visible. And just to be certain, the classical actions computed along this trajectory by both methods was verified to be equivalent also (Figure 3.27).

Evaluating the integral: sampling initial conditions

Here, we confront the issue of correct evaluation of the integrals in (3.32). Recall that our sampling function,

$$f(\mathbf{p}_i, \mathbf{q}_i; \mathbf{p}_0, \mathbf{q}_0) = \left(\frac{1}{4\pi}\right)^N \exp\left[-\frac{1}{4}\gamma(\mathbf{q}_i - \mathbf{q}_0)^2 - \frac{1}{4\hbar^2}\gamma^{-1}(\mathbf{p}_i - \mathbf{p}_0)^2\right] , \tag{3.37}$$

was taken from the overlap, $\langle g^{\gamma}_{\mathbf{p}_i\mathbf{q}_i}|\Psi_0\rangle$. Initial conditions sampled directly from this distribution will almost certainly not satisfy our constraints. Formally, we would like to screen these initial conditions with our Dirac delta functions, $\delta(\sigma)$. In practice, however, this would be exceedingly toilsome. The probability of selecting initial conditions which happen to satisfy our constraints to a tolerance on the order of 10^{-6} au is very small indeed. Furthermore, we are only interested in one of the three *internal* coordinates. We have not yet made mention of the six degrees of freedom associated with the centre of mass. That is, even after our internal coordinates check out, we should

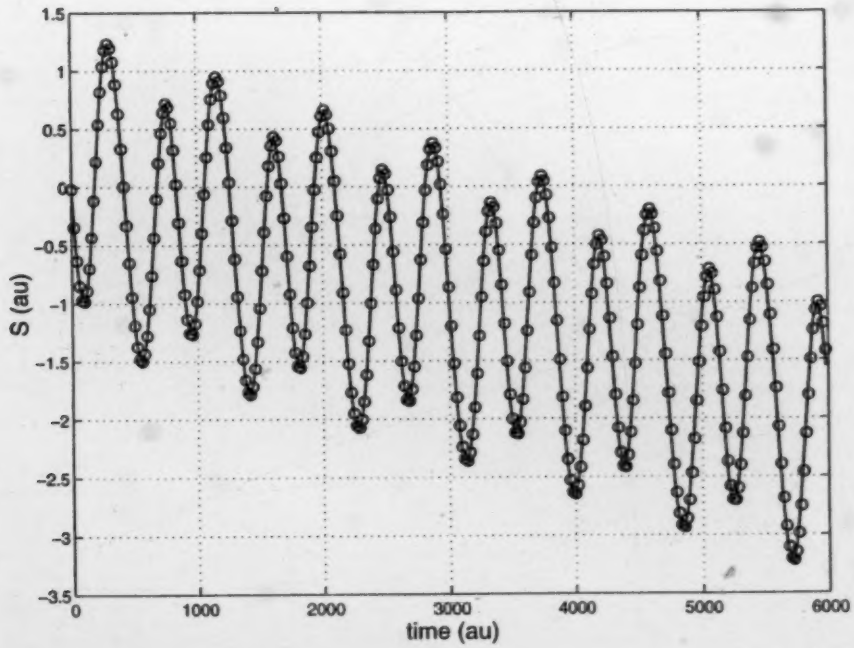

Figure 3.27: A plot of the action calculated along a trajectory with initial conditions ($\theta_0 = 80.0°, p_{\theta 0} = 0.0$). For the solid line, the dynamics were performed in angular coordinates, and the circles, in Cartesian coordinates.

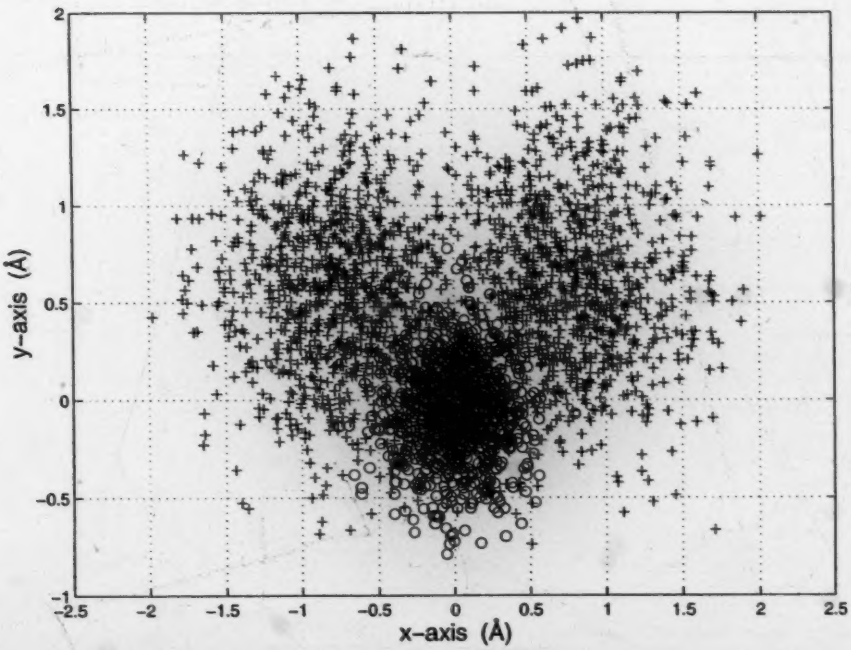

Figure 3.28: A "top view" of the distribution of configurations initially sampled (*ie.* they don't obey the constraints). The hydrogens are depicted by crosses and the oxygens, by circles. Configurations were sampled about $\theta_0 = 80°$ with wavepacket widths, $(\gamma_H = 2.868, \gamma_O = 9.807)$. 1000 sets of initial conditions are represented.

apply yet another delta function in order to remove centre-of-mass translations and rotations.

We propose an *ad hoc* method for obtaining suitable initial conditions, and compare the distributions obtained to those of Section 3.2.2. As a point of reference, Figures 3.28 and 3.29 are plots of the configurations and momenta sampled directly from (3.37). Notice that these results are consistent with the Uncertainty Principle; the reciprocal nature of the $\mathbf{p}$ and $\mathbf{q}$ distributions is observed (recall that coherent states are minimum-uncertainty wavepackets).

Taking these initial conditions as a starting point, we first shift the centre of mass to the origin (which should have no effect on anything). Next, instead of discarding the initial conditions which violate our constraints, we "repair" them by applying a single Rattle timestep. Finally, we remove centre-of-mass motions. Removing net translation is trivial, so I will just describe the method for removing rigid-body rotations. To do this, we first compute the total angular momentum, $\mathbf{L}$, by:

$$\mathbf{L} = \sum_{j=1}^{\text{atoms}} m_j(\mathbf{r}_j \times \mathbf{v}_j) \,, \tag{3.38}$$

where $\mathbf{r}_j$ and $\mathbf{v}_j$ are the three-dimensional position and velocity vectors for atom j. Next, we find

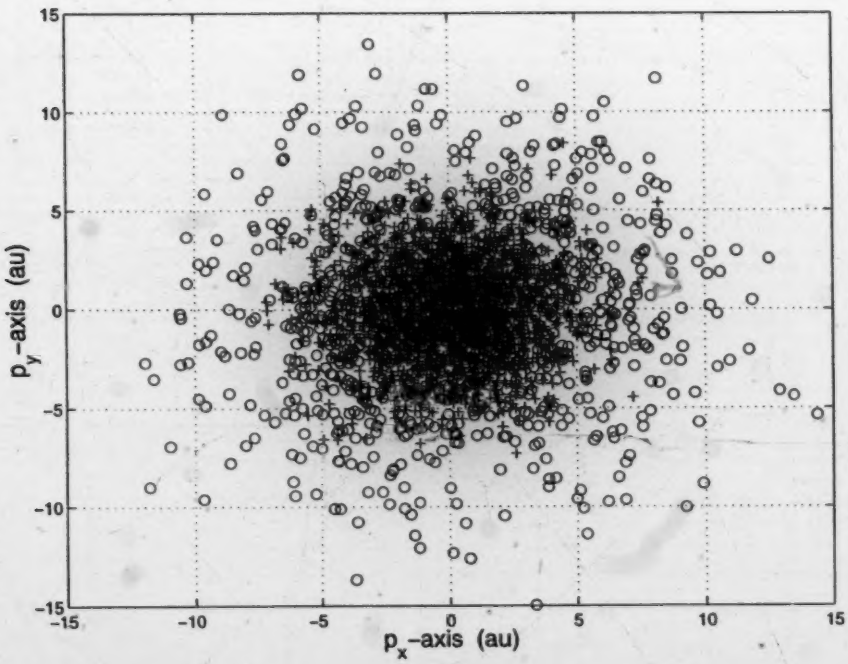

Figure 3.29: A "top view" of the distribution of momenta initially sampled (*i.e.* they do not obey the constraints). The momenta associated with the hydrogens are depicted by crosses and those of the oxygens, by circles. Momenta were sampled about $p_{\theta 0} = 0$ with wavepacket widths, $(\gamma_H = 2.868, \gamma_O = 9.807)$. 1000 sets of initial conditions are represented.

the total angular velocity, ω, in terms of $\mathbf{L}$ and the 3×3 inertial tensor, $\mathbb{I}$: [29]

$$\omega = \mathbb{I}^{-1}\mathbf{L} \, . \tag{3.39}$$

Subtracting this angular velocity from each atom, according to

$$\mathbf{v}_j = \omega \times \mathbf{r}_j \, , \tag{3.40}$$

leads to an expression for the new velocity of atom j in terms of the old:

$$\begin{aligned} \mathbf{v}_j^{\text{new}} &= \mathbf{v}_j^{\text{old}} - (\omega \times \mathbf{r}_j) \\ &= \mathbf{v}_j^{\text{old}} - \left(\mathbb{I}^{-1}\mathbf{L} \times \mathbf{r}_j\right) \, . \end{aligned} \tag{3.41}$$

These new velocities will give $\mathbf{L} = \mathbf{0}$, by (3.38). Our hope is that the distribution which is obtained from the above procedure will be sufficiently similar to one where the delta functions are applied.

Figure 3.30 gives a "top view" of the set of configurations obtained. Because we have shifted the centre of mass back to the origin, it is difficult to comment on how localised the oxygen is, for example. We do observe, however, that the O-H bonds all have length, r_0; the hydrogens within the outer circle are simply not on the xy-plane.

Figure 3.31 shows that the momentum distribution has also been significantly changed: our initial conditions have considerably less kinetic energy than they did initially. Figure 3.32 shows how the distribution of kinetic energy (over the initial conditions) changes at various stages of the above procedure. The most profound change in this distribution is observed after the rotations are removed: the distribution is now centred on zero.

It is interesting to compare these distributions with those obtained in the curvilinear coordinates of Section 3.2.2, since ultimately we will be comparing their corresponding ACF's. This comparison appears in Figures 3.35 and 3.36. The results are very encouraging, given the "make-it-up-as-you-go" nature of our sampling scheme.

Now that we have generated a large set of acceptable initial conditions, we turn our attention to the final significant obstacle: the evaluation of the HK-prefactor. As yet another reference point, Figures 3.37 and 3.38 show the ACF and power spectrum we are able to calculate at this stage: everything in 9D except the HK-prefactor, which is computed in 1D by determining p_θ and θ from the Cartesian positions and momenta. We could register minor complaints about this result: sharp oscillations in our ACF occurring near 5000 au leads to a poor line-shape in our spectrum, and it is presently unclear to me why this should be. The zero point energy is captured to respectable accuracy, though, and the spacing of the peaks is approximately correct.

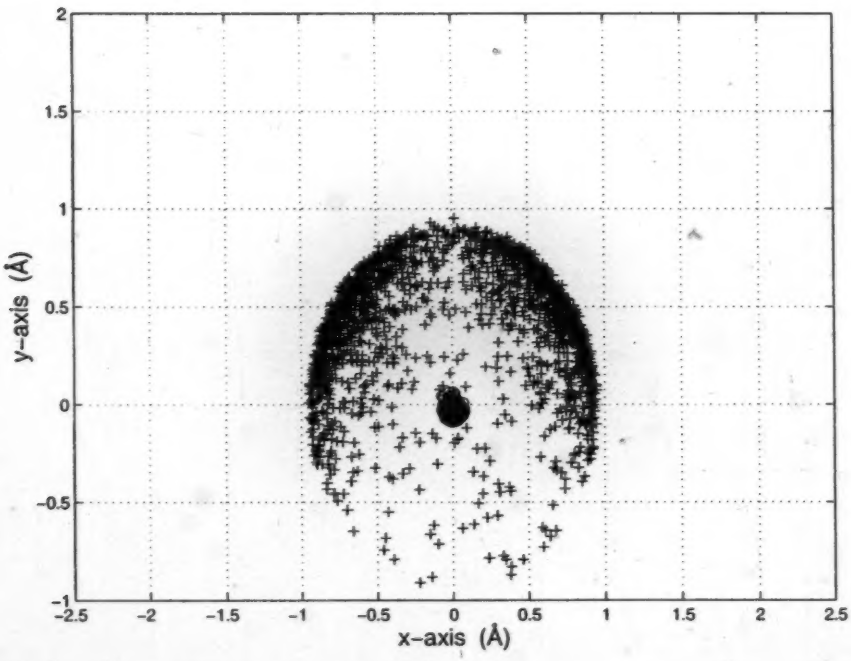

Figure 3.30: The distribution of initial configurations, after the application of Rattle and removal of centre-of-mass motions.

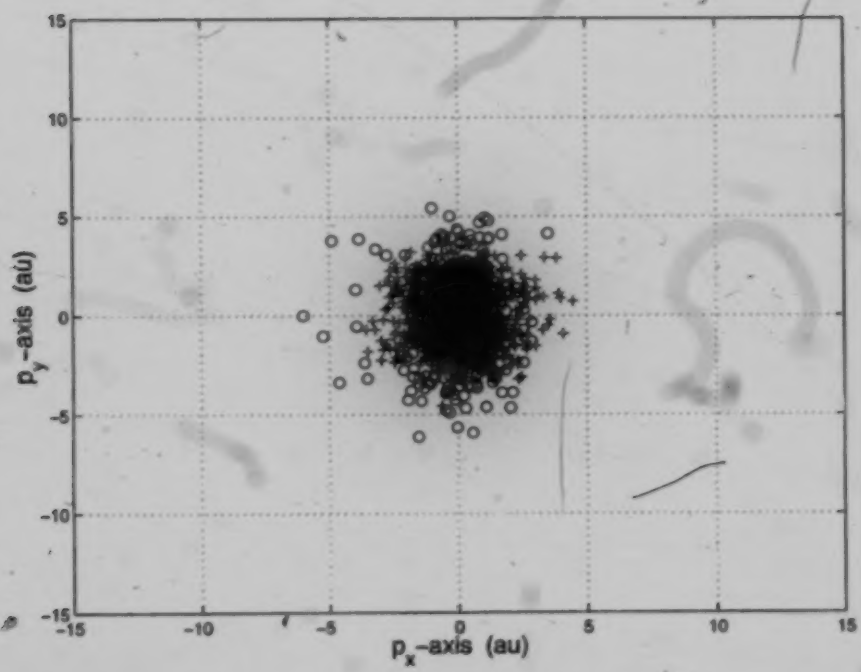

Figure 3.31: The distribution of initial momenta, after the application of Rattle and removal of centre-of-mass motions.

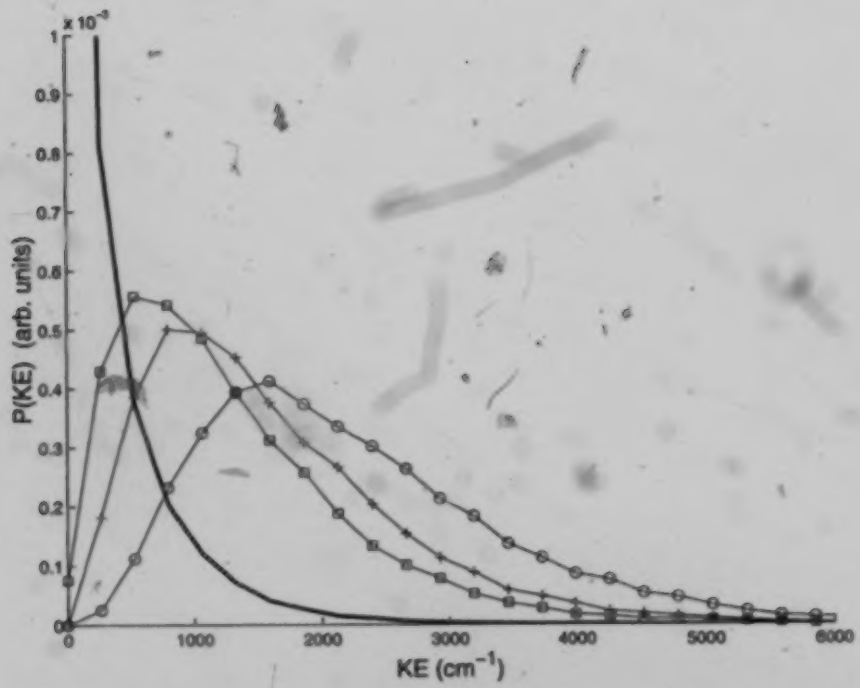

Figure 3.32: The distributions of kinetic energy of the initial conditions (sampled in Cartesian coordinates) at the different stages of preparation. The distribution directly sampled is shown with circles, after the application of Rattle in crosses, after removing translations in squares, and the distribution (not completely shown) after removing rigid-body rotations is shown as the bold solid line. These plots were obtained from 80000 sets of initial conditions.

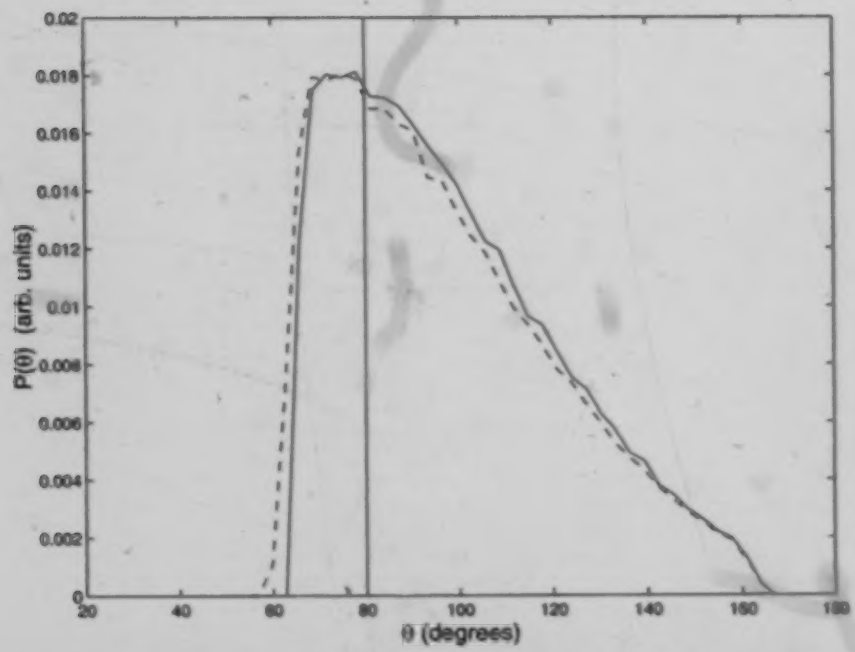

Figure 3.33: The distributions of θ sampled from Ψ_0 in Cartesian coordinates. The dashed line is the distribution obtained from coordinates sampled directly (subject to an energy cutoff, E_{max} = 10000cm^{-1}), while the solid line shows this distribution after Rattle is applied. This plot was obtained from 80000 sets of initial conditions.

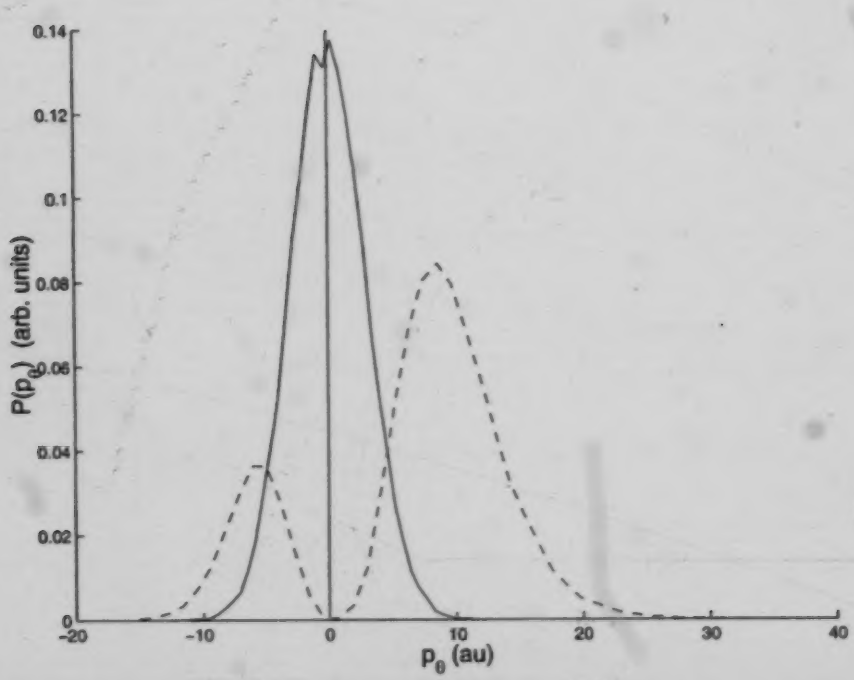

Figure 3.34: The distributions of p_θ sampled from Ψ_0 in Cartesian coordinates. The dashed line is the distribution obtained from momenta sampled directly (subjected to an energy cutoff, E_{max} = 10000cm^{-1}), while the solid line shows the distribution after Rattle is applied and centre-of-mass motion is subtracted. This plot was obtained from 80000 sets of initial conditions.

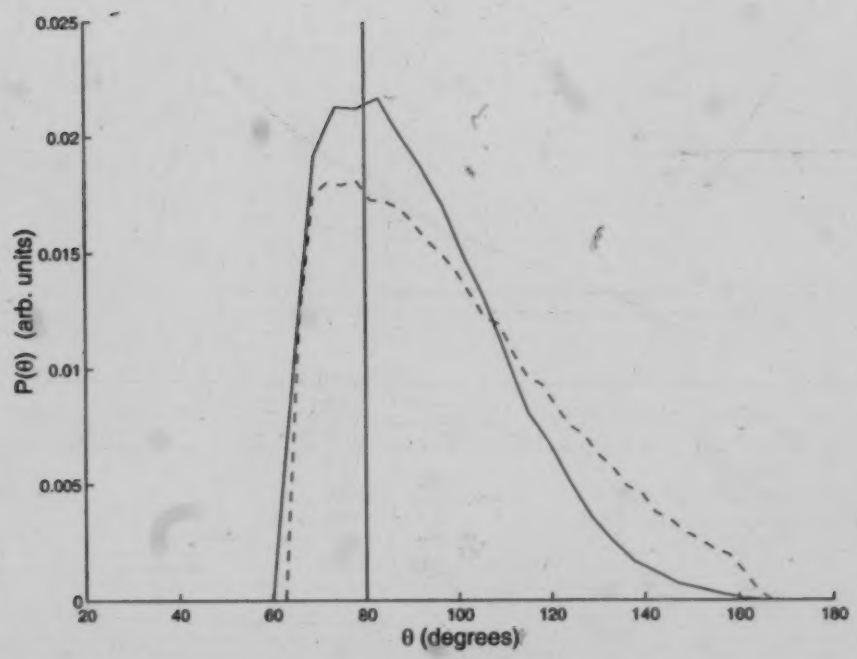

Figure 3.35: A comparison of the values of θ used in the initial conditions, obtained in both angular (solid line) and Cartesian (dashed line) coordinates.

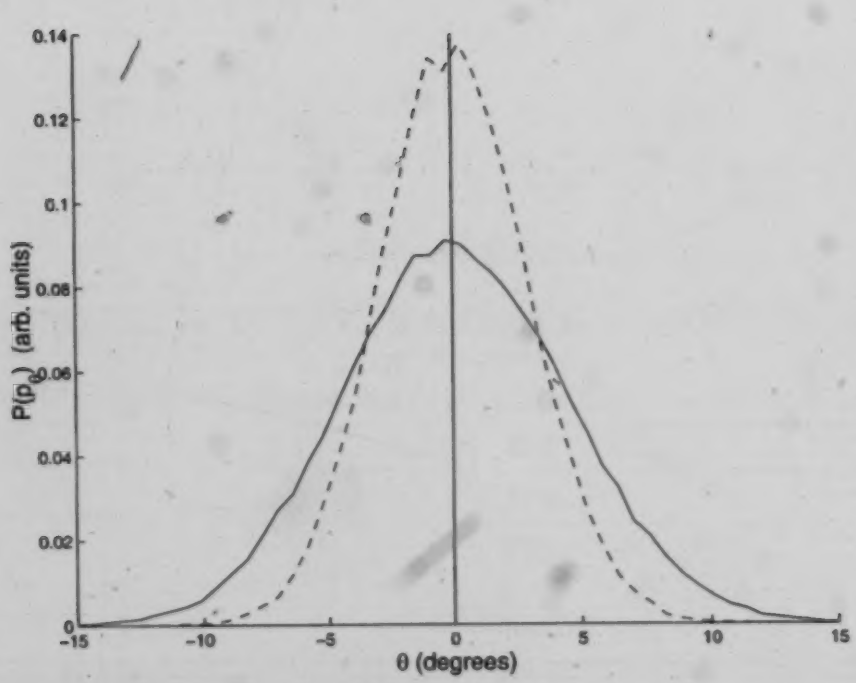

Figure 3.36: A comparison of the values of p_θ used in the initial conditions, obtained in both angular (solid line) and Cartesian (dashed line) coordinates.

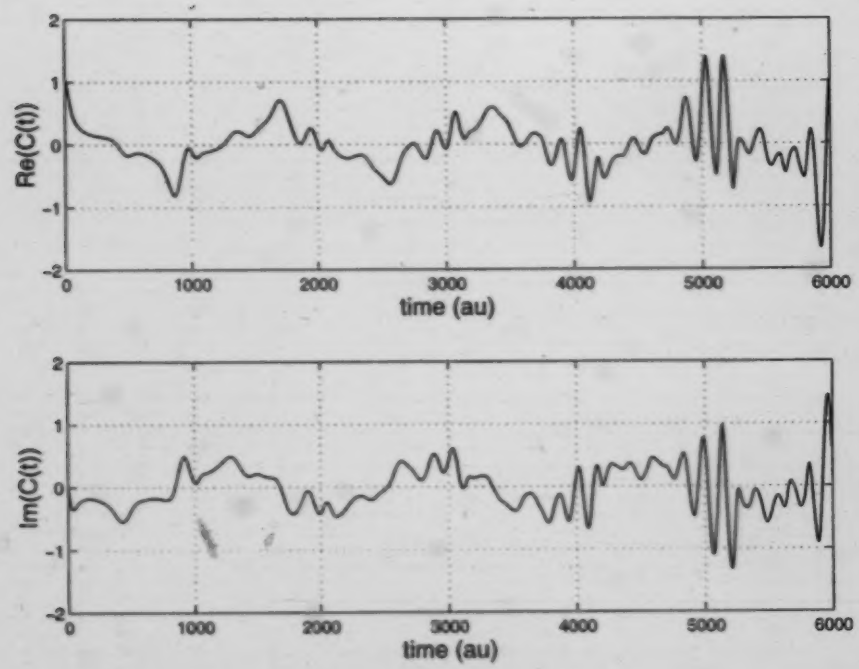

Figure 3.37: The HK-IVR autocorrelation function calculated for the water-bender in Cartesian coordinates, except for the prefactor, which is calculated from the 1D Hessian.

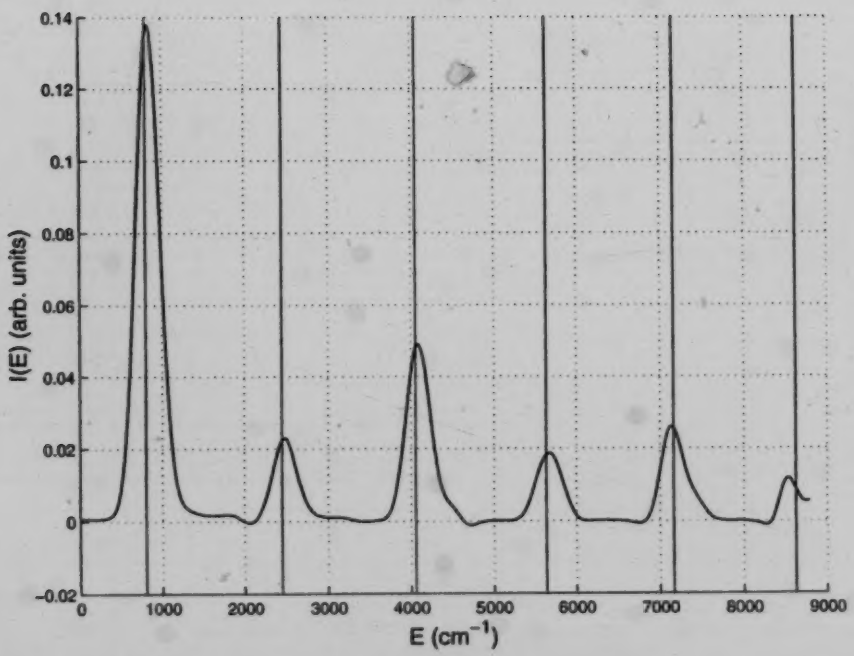

Figure 3.38: The HK-IVR power spectrum calculated for the water-bender in Cartesian coordinates, except for the prefactor, which is calculated from the 1D Hessian.

Evaluating the HK-prefactor

Here, we focus our attention on the "Johnson's multichannel WKB" approximation to the log-derivative prefactor [23] presented in Appendix F. This is:

$$R_{\mathbf{p}_i^c \mathbf{q}_i^c t} \approx \exp\left[-\frac{i}{\hbar}\int_0^t \mathrm{d}t' \sum_{j=1}^{N} \frac{1}{2}\hbar\omega_j^c(t')\right] , \tag{3.42}$$

where $\omega_j^c(t')$ is the frequency of the jth mode for the constrained system. All N of these frequencies are obtained by diagonalising the fully projected mass-weighted Hessian. Here, we expect $6+C$ of them to be zero, where C is the number of constraints we apply (*i.e.* 2).

The appeal of this particular form for the prefactor lies in its ease of computation. Aside from a single diagonalisation, all computationally intensive matrix manipulation is avoided. Furthermore, we have lost the square root of a complex number, so the branch-cut problem is effectively avoided. In the Section 3.2.2, it was determined that (at least for this model system) Equation (3.42) demonstrates favourable performance when compared to the exact log-derivative formulation: the ACF's gave power spectra with a more desirable line-shape, and Monte Carlo convergence of our integral required fewer trajectories. Now, the only thing we need to worry about is getting the correct Hessian (*i.e.* the ω_j^c's).

Since we are in Cartesian coordinates, mass weighting our Hessian is straightforward

$$\mathbf{F}^{\mathrm{mw}} = \mu^{-1} \cdot \mathbf{F} \cdot \mu^{-1} , \tag{3.43}$$

where μ^{-1} is a diagonal $N \times N$ matrix defined by

$$(\mu^{-1})_{ij} = \sqrt{\frac{1}{m_i}}\delta_{ij} . \tag{3.44}$$

Before we begin our discussion of the projection method, we look at the frequencies obtained by diagonalising $\mathbf{F}^{\mathrm{mw}}$ (Figure 3.39). The three translations are effectively zero, and the 3 internal modes compare almost identically with Figure 3.17. The three modes corresponding to rigid-body rotations are troublesome, however, since they are imaginary ($\omega^2 < 0$, except at the equilibrium structure where $\omega^2 = 0$) and are on the same order of magnitude as the bend mode. This leads to difficulties: imaginary modes give rise to a positive real exponent in (3.42), leading to very large values for the prefactor. This problem plagued this work in its earlier stages (our prefactor kept blowing up), before rotations were removed. This limitation does not cause us too much concern, however; it simply restricts our scope to problems concerning internal degrees of freedom.

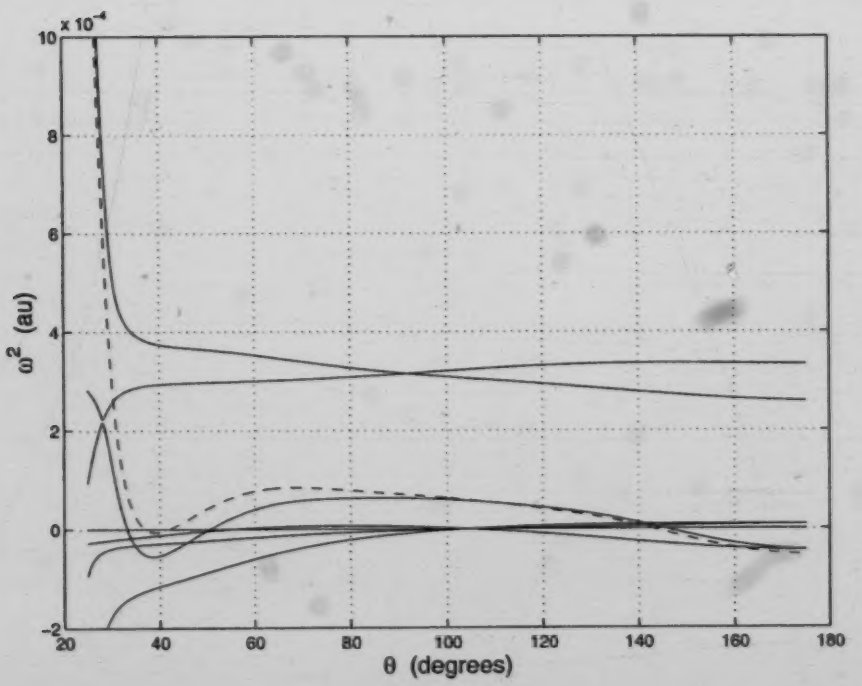

Figure 3.39: The eigenvalues of the unprojected, mass-weighted Hessian matrix in Cartesian coordinates ($\mu^{-1} \cdot \mathbf{F} \cdot \mu^{-1}$). The three modes corresponding to translations are zero. Those corresponding to the three rigid-body rotations are negative (*i.e.* give imaginary frequencies) for most non-equilibrium conformations. The remaining three solid lines correspond to the internal modes. The dashed line indicates the bend mode, calculated in 1D as $G_{33}F_{33}$.

The projection method of Hinsen and Kneller

In this section, we present the general method used to construct a matrix which will effectively project constrained motions out of the Hessian matrix.[3] The method was originally developed by Hinsen and Kneller [44] for use in classical MD simulations of macromolecules. This helps to illustrate one of the chief advantages of our approach: by staying Cartesian, we stay *general*. That is, our method will conveniently interface with the molecular potentials and dynamics algorithms of classical MD. This enables us to freely make use of existing codes and methods when the need arises, rather than waste our time "reinventing the wheel".

The essence of this method is to characterise the subspace of interesting motions (*i.e.* those which are not constrained) by a set of (possibly linearly dependent) vectors which describe infinitesimal elementary displacements. That is, rather than specify which motions are to be removed from the Hessian, we define which motions are going to be allowed, about an infinitesimal displacement from the present configuration. This technique is especially useful when dealing with large systems exhibiting motions on a number of different timescales; normal mode analysis is possible for large biomolecules, when extremely low-frequency normal modes (say, $\sim 500\text{cm}^{-1}$) are being investigated.

The basic procedure is as follows. Once we have specified the complete set of permissible motions, we construct corresponding vectors (we call them $\mathbf{d}^{(k)}$) according to a simple recipe. There are formulas for describing rigid-body translations and rotations, arbitrary motions of individual atoms, and bond stretches.[4] Next, the complete set of these vectors are assembled to form the columns of the *displacement matrix*, $\mathbf{D}$:

$$\mathbf{D} = (\mathbf{d}^{(1)}, \cdots, \mathbf{d}^{(M)}) \,, \tag{3.45}$$

where M is the total number of elementary displacements. This matrix is then orthonormalised. Although perhaps the best known routine for this is the Gram-Schmidt method, a more numerically stable option is *singular-value decomposition* (SVD), which decomposes $\mathbf{D}$ as

$$\mathbf{D} = \mathbf{U} \cdot \mathbf{\Sigma} \cdot \mathbf{V}^T \,. \tag{3.46}$$

Here, $\mathbf{D}$ is an $N \times M$ matrix, $\mathbf{U}$ is $N \times M$ and contains the orthonormal column vectors, $\mathbf{\Sigma}$ is an M-dimensional diagonal matrix containing the eigenvalues of $\mathbf{D}^T \cdot \mathbf{D}$ (these are called the *singular-values* of $\mathbf{D}$). The number of non-zero singular values corresponds to the dimensionality of the subspace of infinitesimal displacements.[5] Finally, $\mathbf{V}$ is an orthogonal $M \times M$ matrix which we have no interest in.

[3] Note that our "constrained motions" include the two frozen bonds *plus* the translations and rigid-body rotations which are associated with the centre of mass.

[4] Here, our bend is rendered by removing components of the H-H stretch vector corresponding to the O-H stretches.

[5] For our water-bender, the dimensionality of this subspace is one.

After removing the columns of U which correspond to zero singular-values, we form the projection matrix, Δ, as

$$\Delta = \mathbf{U} \cdot \mathbf{U}^T \,. \tag{3.47}$$

This projector is then used to bring the Hessian matrix (as well as the matrix used to mass-weigh our coordinate) into the desired subspace.

$$\mathbf{F}^c = \Delta \cdot \mathbf{F} \cdot \Delta \tag{3.48}$$

$$(\mu^{-1})^c = \Delta \cdot \mu^{-1} \cdot \Delta \,. \tag{3.49}$$

Therefore, the final Hessian matrix, H, is calculated as

$$\begin{aligned} \mathbf{H} &= (\Delta \cdot \mu^{-1} \cdot \Delta) \cdot (\Delta \cdot \mathbf{F} \cdot \Delta) \cdot (\Delta \cdot \mu^{-1} \cdot \Delta) \\ &= \Delta \cdot \mu^{-1} \cdot \Delta \cdot \mathbf{F} \cdot \Delta \cdot \mu^{-1} \cdot \Delta \,, \end{aligned} \tag{3.50}$$

where, in the last step, we made use of the following property (*idempotency*) of the projection matrix:

$$\Delta \cdot \Delta = \Delta \,. \tag{3.51}$$

Figure 3.40 displays the eigenvalues of H, calculated as a function of θ. Aside from our bend mode, the rest are now true zero-frequency. Therefore, only this mode contributes to the sum in (3.42).

The semiclassical autocorrelation function

We are now ready to calculate the autocorrelation function by combining the components of the 9D constrained expression. The autocorrelation function and its associated power spectrum appear in Figures 3.41 and 3.42, respectively. Notice that we were able to estimate the quantum energy levels to high accuracy, which is encouraging. The key results of this project are summarised in Tables 3.2 and 3.3. Table 3.3 is a compilation of the peak positions for our water bender, and Table 3.4 shows the percent error in the peak spacing which is not associated with error in the zero point energy. We conclude that our proposed method is justified.

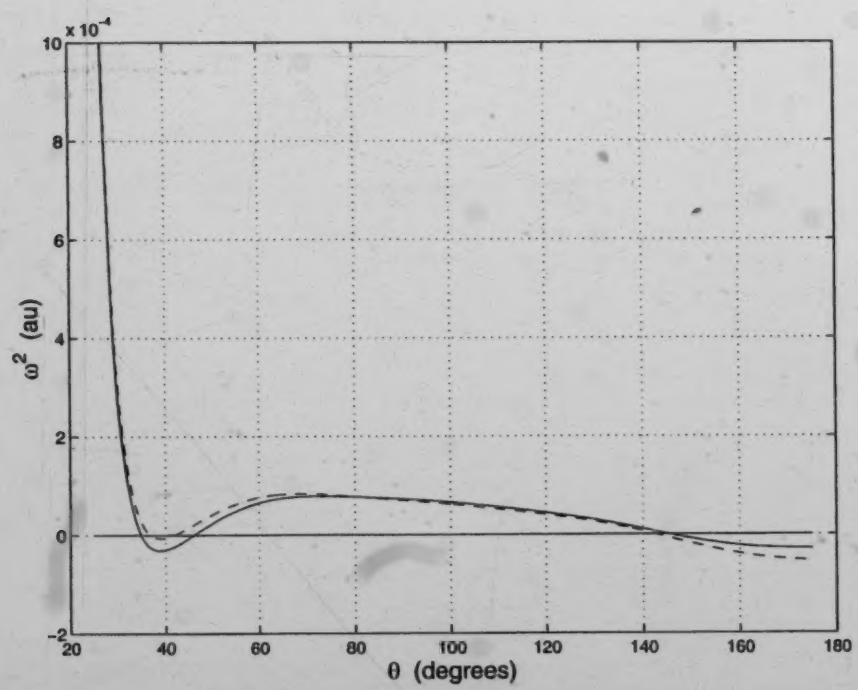

Figure 3.40: Square frequencies obtained by diagonalising $\Delta \cdot \mu^{-1} \cdot \Delta \cdot \mathbf{F} \cdot \Delta \cdot \mu^{-1} \cdot \Delta$. The dashed line corresponds to the bend mode calculated in 1D by $G_{33}F_{33}$. Notice that in two places, our bend mode is imaginary (*i.e.* the curve goes below zero), and this can lead to problems in the evaluation of the HK-prefactor. The region around 160° indicates a transition state (we are approaching the inversion barrier of the potential), while the "dip" near 40° is a feature of the curvature of the potential (perhaps not physically relevant). Either way, these regions correspond to high energies and are not visited frequently in our trajectories.

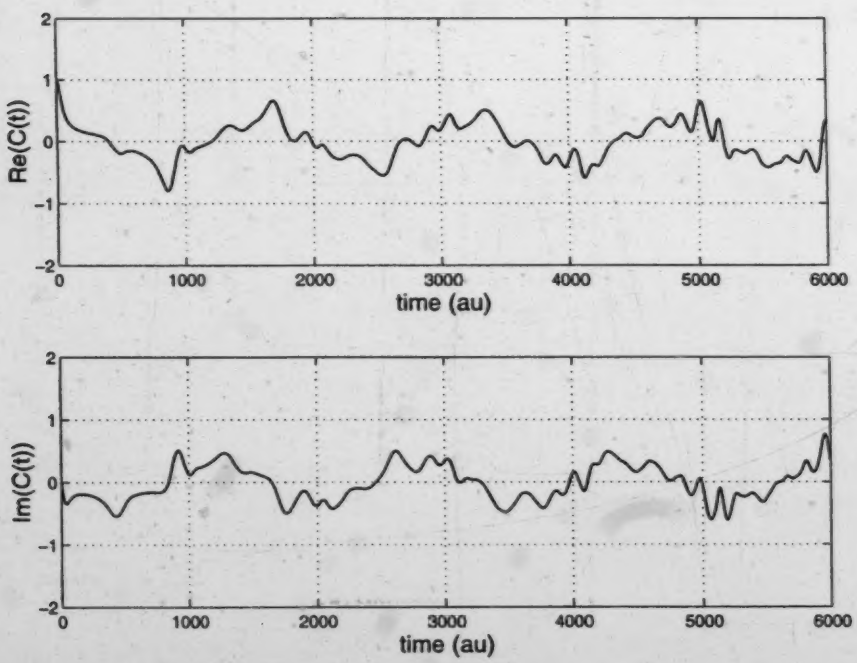

Figure 3.41: The HK-IVR autocorrelation function calculated for the water-bender in Cartesian coordinates, using the "multichannel-WKB" approximation to the prefactor.

Table 3.2: Accuracy in capturing zero point energy. This accuracy is due entirely to the HK-prefactor. By introducing the approximate form, we gain an additional 0.6% error; by going to the projected 9D Hessian, our error roughly doubles. The latter result can be explained by noticing that the frequency of our bend mode spends more time in the imaginary region than does the frequency computed in 1D.

method of calculation	ZPE (cm^{-1})	error %
QM	808.0	0.0
1D SC-IVR		
no R-factor	0.0	-
approximate R-factor	833.5	3.2
exact R-factor	828.8	2.6
9D SC-IVR (approximate R-factor)		
no R-factor	0.0	-
1D hessian	834.8	3.3
9D projected hessian	861.6	6.6

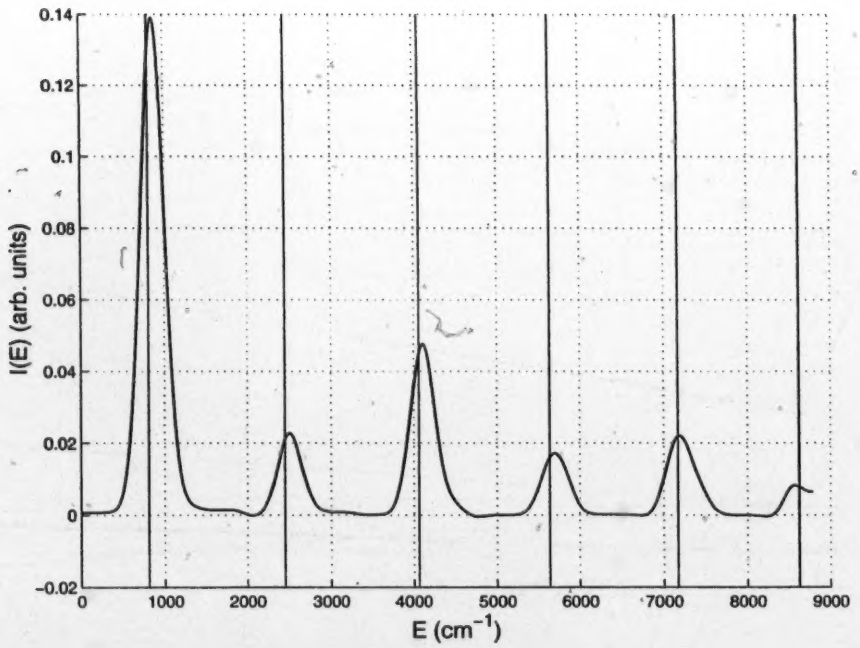

Figure 3.42: The HK-IVR power spectrum calculated for the water-bender in Cartesian coordinates, using the "multichannel-WKB" approximation to the prefactor.

Table 3.3: Final table of calculated energy levels (raw data) in cm^{-1}. The numbers in brackets are uncertainties.

		1D SC-IVR			9D SC-IVR		
peak	QM	no R-factor	approximate R-factor	exact R-factor	no R-factor	1D hessian	9D projected hessian
0	808.0	0.0	833.5	828.8	0.0	834.8	861.6
1	1641.5	858.6	1661.1	1652.2	871.7	1673.0	1698.4
2	3253.1	2488.9	3262.3	3262.6	2492.3	3278.0	3302.1
3	4828.3	4096.3	4823.1	4834.6	4114.3	4865.0	4889.5
4	6355.6	5697.5	6363.3	6389.1	5687.1	6333.7	6373.5
5	7815.0	7291.4	7880.3	7928.0	7232.7	7900.0 (20)	7905.6 (20)

Table 3.4: The percent errors on the peak positions, compared to the corresponding quantum results. This error reflects peak spacings only; peaks values were shifted so that the error associated with zero point energy is 0.

	1D SC-IVR			9D SC-IVR		
peak	no R-factor	approximate R-factor	exact R-factor	no R-factor	1D hessian	9D projected hessian
0	0.0	0.0	0.0	0.0	0.0	0.0
1	1.5	-0.4	-0.6	2.3	0.3	0.2
2	1.3	-0.5	-0.3	1.5	-0.1	-0.1
3	1.6	-0.6	-0.3	1.9	0.2	0.2
4	2.4	-0.3	0.2	2.2	-0.7	-0.6
5	3.6	0.5	1.2	2.9	0.7	0.4

Chapter 4

Conclusions

The principal conclusion that we make with regards to the results of the preceding chapter is: "our method works". That is, no significant error was found to be associated with our method, *vis-a-vis* computation of the HK-IVR in curvilinear coordinates. Again, the primary appeal of our method derives from its generality: it is amenable to large-scale simulation of arbitrary constrained molecular systems. We also report that the computational methodology is parallelised in a straightforward way,[1] with total processor time approximately equal to that used in corresponding serial calculations on a single processor.

Limitations of our method

It must be mentioned that, for the simple systems discussed here, our method requires considerably more CPU time than do the corresponding quantum and traditional semiclassical calculations. If a model under investigation already has an existing curvilinear coordinate (*i.e.* the Hamiltonian has been worked out), then our method will lose. But, our approach is aimed at complex situations where these coordinates are not available.[2] Furthermore, when compared to exact quantum methods, our approach exhibits far more favourable scaling: our computational bottleneck amounts to one singular-value decomposition and one diagonalisation per timestep. The total number of these operations is given by:

$$\begin{pmatrix} \text{number of diagonalisations/} \\ \text{singular-value decompositions} \end{pmatrix} = \begin{pmatrix} \text{number of Monte} \\ \text{Carlo trajectories} \end{pmatrix} \times \begin{pmatrix} \text{number of timesteps} \\ \text{per trajectory} \end{pmatrix},$$

and each of these operations is performed on a (roughly) $N \times N$ matrix. A comparable quantum mechanical calculation requires only one matrix diagonalisation, but this matrix becomes very large for systems of moderate complexity, as outlined in Section 1.4.

[1] We launch different Monte Carlo trajectories on different processors, and average results after they are complete. In this sense, we affectionately refer to our MPI code as *dumb parallelisation*.

[2] At the present time, there exist kinetic energy operators for 4-atom models, and these are exceedingly complicated constructions.

Also, we acknowledge that our method is not yet capable of addressing problems which include rotational degrees of freedom. Rotations can become especially important when confronting intermolecular dynamics problems.

So far, we have restricted ourselves to a coherent state initial wavefunction. This may be a poor representation for the physical system at hand in certain instances. Heller [21] has a way to decompose any arbitrary wavefunction in terms of FG's, and this may need to be employed in certain cases.

Here, we have reported a *numerical* justification for our procedure, rather than a formal mathematical proof. We may conclude that our method is adequate to capture zero-point effects, and proper quantisation in an anharmonic potential. The *ad hoc* way in which we proposed our sampling procedure would have been especially troubling, had it not led to success. Our sampling procedure is certainly a target for future analysis.

The way we have elected to compute the HK-prefactor is susceptible to the scaling of both SVD and diagonalisation routines. Because this is the computational bottleneck in our procedure, it is a strong candidate for potential improvement.

Last, within the framework we have developed, there is no systematic way of dealing with so-called *problematic trajectories*. Such trajectories hinder the convergence of our ACF, and in some cases, cause the integrand to "blow up". This is widely reported in the literature: Miller [45] screened his initial conditions, and discarded those which lead to dissociation. Manolopoulos [46] did likewise, and furthermore discarded trajectories which were deemed to be chaotic. These were identified by their large HK-prefactors.[3] In this work, we found it sufficient to apply a simple energy cutoff. In the case of our water bender model, this cutoff was chosen to be slightly lower than the inversion barrier.

Future directions

The following improvements can be made in the way with which our method is implemented. First, we could employ an integral conditioning technique in order to reduce the oscillations of our integrand. Examples of such "smoothing" or "filtering" procedures which have been developed especially for frozen Gaussian wave-propagation are Miller's *Filinov* [24] or *generalised Filinov* [26], and Heller's *cellular dynamics*.[8] I point out that these methods are formally equivalent, although there is some dispute over which performs better. We remind the reader that the application of holonomic constraints can be viewed as a smoothing technique, as described in the introduction to Chapter 3.

Again, our method is presently incapable of addressing rotational degrees of freedom, and this will

[3]Recall that propagation of the HK-prefactor involves elements of the monodromy matrix. This matrix is a measure of stability for the dynamics. Therefore, the assessment of a set of initial conditions on the basis of the HK-prefactor is called a *stability criterion*.

be a high priority in the future. The problems with rotations enter our method as the orientational dependence of the constrained Hessian matrix, giving rise to superfluous imaginary frequencies when it is computed for any geometry apart from the equilibrium structure.

Because our method is general, it can be interfaced quite readily to other codes. In conjunction with MMTK (the Molecular Modeling Toolkit developed by Konrad Hinsen [47]), we would be able to make use of the expansive resources for classical molecular dynamics found therein. Recently, the HK-IVR has been used in conjunction with Feynman's path integral techniques. [48] Our code could be modified to launch *ab initio* software to enable "on-the-fly" computation of potentials, gradients, and Hessians directly on the BO-PES. Finally, we could apply our propagator to the *forward-backward* IVR (FB-IVR) of Miller ([49, 50], for example). This was designed for the calculation of finite-temperature averages.

There are a number of applications of our method which will be potential candidates for research in this group. I conclude with a brief enumeration of these.

1. Simulations of molecular species embedded in a liquid helium environment. For example, the dependence of the O-C stretch frequency in OCS-He_n on the number of He atoms comprising the cluster.

2. Simulation of intermolecular degrees of freedom. We could take as an example the HCl dimer, and compare to results obtained with the HK-IVR in curvilinear coordinates.[45] This model would also establish the capabilities of our method in handling particle symmetry and in capturing the quantum effect of *tunneling-splitting*.

3. Simulation of photoelectronic spectra of hydrogen-bonded complexes. A number of potential models exist here including water-clusters and a phenol-water dimer.

Bibliography

[1] W. S. Struve, *Fundamentals of Molecular Spectroscopy* (Wiley, 1989).

[2] A. Messiah, *Quantum Mechanics* (Dover Publications, 1999).

[3] The nobel prize in chemistry 1998, the royal swedish academy of sciences.

[4] M. P. Allen and D. J. Tildesley, *Computer Simulation of Liquids* (Oxford University Press, 1987).

[5] D. Chandler, *Introduction to Modern Statistical Mechanics* (Oxford University Press, 1987).

[6] D. C. Rapaport, *The Art of Molecular Dynamics Simulation* (Cambridge University Press, 1995).

[7] E. J. Heller, J. Chem. Phys. **62**, 1544 (1975).

[8] E. J. Heller, J. Chem. Phys. **94**, 2723 (1991).

[9] J. C. Light, Adv. Chem. Phys. **114**, 263 (2000).

[10] P. A. M. Dirac, *The Principals of Quantum Mechanics, 4th ed.* (Oxford University Press, 1958).

[11] R. P. Feynmann and A. R. Hibbs, *Quantum Mechanics and Path Integrals* (McGraw-Hill, 1965).

[12] J. H. V. Vleck, Proc. Nat. Acad. Sci. **14**, 178 (1928).

[13] W. H. Miller, J. Chem. Phys. **95**, 9428 (1991).

[14] E. J. Heller, J. Chem. Phys. **95**, 9431 (1991).

[15] M. F. Herman and E. Kluk, Chem. Phys. **91**, 27 (1984).

[16] M. F. Herman, Chem. Phys. Lett. **275**, 445 (1997).

[17] K. G. Kay, J. Chem. Phys. **100**, 4377 (1993).

[18] K. G. Kay, J. Chem. Phys. **100**, 4432 (1994).

[19] K. G. Kay, J. Chem. Phys. **101**, 2250 (1994).

[20] Y. Elran and K. G. Kay, J. Chem. Phys. **110**, 3653 (1999).

[21] E. J. Heller, J. Chem. Phys. **75**, 2923 (1981).

[22] S. Garashchuk and J. C. Light, J. Chem. Phys. **113**, 9390 (2000).

[23] R. Gelabert, X. Gimenez, M. Thoss, H. Wang, and W. H. Miller, J. Phys. Chem. A **104**, 10321 (2000).

[24] V. S. Filinov, Nuc. Phys. B , 717 (1986).

[25] N. Makri and W. H. Miller, Chem. Phys. Lett. **139**, 10 (1987).

[26] H. Wang, D. E. Manolopoulos, and W. H. Miller, J. Chem. Phys. **115**, 6317 (2001).

[27] L. S. Schulman, *Techniques and Applications of Path Integration* (Wiley, 1996).

[28] D. A. McQuarrie, *Statistical Mechanics* (Harper and Row, 1976).

[29] H. Goldstein, C. Poole, and J. Safko, *Classical Mechanics, 3rd ed.* (Addison Wesley, 2002).

[30] P. R. Holland, *The Quantum Theory of Motion* (Cambridge University Press, 1993).

[31] M. Brack and R. K. Bhaduri, *Semiclassical Physics* (Addison-Wesley Publishing Company, Inc., 1997).

[32] M. Gutzwiller, *Chaos in Classical and Quantum Mechanics* (Springer Verlag, New York, 1990).

[33] P. A. M. Dirac, Proc. Roy. Soc. London **113 A**, 621 (1927).

[34] P. Jordan, Zeits. Physik **40**, 809 (1927).

[35] G. B. Arfken and H. J. Weber, *Mathematical Methods for Physicists, 5th ed.* (Harcourt Academic Press, 2001).

[36] W. H. Press, S. A. Teukolsky, W. T. Vetterling, and B. P. Flannery, *Numerical Recipes in C, 2nd ed.* (Cambridge University Press, 1992).

[37] Maple 6, copyright (c) 2000 by waterloo maple inc.

[38] J.-P. Ryckaert, G. Ciccotti, and H. J. C. Berendsen, J. Comput. Phys. **23**, 327 (1977).

[39] H. C. Andersen, J. Comput. Phys. **52**, 24 (1983).

[40] O. L. Polyansky, P. Jensen, and J. Tennyson, J. Chem. Phys. **105**, 6490 (1996).

[41] C. Eckart, Phys. Rev. **46**, 383 (1934).

[42] H. Wei and T. Carrington, J. Chem. Phys. **101**, 1343 (1994).

[43] E. B. Wilson, J. C. Decius, and P. C. Cross, *Molecular Vibrations: The theory of infrared and Raman vibrational spectra.* (Dover Publications, Inc. New York., 1955).

[44] K. Hinsen and G. R. Kneller, Mol. Sim. **23**, 275 (2000).

[45] X. Sun and W. H. Miller, J. Chem. Phys. **108**, 8870 (1998).

[46] A. R. Walton and D. E. Manolopoulos, Mol. Phys. **87**, 961 (1996).

[47] K. Hinsen, J. Comp. Chem. **21**, 79 (2000).

[48] J. C. Burant and V. S. Batista, J. Chem. Phys. **116**, 2748 (2002).

[49] X. Sun and W. H. Miller, J. Chem. Phys. **110**, 6635 (1999).

[50] W. H. Miller, J. Chem. Phys. **116**, 9207 (2002).

Appendix A

Multidimensional Gaussian Integrals

Here, we simply generalise the well-known (and by me, well-used) analytical formula for a 1-D Gaussian integral,

$$\begin{aligned} I^{1D} &= \int_{-\infty}^{+\infty} \mathrm{d}x e^{ax^2+bx+c} \\ &= \sqrt{-\frac{\pi}{a}} e^{-b^2/4a+c}, \end{aligned} \tag{A.1}$$

to N-dimensions.

$$I = \int_{-\infty}^{+\infty} \mathrm{d}\mathbf{x} \exp\left[\mathbf{x}^T \cdot \mathcal{A} \cdot \mathbf{x} + \mathbf{x}^T \cdot \mathbf{b} + c\right]. \tag{A.2}$$

Here, we assume that the elements of $\mathcal{A}$ are real and negative, and also that it has an inverse. We now change to a new basis, $\mathbf{y}$, in which $\mathcal{A}$ is diagonal, so that we may rewrite (A.2) as a product:

$$\begin{aligned} I &= \int_{-\infty}^{+\infty} \mathrm{d}\mathbf{y} \exp\left[\mathbf{y}^T \cdot \tilde{\mathcal{A}} \cdot \mathbf{y} + \mathbf{y}^T \cdot \tilde{\mathbf{b}} + c\right] \\ &= \prod_{k=1}^{N} \int_{-\infty}^{+\infty} \mathrm{d}y_k \exp\left[\tilde{A}_{kk} y_k^2 + \tilde{b}_k y_k + c\right] \\ &= \prod_{k=1}^{N} \left\{\sqrt{-\frac{\pi}{\tilde{A}_{kk}}} \exp\left[-\tilde{b}_k^2/4\tilde{A}_{kk} + c\right]\right\} \\ &= \sqrt{-\frac{\pi}{\det \tilde{\mathcal{A}}}} \exp\left\{\sum_{k=1}^{N} \frac{\tilde{b}_k \tilde{A}_{kk}^{-1} \tilde{b}_k}{4} + c\right\}. \end{aligned} \tag{A.3}$$

Recalling that a determinant does not depend upon basis,

$$\sqrt{-\frac{\pi}{\det \tilde{\mathcal{A}}}} = \sqrt{-\frac{\pi}{\det \mathcal{A}}}. \tag{A.4}$$

Also, since $\tilde{A}$ is diagonal,

$$\begin{aligned}\sum_{k=1}^{N} \tilde{b}_k \tilde{A}_{kk}^{-1} \tilde{b}_k &= \tilde{\mathbf{b}}^T \cdot \tilde{\mathcal{A}}^{-1} \cdot \tilde{\mathbf{b}} \\ &= \mathbf{b}^T \cdot \mathcal{A}^{-1} \cdot \mathbf{b}. \end{aligned} \tag{A.5}$$

The last step was made recalling that a linear change of basis matrix is orthogonal. So, our final result is:

$$\int_{-\infty}^{+\infty} \mathrm{d}\mathbf{x} \exp\left[\mathbf{x}^T \cdot \mathcal{A} \cdot \mathbf{x} + \mathbf{x}^T \cdot \mathbf{b} + c\right] = \sqrt{-\frac{\pi}{\det \mathcal{A}}} \exp\left[\frac{\mathbf{b}^T \cdot \mathcal{A}^{-1} \cdot \mathbf{b}}{4} + c\right]. \tag{A.6}$$

Appendix B

The Stationary-Phase Approximation

Here, I derive the *Stationary-Phase Approximation* [27] which provides us with a means of evaluating multidimensional integrals of the form:

$$I = \int \mathrm{d}\mathbf{x} g(\mathbf{x}) \exp\left(\frac{i}{\hbar} f(\mathbf{x})\right). \tag{B.1}$$

Difficulties in evaluating this integral by conventional means arise due to the highly oscillatory nature of the integrand. Because of this rapid oscillation, there will be a large degree of cancellation between positive and negative areas. Therefore, we expect the main contributions to the overall integral to come from points where the phase is *stationary*, that is, where

$$f'(\mathbf{x}) = \mathbf{0}. \tag{B.2}$$

We are therefore justified in expanding the phase ($f(\mathbf{x})$) to second order and the pre-exponential function ($g(\mathbf{x})$) to zeroth order about these *stationary points*, which will be denoted $\mathbf{x}_k$:

$$g(\mathbf{x})\Big|_{\mathbf{x}=\mathbf{x}_k} \approx g(\mathbf{x}_k) \tag{B.3}$$

$$f(\mathbf{x})\Big|_{\mathbf{x}=\mathbf{x}_k} \approx f(\mathbf{x}_k) + \frac{1}{2}(\mathbf{x}-\mathbf{x}_k)^T \cdot f''(\mathbf{x}_k) \cdot (\mathbf{x}-\mathbf{x}_k). \tag{B.4}$$

Notice that the linear term of (B.4) does not appear because of (B.2). Substituting (B.3) and (B.4) into (B.1), we obtain for a single stationary point:

$$I_k = g(\mathbf{x}_k) \int \mathrm{d}\mathbf{x} \exp\left(\frac{i}{\hbar} f(\mathbf{x}_k) + \frac{i}{2\hbar}(\mathbf{x}-\mathbf{x}_k)^T \cdot f''(\mathbf{x}_k) \cdot (\mathbf{x}-\mathbf{x}_k)\right). \tag{B.5}$$

Once again, we have a multidimensional Gaussian integral which can be evaluated as per Appendix A. This gives us:

$$\begin{aligned} I_k &= g(\mathbf{x}_k)\left(-\frac{(2\pi)^N}{\sqrt{\det(\frac{i}{\hbar}f''(\mathbf{x}_k))}}\right)\exp\left[\frac{i}{\hbar}f(\mathbf{x}_k)\right] \\ &= g(\mathbf{x}_k)\left(\frac{(2\pi i\hbar)^N}{\sqrt{\det f''(\mathbf{x}_k)}}\right)\exp\left[\frac{i}{\hbar}f(\mathbf{x}_k)\right]. \end{aligned} \tag{B.6}$$

Finally, the overall integral is computed as a sum over the contributions from each of these stationary points:

$$\begin{aligned} I &= \sum_{k=1}^{st.pts.} I_k \\ &= (2\pi i\hbar)^N \sum_{k=1}^{st.pts.} g(\mathbf{x}_k)\frac{1}{\sqrt{\det f''(\mathbf{x}_k)}}\exp\left[\frac{i}{\hbar}f(\mathbf{x}_k)\right]. \end{aligned} \tag{B.7}$$

This final expression is an approximation to (B.1), accurate to $\mathcal{O}(\hbar)$.

Appendix C

The Power Spectrum from the Autocorrelation Function

In this section, we demonstrate that the Fourier transform of the autocorrelation function, $C(t)$, is in fact a power spectrum. Beginning with the definition of the autocorrelation function,

$$C(t) = \langle \psi_0 | e^{-i\hat{H}t/\hbar} | \psi_0 \rangle \ , \tag{C.1}$$

we take the Fourier transform into the energy domain:

$$I(E) = \frac{1}{2\pi} \int_{-\infty}^{+\infty} \mathrm{d}t e^{+iEt/\hbar} \langle \psi_0 | e^{-i\hat{H}t/\hbar} | \psi_0 \rangle \ . \tag{C.2}$$

Inserting a complete set of stationary states allows us to evaluate the Hamiltonian operator:

$$\begin{aligned} I(E) &= \frac{1}{2\pi} \int_{-\infty}^{+\infty} \mathrm{d}t e^{+iEt/\hbar} \sum_{n=0}^{\infty} \langle \psi_0 | e^{-i\hat{H}t/\hbar} | n \rangle \langle n | \psi_0 \rangle \\ &= \frac{1}{2\pi} \sum_{n=0}^{\infty} \int_{-\infty}^{+\infty} \mathrm{d}t e^{+iEt/\hbar} e^{-iE_n t/\hbar} \langle \psi_0 | n \rangle \langle n | \psi_0 \rangle \\ &= \sum_{n=0}^{\infty} |\langle n | \psi_0 \rangle|^2 \frac{1}{2\pi} \int_{-\infty}^{+\infty} \mathrm{d}t \exp\left[\frac{i(E - E_n)t}{\hbar}\right] \\ &= \sum_{n=0}^{\infty} |\langle n | \psi_0 \rangle|^2 \delta(E - E_n) \ . \end{aligned} \tag{C.3}$$

In the last step we have identified the Fourier representation of the Dirac delta function. Therefore, we find that the energy spectrum consists, in theory, of a sum of Dirac delta functions. Although these functions are defined as having infinitesimal width (yet still integrate to unity), in practice, we do not evaluate the Fourier transform to infinite time. In fact, we compute $I(E)$ as twice the real part of (C.2), integrated only to some positive, finite time:

$$I(E) \approx \frac{1}{\pi} \mathrm{Re} \int_0^T \mathrm{d}t e^{+iEt/\hbar} \langle \psi_0 | e^{-i\hat{H}t/\hbar} | \psi_0 \rangle \ . \tag{C.4}$$

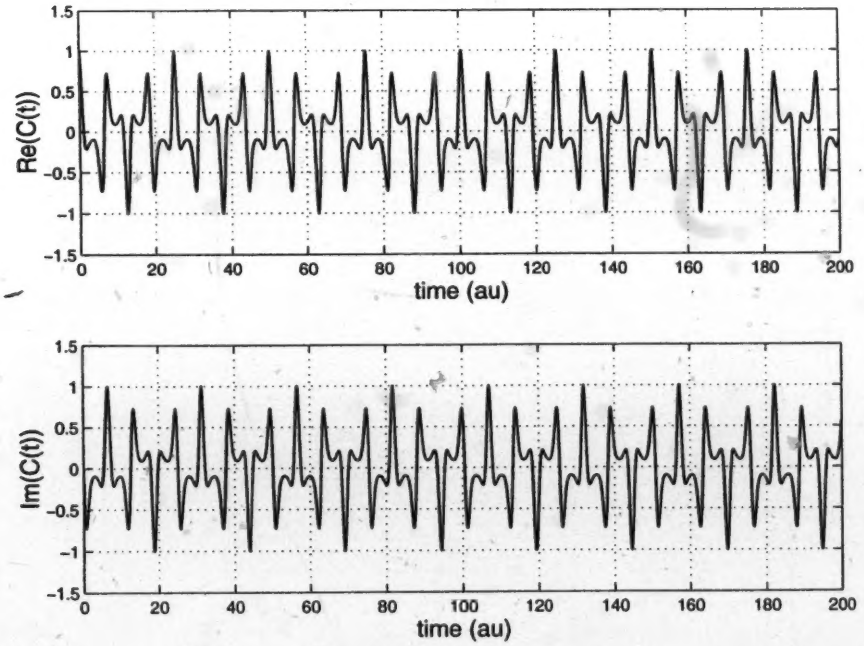

Figure C.1: The quantum autocorrelation function for two particles in a harmonic well.

This gives rise to *sink functions* which have finite amplitude. The amplitude of a peak corresponding to E_n is related to the overlap $|\langle n|\psi_0\rangle|$. In principal, our wavefunction $|\psi_0\rangle$ could have significant overlap with any or all of the stationary states. However in practice, we define it such that only the first several peaks are observed.

To illustrate this relationship between the autocorrelation function and the energy spectrum, I will provide an example: the harmonic oscillator model presented in section 3.1. The quantum ACF calculated is shown again in Figure C.1. The energy spectrum, computed as Equation (C.4) is shown in Figure C.2. The line-shape of the peaks is undesirable since, for more complicated spectra, it can pose difficulties in identifying the precise positions of individual peaks. Furthermore, for the least attractive spectra, it is sometimes difficult to identify which features are true peaks, and which are artifacts of the numerical transform procedure.

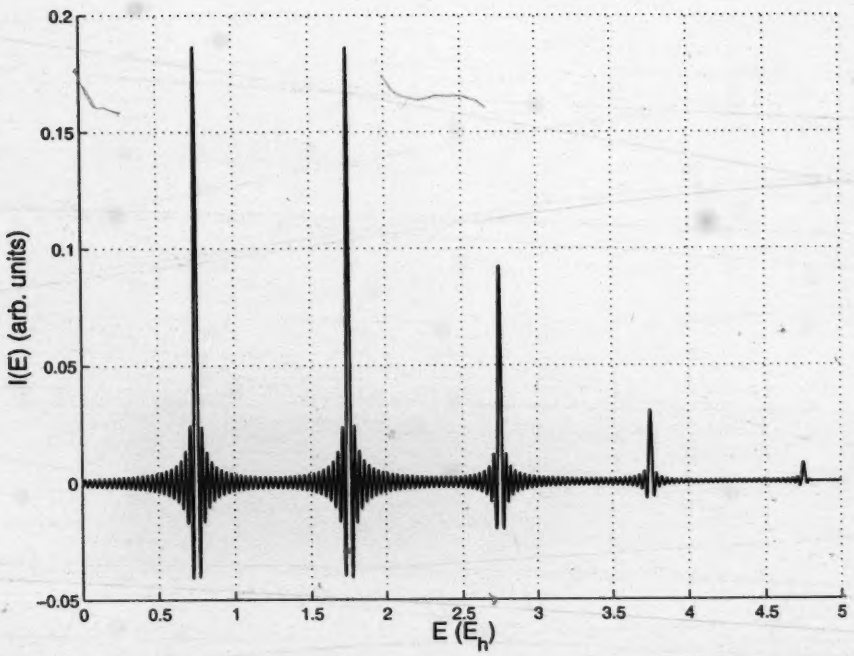

Figure C.2: The quantum power spectrum for two particles in a harmonic well, taken as the Fourier transform of the autocorrelation function.

Appendix D

The Gaussian Window Function Applied to the Autocorrelation Function

In order to accurately determine the positions of the peaks in the power spectrum, we apply a conditioning technique which transforms the approximate Dirac delta functions with smooth Gaussians. The method is simple. We simply multiply our autocorrelation function by a Gaussian ($g^{\alpha}(t) = \exp(-\alpha t^2)$) prior to Fourier transforming it:

$$C^{gw}(t) = g^{\alpha}(t)C(t). \tag{D.1}$$

Again, we evaluate the FT of the above expression:

$$\begin{aligned} I^{gw}(E) &= \frac{1}{2\pi}\int_{-\infty}^{+\infty} \mathrm{d}t e^{iEt/\hbar} C^{gw}(t) \\ &= \frac{1}{2\pi}\int_{-\infty}^{+\infty} \mathrm{d}t e^{iEt/\hbar}\left\{ e^{-\alpha t^2}\sum_{n=0}^{\infty}\langle\psi_0|e^{-i\hat{H}t/\hbar}|n\rangle\langle n|\psi_0\rangle\right\} \\ &= \frac{1}{2\pi}\sum_{n=0}^{\infty}|\langle n|\psi_0\rangle|^2\int_{-\infty}^{+\infty}\mathrm{d}t\exp\left[-\alpha t^2 + \frac{i(E-E_n)}{\hbar}t\right]. \end{aligned} \tag{D.2}$$

We observe yet another Gaussian integral, which is performed analytically:

$$\begin{aligned} I^{gw}(E) &= \frac{1}{2\pi}\sum_{n=0}^{\infty}|\langle n|\psi_0\rangle|^2\sqrt{\frac{\pi}{\alpha}}\exp\left[\left(\frac{i(E-E_n)}{\hbar}\right)\left(\frac{-1}{4\alpha}\right)\right] \\ &= \frac{1}{2}\sqrt{\frac{1}{\pi\alpha}}\sum_{n=0}^{\infty}|\langle n|\psi_0\rangle|^2\exp\left[-\frac{1}{4\hbar^2\alpha}(E-E_n)^2\right]. \end{aligned} \tag{D.3}$$

Our final result, (D.3), is analogous to that of Appendix C, except our sum over Dirac delta functions had been replaced with a sum over Gaussians, each with width $\frac{1}{4\hbar^2\alpha}$. The width parameter is arbitrary in principal, but is selected so that the autocorrelation function decays to zero close to the end of the time-frame of the experiment.

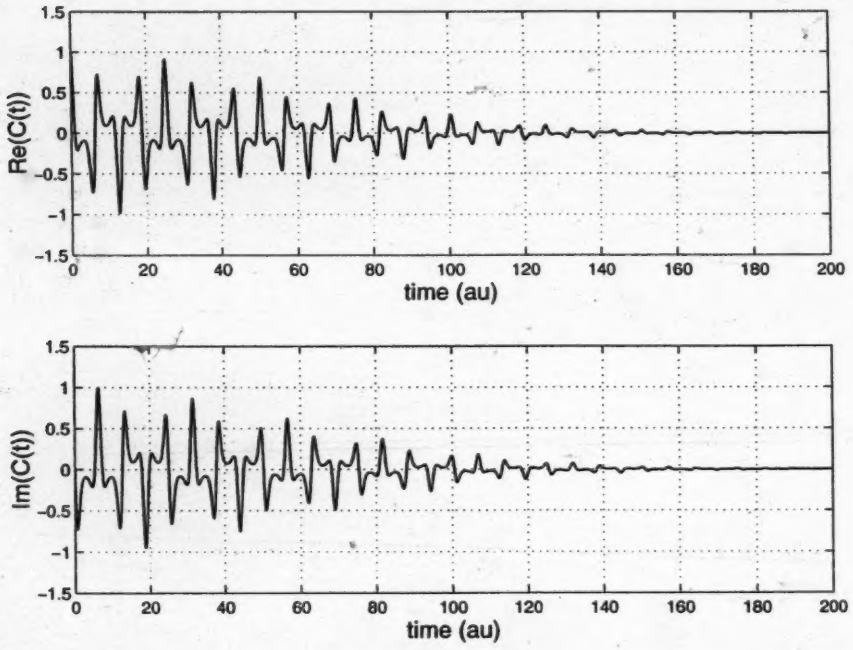

Figure D.1: The windowed quantum autocorrelation function for two particles in a harmonic well.

To illustrate the effect of this technique, I provide an example for comparison to Appendix C. Figure D.1 shows the windowed autocorrelation function corresponding to Figure C.1, while Figure D.2 gives the Fourier Transform. Notice that our peaks now have a Gaussian line-shape.

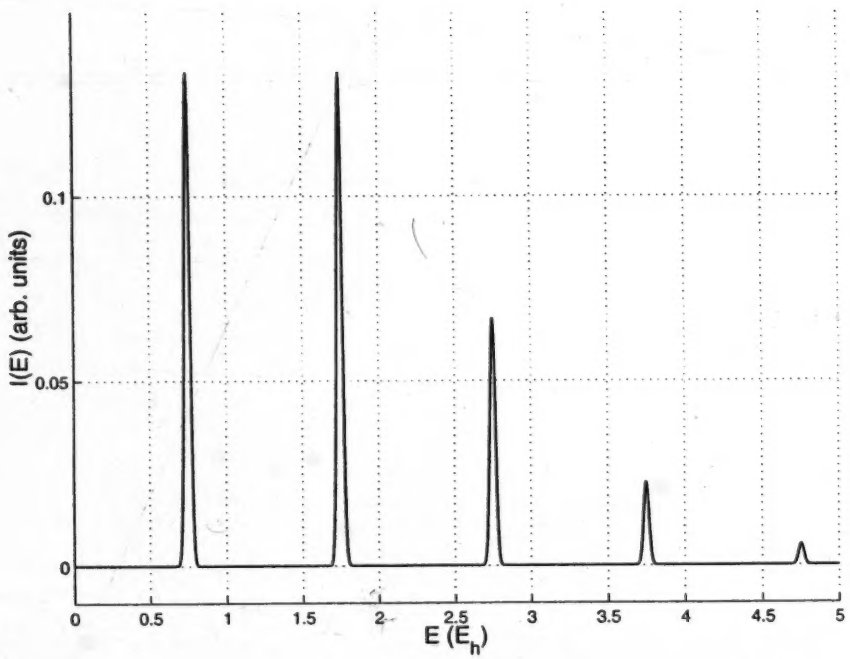

Figure D.2: The quantum power spectrum for two particles in a harmonic well taken as the Fourier transform of the windowed autocorrelation function.

Appendix E

Selection of the Coherent State Width Parameters

We want the widths of our wavepackets appearing both in our initial wavefunction as well as in the coherent states to reflect both the mass of the atom it is assigned to, as well as the shape of the potential the atom is in. We know that heavier atoms should be more localised in coordinate space. Furthermore, in accordance with the Frozen Gaussian Approximation (in section 2.6.2), we would like atoms located in regions of the potential with a large curvature to be more localised.

Therefore, we calculate a general element of the width matrix, γ, (corresponding to the k^{th} atom) as:

$$\begin{aligned} \gamma_k &\propto \sqrt{\langle \frac{\partial^2 V}{\partial \mathbf{q}_k^2} \rangle_{xyz} \times m_k} \\ &= C\sqrt{\langle \frac{\partial^2 V}{\partial \mathbf{q}_k^2} \rangle_{xyz} \times m_k}\,, \end{aligned} \tag{E.1}$$

where m_k is the mass of the k^{th} atom, and $\langle \frac{\partial^2 V}{\partial \mathbf{q}_k^2} \rangle_{xyz}$ denotes the average of the x, y, z terms of the (diagonalised) second derivative matrix of the potential corresponding to the k^{th} atom. C is a global width parameter, selected at our discretion so that our autocorrelation function has a desirable shape.

Appendix F

Miller's Log-Derivative Formulation for the Herman-Kluk Prefactor

Here, I present an alternate method of evaluating the Herman-Kluk prefactor which is due to Miller. [23] It is not only computationally less intensive than propagating the monodromy matrix (via the auxiliary equations presented in Section 2.7.2), but also claims to bypass the *branch-cut* problem, which arises when we take the square root of a complex number. Perhaps the most attractive feature of this method is that it can be successively approximated to suit the computational demands of the problem at hand.

Recall that the Herman-Kluk prefactor is

$$R^2_{\mathbf{p}_t\mathbf{q}_t t} = \det\left\{\frac{1}{2}\left[\mathbf{M}_{qq} + \gamma^{-1}\mathbf{M}_{pp}\gamma + \frac{i}{\hbar}\gamma^{-1}\mathbf{M}_{pq} + \frac{\hbar}{i}\mathbf{M}_{qp}\gamma\right]\right\}, \tag{F.1}$$

where $\mathbf{M}_{qq}, \mathbf{M}_{qp}, \mathbf{M}_{pq}$ and $\mathbf{M}_{pp}$ are elements of the monodromy matrix. For brevity, I will refer to the mass-weighted second derivative matrix for the potential as $\kappa_t = \frac{\partial^2 V}{\partial \mathbf{q}_t^2}$. Miller begins by defining a matrix, $\mathbf{Q}$, as

$$\begin{aligned}
\mathbf{Q}_t &= \mathbf{M}_{qq} + \frac{\hbar}{i}\mathbf{M}_{qp}\gamma && \text{(F.2)}\\
\dot{\mathbf{Q}}_t &= \dot{\mathbf{M}}_{qq} + \frac{\hbar}{i}\dot{\mathbf{M}}_{qp}\gamma \\
&= \mathbf{M}_{pq} + \frac{\hbar}{i}\mathbf{M}_{pp}\gamma && \text{(F.3)}\\
\ddot{\mathbf{Q}}_t &= \dot{\mathbf{M}}_{pq} + \frac{\hbar}{i}\dot{\mathbf{M}}_{pp}\gamma \\
&= -\kappa_t\mathbf{M}_{qq} - \frac{\hbar}{i}\kappa_t\mathbf{M}_{qp}\gamma. && \text{(F.4)}
\end{aligned}$$

Here, he has made use of the auxiliary equations, (2.128). He notes that (F.1) can be written

$$R^2_{\mathbf{p}_t\mathbf{q}_t t} = \det\left\{\frac{1}{2}\left[\mathbf{Q}_t + \frac{i}{\hbar}\gamma^{-1}\dot{\mathbf{Q}}_t\right]\right\}. \tag{F.5}$$

and that

$$\ddot{\mathbf{Q}}_t + \kappa_t \mathbf{Q}_t = -\kappa_t \left[\mathbf{M}_{qq} + \frac{\hbar}{i}\mathbf{M}_{qp}\gamma\right] + \kappa_t \left[\mathbf{M}_{qq} + \frac{\hbar}{i}\mathbf{M}_{qp}\gamma\right] = \mathbf{0}. \tag{F.6}$$

The log-derivative matrix, $\mathbf{R}_t$ (not to be confused with the prefactor, $R_{\mathbf{p}_i\mathbf{q}_i t}$) is now defined as:

$$\mathbf{R}_t = \dot{\mathbf{Q}}_t \mathbf{Q}_t^{-1}. \tag{F.7}$$

After a little fiddling,

$$\begin{aligned}
\mathbf{R}_t\mathbf{Q}_t &= \dot{\mathbf{Q}}_t\mathbf{Q}_t^{-1}\mathbf{Q}_t \\
&= \dot{\mathbf{Q}}_t \\
\therefore \ddot{\mathbf{Q}}_t &= \dot{\mathbf{R}}_t\mathbf{Q}_t + \mathbf{R}_t\dot{\mathbf{Q}}_t \\
\therefore -\kappa_t\mathbf{Q}_t &= \dot{\mathbf{R}}_t\mathbf{Q}_t + \mathbf{R}_t\mathbf{R}_t\mathbf{Q}_t \\
&= \left(\dot{\mathbf{R}}_t + \mathbf{R}_t^2\right)\mathbf{Q}_t \\
\therefore -\kappa_t &= \dot{\mathbf{R}}_t + \mathbf{R}_t^2.
\end{aligned}$$

We have made use of (F.4) in the second last step. Therefore, $\mathbf{R}_t$ evolves according to

$$\dot{\mathbf{R}}_t = -\kappa_t - \mathbf{R}_t^2. \tag{F.8}$$

Now, we determine the initial condition for $\mathbf{R}_t$. Since at $t = 0$, $\mathbf{M}_{qq} = \mathbf{M}_{pp} = \mathbf{1}$ and $\mathbf{M}_{qp} = \mathbf{M}_{pq} = \mathbf{0}$, it follows that $\mathbf{Q}_0 = \mathbf{1}$, $\dot{\mathbf{Q}}_0 = \frac{\hbar}{i}\gamma$, and therefore, by (F.7):

$$\mathbf{R}_0 = \frac{\hbar}{i}\gamma. \tag{F.9}$$

To arrive at the final expression for the prefactor in terms of the log-derivative, we notice that, with the help of (F.7), (F.5) can be factored as

$$\begin{aligned}
\det\left[\frac{1}{2}\left(\mathbf{Q}_t + \frac{i}{\hbar}\gamma^{-1}\dot{\mathbf{Q}}_t\right)\right] &= \det\left[\frac{1}{2}\left(\mathbf{1} + \frac{i}{\hbar}\gamma^{-1}\mathbf{R}_t\right)\mathbf{Q}_t\right] \\
&= \det\left[\frac{1}{2}\left(\mathbf{1} + \frac{i}{\hbar}\gamma^{-1}\mathbf{R}_t\right)\right]\det\mathbf{Q}_t.
\end{aligned} \tag{F.10}$$

Now, we must express $\det\mathbf{Q}_t$ in terms of the log-derivative. Solving (F.7) for $\mathbf{Q}_t$ gives:

$$\mathbf{Q}_t = \mathbf{T}\exp\left[\int_0^t \mathrm{d}t'\mathbf{R}_{t'}\right], \tag{F.11}$$

where $\mathbf{T}$ is the time-ordering operator, although it disappears when the determinant is taken:

$$\begin{aligned}
\det\mathbf{Q}_t &= \det\left\{\mathbf{T}\exp\left[\int_0^t \mathrm{d}t'\mathbf{R}_{t'}\right]\right\} \\
&= \exp\left[\int_0^t \mathrm{d}t'\mathrm{Tr}\mathbf{R}_{t'}\right].
\end{aligned} \tag{F.12}$$

To arrive at (F.12), we've diagonalised $\mathbf{R}_{t'}$, so we are able to write the determinant as a product, and then made use of the basis-invariance of the trace operation. So, our final expression for the prefactor is:

$$R_{\mathbf{p}_i\mathbf{q}_i t} = \sqrt{\det\left[\frac{1}{2}\left(\mathbf{1} + \frac{i}{\hbar}\gamma^{-1}\mathbf{R}_t\right)\right]}\exp\left[\frac{1}{2}\int_0^t \mathrm{d}t' \mathrm{Tr}\mathbf{R}_{t'}\right]. \tag{F.13}$$

Note that this result is formally exact. Taken with (F.8) and (F.9), (F.13) provides us with a practical means of computing $R_{\mathbf{p}_i\mathbf{q}_i t}$.

Now we turn our attention to two approximate treatments. The first was not used to produce any of the results in this thesis, so I won't provide the details of its derivation. It assumes that the force constant matrix varies slowly in time, *i.e.*:

$$\frac{\mathrm{d}\kappa_t}{\mathrm{d}t} = \frac{\partial^3 V}{\partial \mathbf{q}_t^3}\dot{\mathbf{q}} \approx \mathbf{0}. \tag{F.14}$$

This gives the following expression for the prefactor:

$$R_{\mathbf{p}_i\mathbf{q}_i t} = \exp\left[\frac{1}{2}\int_0^t \mathrm{d}t' \mathrm{Tr}\tilde{\mathbf{R}}_{t'}\right]. \tag{F.15}$$

Notice that this obviates the need to calculate any determinant, thereby reducing the computational cost. This new matrix, $\tilde{\mathbf{R}}_t$, has the same time-dependence as $\mathbf{R}_t$, but with a different initial condition:

$$\tilde{\mathbf{R}}_0 = -\frac{i}{2}\left(\frac{1}{\hbar}\gamma^{-1}\kappa_0 + \hbar\gamma\right). \tag{F.16}$$

The other approximate scheme goes a step further: we assume that the log-derivative matrix itself varies slowly with time:

$$\dot{\mathbf{R}}_t \approx \mathbf{0}. \tag{F.17}$$

Miller refers to this as "Johnson's multichannel WKB approximation". Equation (F.17) enables us to simplify (F.8) as:

$$\mathbf{R}_t = (-\kappa_t)^{1/2} = -i(\kappa_t)^{1/2} \tag{F.18}$$

Taking $\mathbf{R}_t$ as (F.9) in the determinant and as (F.18) in the exponent dramatically simplifies (F.13):

$$\begin{aligned} R_{\mathbf{p}_i\mathbf{q}_i t} &= \sqrt{\det\left[\frac{1}{2}\left(\mathbf{1} + \frac{i}{\hbar}\gamma^{-1}\left\{\frac{\hbar}{i}\gamma\right\}\right)\right]}\exp\left[\frac{1}{2}\int_0^t \mathrm{d}t' \mathrm{Tr}\left\{-i(\kappa_{t'})^{1/2}\right\}\right] \\ &= \sqrt{\det\left[\mathbf{1}\right]}\exp\left[-\frac{i}{\hbar}\int_0^t \mathrm{d}t' \frac{\hbar}{2}\mathrm{Tr}(\kappa_{t'})^{1/2}\right] \\ &= \exp\left[-\frac{i}{\hbar}\int_0^t \mathrm{d}t' \sum_{j=1}^{N}\frac{1}{2}\hbar\omega_j(t')\right]. \end{aligned} \tag{F.19}$$

For the last step, we have recognised that the trace of the square root of the force-constant matrix is equivalent to the sum of the frequencies obtained by diagonalising κ_t ($\omega_j^2(t)$ are the eigenvalues

of the κ_t). Notice that now all that is required to propagate the HK-prefactor is to compute κ_t and diagonalise it once per timestep. Notice also that imaginary frequencies (encountered in "concave-down" regions of the potential) will give rise to rather large contributions to $R_{\mathbf{p}_t\mathbf{q}_t t}$. This was a problem encountered in Section 3.2.3, before rigid-body rotations were removed from our water model.

Appendix G

Schematic for Computer Code Used in this Thesis

Below is a schematic outline of the code used in this thesis. Codes were written in C++, and extensive use was made of the object oriented philosophy. I present the classes used in the evaluation of the HK-IVR ACF in a format modeled after Hinsen's MMTK documentation. [47]

class *molecule* :
This class models a molecular system, and is used to compute common quantities (angular momentum, bond distances and angles, the location of the centre of mass, etc.).

members :

- natoms
  The number of atoms in our molecule.
- molecule_name
  The name of our molecular system. For our water-bender, this was "`water`".
- atom_label
  The chemical symbols of all of the atoms in the system. Each atom is defined by two characters (our water-bender was specified by "`O␣H␣H␣`").
- atom_chg
  The charges, Z, of the nuclei.
- pos
  The present configuration.

- vel

  The present velocities.

- acc

  The present accelerations.

- mass

  The atomic masses.

- M

  The total mass.

- animation

  A filestream for writing a *jmol* animation to file.

methods :

- molecule(*molecule_name, atom_labels*)

  The constructor: initialise the molecule name and its atom labels. Fill atom_chg and mass with appropriate values.

- init(*pos, vel*)

  Initialise position and velocity.

- write_xyz(*filename*)

  Write the molecular configuration to file in *xyz* format.

- distance(*atom_1, atom_2*)

  Return the distance between atom_1 and atom_2.

- angle(*atom_1, atom_2, atom_3*)

  Return the angle formed by atom_1, atom_2 and atom_3.

- position(*atom, coord*)

  Return the x, y or z component (specified by coord) of the position of atom, atom.

- velocity(*atom, coord*)

  Return the x, y or z component (specified by coord) of the velocity of atom, atom.

- acceleration(*atom, coord*)

  Return the x, y or z component (specified by coord) of the acceleration of atom, atom.

- remove_translations()

  Remove net translations.

- remove_rotations()

  Remove net angular momentum, so that $\mathbf{L} = \mathbf{0}$.

- moment_of_inertia()

  Return the 3×3 inertial tensor.

- cm_at_origin()

  Shift the centre of mass to the origin.

- total_mass()

  Return the total mass of the molecular system.

- total_L()

  Return the total angular momentum of the molecular system.

- return_qcm()

  Return the position of the centre of mass.

- return_pcm()

  Return the momentum associated with the centre of mass.

- animate_jmol()

  Add the present configuration to the animation file, in *jmol* format.

class *waterpot* :

This class make use of the molecular potential of Reference [40] (*i.e.* it calls the FORTRAN function), in order to compute the potential and its relevant derivatives.

members :

- fdiff

  The finite difference value for computing derivatives of the potential.

methods :

- waterpot(*fdiff*)

  The constructor: initialise fdiff.

- potential(*pos*)

  Return the value of the potential, $V(\mathbf{q})$, calculated at the input configuration, pos.

- gradient(*pos*)

  Return the gradient, $\frac{\partial V(\mathbf{q})}{\partial \mathbf{q}}$, calculated at the input configuration, pos.

- hessian(*pos*)

  Return the Hessian, $\frac{\partial^2 V(\mathbf{q})}{\partial \mathbf{q}^2}$, calculated at the input configuration, pos.

- projector(*pos*)

  Calculate the elementary displacement matrix, $\mathbf{D}$, at the configuration, pos, and return the corresponding projection matrix, Δ.

class *rattle* :

This class computes classical trajectories for constrained systems in Cartesian coordinates.

members :

- natoms

  The number of atoms in our molecule.

- nconsts

  The number of holonomic constraints.

- dt

  The value of the timestep for the dynamics.

- constraint

  The complete set of constraints, $\{d_{ij}^{(k)}\}$. Each constraint specifies the two participating atoms and their relative distance.

- mass

  The atomic masses.

- max_iterations

  The maximum number of Rattle iterations to be performed before it gives up and sends an error message (in order to prevent an infinite loop).

- tolerance

  The value of the Rattle tolerance.

methods :

- rattle(*natoms, nconsts, dt, constraint, mass, max_iterations, tolerance*)
  The constructor: initialise members.

- init(*pos, vel, acc, hes, T, V, potcalc*)
  "Repair" position and velocity (to obey the constraints), and compute acceleration, the Hessian, and kinetic and potential energy at the beginning of a trajectory (potcalc is an instance of the waterpot class).

- timestep(*pos, vel, acc, hes, T, V, potcalc*)
  Propagate all dynamical variables forward by dt, ensuring that all constraints are satisfied to within tolerance.

class *hk_ivr* :
This class performs the computation of all parts of the HK-integrand. It includes (as members) instances of the classes written for the calculation of the HK-prefactor (see below).

members :

- ndf
  The total number of degrees of freedom of our molecular system.

- dt
  The value of the timestep for the dynamics.

- alpha
  The wavepacket width parameters.

- mass
  The atomic masses.

- pos0
  The configuration of $|\Psi_0\rangle$.

- vel0
  The velocities corresponding to $|\Psi_0\rangle$.

- gpiqi_psi0
  The present value of the overlap, $\langle g^{\gamma}_{\mathbf{p}_i\mathbf{q}_i}|\Psi_0\rangle$, minus the Gaussian sampling function.

- psi0_gptqt

  The present value of the overlap, $\langle \Psi_0 | g^{\gamma}_{\mathbf{p}_t \mathbf{q}_t} \rangle$.

- action

  The present value of the classical action, $S_{\mathbf{p}_t \mathbf{q}_t t}$.

- intgnd

  The present value of the HK-integrand, minus the prefactor (*i.e.* the overlaps multiplied by the phase term).

- r_wkb

  An instance of the class for computing the approximate HK-prefactor.

- r_ext

  An instance of the class for computing the formally exact HK-prefactor.

methods :

- hk_ivr(*natoms, dt, alpha, mass, pos0, vel0*)

  The constructor: initialise members.

- sample_ics(*posi, veli, rand*)

  Sample initial positions and velocities from the Gaussian distribution, centred on $|\Psi_0\rangle$ (using the random number generator, rand), and place these in posi and veli.

- init(*posi, veli*)

  The classical action is reset to 0, and the HK-prefactor to 1. The initial positions and velocities (posi and veli) for this trajectory are used in evaluating the overlaps; $\langle g^{\gamma}_{\mathbf{p}_i \mathbf{q}_i} | \Psi_0 \rangle$ is computed only once per trajectory since it is time-independent.

- update(*post, velt, hest, T, V*)

  Update all members based on the input dynamical variables: The overlap, $\langle \Psi_0 | g^{\gamma}_{\mathbf{p}_t \mathbf{q}_t} \rangle$ is computed using the present position and velocity (post and velt). The classical action is updated using the kinetic and potential energy (T and V). The HK-prefactor is updated using the projected, mass-weighted Hessian (hest).

- intgnd_nor()

  Return the present value of the HK-integrand without the prefactor. This gives rise to Heller's primitive IVR.

- intgnd_wkb()

  Return the present value of the HK-integrand, where the prefactor has been computed by the approximate method of Appendix F.

- intgnd_ext()

  Return the present value of the HK-integrand, where the prefactor has been computed by the formally exact method of Appendix F.

class *r_logwkb* :

A class for computing the HK-prefactor by the approximate method presented in Appendix F, $R_{\mathbf{p}_i\mathbf{q}_i t} \approx \exp\left[-\frac{i}{\hbar}\int_0^t \mathrm{d}t' \sum_{j=1}^{N} \frac{1}{2}\hbar\omega_j(t')\right]$.

members :

- ndf

  The total number of degrees of freedom of our molecular system.

- dt

  The value of the timestep for the dynamics.

- int_sum_w

  The present value of the integral in the exponent (see above).

methods :

- r_logwkb(*ndf, dt*)

  The constructor: initialise members.

- init()

  Start off with $R_{\mathbf{p}_i\mathbf{q}_i t} = 1$.

- update(*hes*)

  Update the value of the prefactor using the eigenvalues of the projected mass-weighted Hessian, hes.

- value()

  Return the present value of the prefactor.

class *r_logext* :

A class for computing the HK-prefactor by the formally exact method presented in Appendix F,

$R_{\mathbf{p};\mathbf{q};t} = \sqrt{\det\left[\frac{1}{2}\left(1 + \frac{i}{\hbar}\gamma^{-1}\mathbf{R}_t\right)\right]} \exp\left[\frac{1}{2}\int_0^t dt' \mathrm{Tr}\mathbf{R}_{t'}\right]$.

members :

- ndf

  The total number of degrees of freedom of our molecular system.

- pfsteps

  The number of "sub-timesteps" which are performed in the propagation of the log-derivative matrix (according to $\dot{\mathbf{R}}_t = -\kappa_t - \mathbf{R}_t^2$) per evaluation of the projected mass-weighted Hessian, κ_t.

- dt

  The value of the timestep for the dynamics, divided by pfsteps.

- R

  The present log-derivative matrix.

- igamma

  The inverse wavepacket width parameters.

- int_Tr_R

  The present value of the integral, $\int_0^t dt' \mathrm{Tr}\mathbf{R}_{t'}$.

- C

  The present value of the HK-prefactor.

- imdet

  The imaginary part of the determinant, $\det\left[\frac{1}{2}\left(1 + \frac{i}{\hbar}\gamma^{-1}\mathbf{R}_t\right)\right]$. We keep track of this in order to keep the prefactor a continuous function of time.

- v

  This quantity is ± 1, and is used to keep the prefactor a continuous function of time.

methods :

- r_logext(*ndf, pfsteps, dt, alpha, mass*)

  The constructor: initialise members.

- init()

  Start off with $R_{\mathbf{p};\mathbf{q};t} = 1$.

- **update(*hes*)**

  Update the value of the prefactor using the projected mass-weighted Hessian, hes.

- **value()**

  Return the present value of the prefactor.